ERDC TR-23-11

US Army Corps
of Engineers®
Engineer Research and
Development Center

ERDC
ENGINEER RESEARCH & DEVELOPMENT CENTER

Mechanical Properties of Steel under Dynamic Loading

Dynamic Material Properties of Grade 50 Steel

Effects of High Strain Rates on ASTM A992 and A572 Grade 50 Steels

Matthew P. Murray, Trace A. Thornton, Stephen P. Rowell,
and Clifford E. Grey

August 2023

Engineer Research and
Development Center

The US Army Engineer Research and Development Center (ERDC) solves the nation's toughest engineering and environmental challenges. ERDC develops innovative solutions in civil and military engineering, geospatial sciences, water resources, and environmental sciences for the Army, the Department of Defense, civilian agencies, and our nation's public good. Find out more at www.erdc.usace.army.mil.

To search for other technical reports published by ERDC, visit the ERDC online library at https://erdclibrary.on.worldcat.org/discovery.

Dynamic Material Properties of Grade 50 Steel

Effects of High Strain Rates on ASTM A992 and A572 Grade 50 Steels

Matthew P. Murray, Trace A. Thornton, and Stephen P. Rowell

US Army Engineer Research and Development Center
Geotechnical and Structures Laboratory
3909 Halls Ferry Road
Vicksburg, MS 39180-6199

Clifford E. Grey

US Army Engineer Research and Development Center
Information Technology Laboratory
3909 Halls Ferry Road
Vicksburg, MS 39180-6199

Final report

Prepared for Department of Defense Explosives Safety Board
4800 Mark Center Drive
Alexandria, VA 22350-3606

Under MIPR 11052312

Abstract

Uniaxial tensile tests were conducted on American Society for Testing Materials International (ASTM) A992 and A572 Grade 50 steels at increasing strain rates to determine the material strength properties of structural members subjected to dynamic loadings. The increase in dynamic yield strength and ultimate tensile strength was determined to update design criteria within UFC 3-340-02, which are currently limited to ASTM A36 and A514 steels. The proposed updates will provide the necessary information required to design blast-resistant structures utilizing modern-day structural steels. The dynamic material properties determined by high-rate tensile tests were compared to static values obtained from ASTM E8 standard tensile tests. The comparisons were used to calculate dynamic increase factors (DIFs) for each steel at strain rates from 2E-3 to 2E0 inch/inch/second. The experiments revealed that the A992 steel exhibited an increase in yield strength up to 45% and ultimate tensile strength up to 20% as strain rate increased over the range tested. The A572-50 steel exhibited a similar increase in yield strength up to 35% and ultimate tensile strength up to 20%. The DIF design curves developed during this research will allow engineers to more efficiently design structural steel components of hardened structures for the protection of our nation's critical infrastructure.

Contents

Figures and Tables

Figures

Tables

Preface

This study was conducted as a part of collaborative efforts between the US Army Corps of Engineers and the US Department of Defense Explosives Safety Board (DDESB), under MIPR 11052312, to update UFC 3-340-02. The technical monitor was William H. Zehrt, Jr. of the DDESB.

The work was performed by the Structural Mechanics Branch (GSM) of the Geosciences and Structures Division (GS), US Army Engineer Research and Development Center, Geotechnical and Structures Laboratory (ERDC-GSL). At the time of publication of this report, Mr. Omar Flores was branch chief; Mr. James L. Davis was division chief; and Ms. Pamela G. Kinnebrew was the technical director for Survivability and Protective Structures. The deputy director of ERDC-GSL was Mr. Charles W. Ertle II, and Mr. Bartley P. Durst was the director.

Additional support was provided by the Sensor Integration Branch of the Computational Science and Engineering Division, ERDC Information Technology Laboratory (ERDC-ITL). At the time of publication of this report, Ms. Amie Burroughs was branch chief; Dr. Jeffrey Hensley was division chief. The deputy director of ERDC-ITL was Dr. Jackie Pettway, and Dr. David Horner was the director.

Portions of this report have been modified and reprinted from Matthew P. Murray, Stephen P. Rowell, and Trace A. Thornton, *Effects of High Strain Rates on ASTM A992 and A572 Grade 50 Steel* (Vicksburg, MS: US Army Engineer Research and Development Center, Geotechnical and Structures Laboratory, 2018), https://ndiastorage.blob.core.usgovcloudapi.net/ndia/2018/intexpsafety/MurrayPaper.pdf. Public domain.

Portions of this report have been modified and reprinted with permission from Matthew P. Murray, "Dynamic Strength Properties of Structural Steel at Elevated Rates of Strain." Master's thesis, Mississippi State University, 2020, https://scholarsjunction.msstate.edu/td/1592, Copyright 2020 Matthew P. Murray.

COL Christian Patterson was the commander of ERDC, and the director was Dr. David W. Pittman.

This page intentionally left blank.

1 Introduction

Many reports document the effects of strain rate on material strength properties of steels such as yield and ultimate tensile strength; however, the majority of the experimental data that were found on the subject date back 30 to 50 yr1. A collection of research on dynamic material properties and related topics is listed in the bibliography sections of this report. The change in material strength values are important to understand for the efficient design of protective structures with requirements to withstand, to a specific degree, dynamic loading generated from an explosion. Chapter 5 of Unified Facilities Criteria (UFC) 3-340-02, *Structures to Resist the Effects of Accidental Explosions*, details the fundamentals of protective design using structural steels (DoD 2014).

All references to ASTM standards were shortened for brevity. For example, ASTM A992/A992M-11 was abbreviated as A992 (ASTM 2011). In some cases, specific chapters and sections are referenced, for example, A6-11.2 refers to Chapter 11, section 2 of A6 (ASTM 2017a). Full specification information used during this research is found in the reference section. All references to A572 steel in this report are specific to A572 Grade 50 steel. All references to strain rate are to average elastic strain rate, which is the average rate of straining up to the material's yield point. All mentioning of static properties and rates refer to those of a quasistatic environment at a rate low enough to be assumed representative of static.

1.1 Background

The mission of the Department of Defense Explosive Safety Board (DDESB) is to provide objective advice to the Secretary of Defense and Service Secretaries on matters concerning explosives safety and to prevent hazardous conditions to life and property on and off Department of Defense (DoD) installations from the explosives and environmental effects of DoD-titled munitions. The DDESB has oversight and approval responsibility for Protective Construction Design Criteria and Methods when used to support explosives safety site plans. Protective construction is typically designed per UFC 3-340-02, referred to as UFC in this report (DoD 2014).

---

1 For a full list of the spelled-out forms of the units of measure and unit conversions used in this document, please refer to *US Government Publishing Office Style Manual*, 31st ed. (Washington, DC: US Government Publishing Office 2016), 248–52 and 345–7, respectively. https://www.govinfo.gov/content/pkg/GPO-STYLEMANUAL-2016/pdf/GPO-STYLEMANUAL-2016.pdf.

Engineers and scientists throughout the protective design community have recognized the cost and performance benefits of incorporating newer, readily available, advanced construction materials into hardened structure designs for protection of personnel, critical assets, and facilities. However, there is currently limited design guidance available in the current UFC to permit efficient use of these materials, specifically A572 and A992 steels, due to the lack of research on these steels at high strain rates.

1.2 Objective

The objective of this effort was to develop the design dynamic increase factor (DIF) versus strain rate values and curves for A992 and A572 structural steels for incorporation into Chapter 5 of UFC 3-340-02 (DoD 2014). Table 1 indicates the rates of strain at which each steel was tested for this research.

Table 1. Designations and abbreviations for the tested strain rates.

Strain Rate (s^{-1})	Test Designation
2E-5 or 2×10^{-5}	Static Rate (SR)
2E-3 or 2×10^{-3}	Dynamic Rate 1 (DR1)
5E-2 or 5×10^{-2}	Dynamic Rate 2 (DR2)
2E-1 or 2×10^{-1}	Dynamic Rate 3 (DR3)
2E0 or 2×10^{0}	Dynamic Rate 4 (DR4)

1.3 Approach

The following tasks were conducted by the US Army Engineer Research and Development Center to obtain the required dynamic material strength properties of A992 and A572 steel.

1. Define baseline yield and ultimate tensile strength by conducting uniaxial tension tests at a static strain rate of 2E-5 s^{-1}.
2. Determine dynamic yield and dynamic ultimate tensile strength by conducting uniaxial tension tests at four increasing strain rates, approximately 2E-3, 5E-2, 2E-1, and 2E0 s^{-1}.
3. Relate the dynamic strength to the average static values to define the DIF for yield strength (DIF_y) and the DIF for ultimate tensile strength (DIF_u) for each steel.
4. Present the experimental data by plotting the DIF versus strain rate results (for both yield and ultimate tensile strength) and generate a design DIF curve for each steel.

2 Experimental Procedure

2.1 Material Selection/Acquisition

2.1.1 American Society for Testing Materials International (ASTM) A572 (Domestic)

Two 4 × 8 ft A572 plates with a nominal $^3/_8$ in. thickness with the same heat designation (W6D665) were procured. The certified mill test report (MTR) indicated the steel also met the specifications of ASTM A709-50 (ASTM 2017b). The chemical composition of the A572 plate is shown in Table 2.

Table 2. Chemical composition of tested materials (weight percentage).

Material*	C	Mn	P	S	Si	Al	Cu	Ni	Cr	Mo	Cb/Nb	V	Ti
A572 Plate	0.17	1.04	0.009	0.002	0.19	0.027	0.22	0.19	0.12	0.07	0.001	0.042	0.002
A992 Beam	0.07	1.21	0.01	0.022	0.2	0.001	0.28	0.1	0.1	0.048	0.001	0.031	—

*Material: carbon, manganese, phosphorus, sulfur, silicon, aluminum, copper, nickel, chromium, molybdenum, columbium/niobium, vanadium, titanium

2.1.2 ASTM A992 (Domestic)

Three 20 ft long S12 × 31.8 beams of A992 with the same heat designation (B125700) were procured for the experiments. The beam was chosen due to the geometry of the web, which had a thickness approximately equal to the $^3/_8$ in. A572 plate. The height of the web also allowed for two specimens of uniform thickness to be cut per unit length of the beam. The MTR indicated that the beams also met specifications of ASTM A6 (ASTM 2017a), A709-50 (ASTM 2017b), A572-50 (ASTM 2015), and A36 (ASTM 2014).

2.2 Specimen Fabrication

2.2.1 Dynamic ASTM A572 Specimen

The dog-bone-shaped specimens were each waterjet cut so that the longitudinal axis of the specimens was transverse to the length of the plate, as per A6-11.2 (ASTM 2017a). The bolt holes for the grips were then drilled using a computer numerical control machine to allow for the high-precision axial alignment of the tensile specimens and the applied load. Best machining practices were followed to ensure that the specimens were free of flaws such as burs, chips, or rough surfaces. Gauge marks were lightly machined into one face of the specimens. The specimen's geometry for both the A572 and A992 steels is shown in Figure 1 and conform to tolerances prescribed in E8 (ASTM 2016).

Figure 1. Dynamic uniaxial tension specimen for A572 and A992.

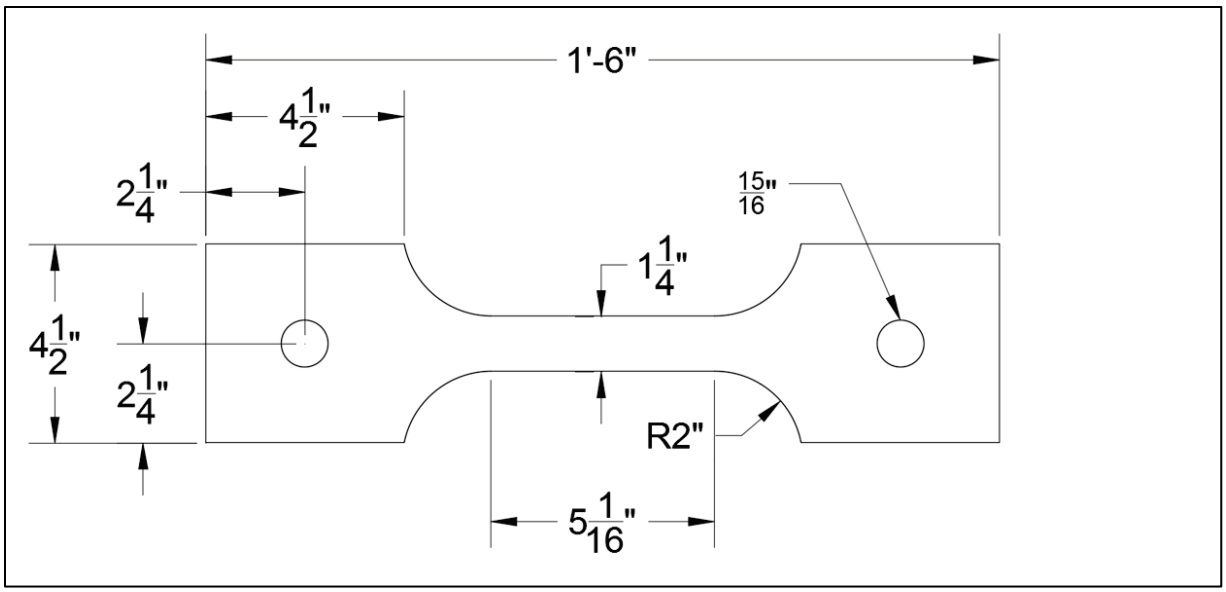

2.2.2 Dynamic ASTM A992 Specimen

The A992 specimens were cut from the webbing of the *S* shape. The machining practices used for this material were the same as listed above for the A572 specimens. Figure 2 shows the orientation of both the static and dynamic specimens cut from the *S* beam.

Figure 2. Sections of the S12 × 31.8 beam after dynamic (*left*) and static (*right*) specimens were cut from the web.

2.2.3 Static Specimen

For both the A572 and the A992 steels, the static-rate specimens were waterjet cut into ASTM E8 standard sheet-type geometries shown in E8-6.2 (ASTM 2016). Figure 3 shows a size comparison of the static and dynamic rate specimen.

Figure 3. Static (*top*) and dynamic (*bottom*) tension specimen.

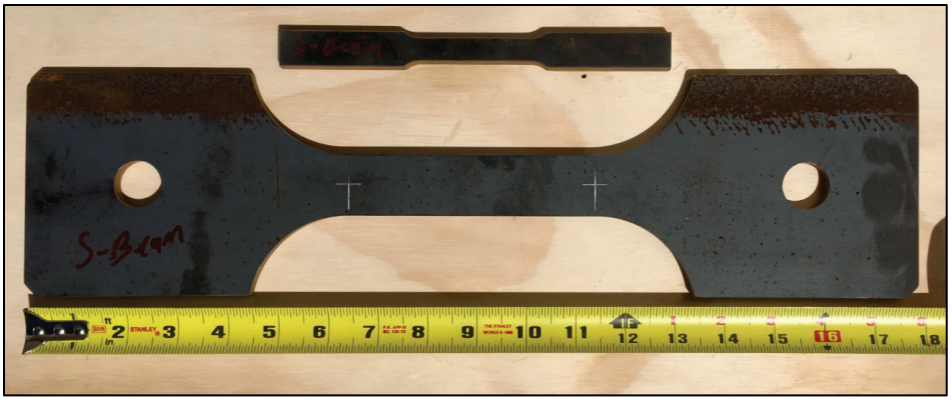

2.3 Static-Rate Testing Device

Baseline material strength properties of the A992 and A572 steels were determined using the 33R4206 Universal Testing System (Instron; Norwood, Massachusetts) (Figure 4) at the Geotechnical and Structures Laboratory (GSL). The apparatus incorporated an optical extensometer to record elongation over time. Specimens were tested at an average strain rate of approximately 2E-5 s^{-1} using this machine.

Figure 4. Instron uniaxial tension test machine used for static-rate testing.

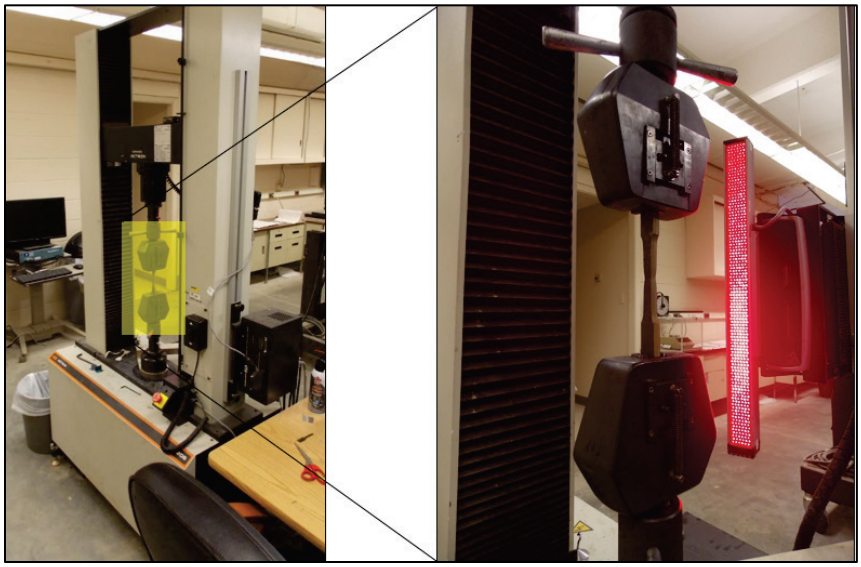

2.4 Dynamic-Rate Testing Device

The 200-kip hydraulic loader of the GSL (Figure 5, Figure 6, and Figure 7) was used to conduct dynamic uniaxial tensile tests. The hydraulic loader has been used since the 1970s to conduct dynamic experimentation on reinforcing steel, splices, and fasteners (Flathau 1971; Weathersby 2003; Rowell and Grey 2009). It has been

periodically renovated to incorporate more advanced methods of control as required for each new set of experiments that were performed. Figure 5 shows a schematic of the pressure chambers. The original configuration shown in this figure relied on rupture disks, which have since been replaced with quick-opening valves.

The device is capable of applying a load with a minimum rise time of 1.3 ms and has a maximum stroke of 6 in. It is designed to apply loads from 10 to 200 kip in either tension or compression. The loading rates can be adjusted to provide test specimen strain rates between 1E-3 to 3.5E0 s^{-1}, depending on the material properties and geometry of the tested specimen. The loader grips can be adjusted to accept test specimens up to 3 ft in length. Adjustments in the tower above the loader can be made to accommodate longer specimens if required.

The device is slowly pressurized by pumping compressible silicon oil into the top and bottom pressure chambers. The pressure in the top chamber is kept at a slightly higher pressure to maintain a small tensile preload (50–1,000 lbf) on the specimen. The preload ensures alignment of the specimen through the bolted connections and also seats the top reaction stem pivot joint to further ensure axial loading of the specimen. Once the desired fluid pressure has been reached, a quick-opening valve leading to an empty expansion tank is opened. The pressure in the lower chamber is rapidly reduced, allowing the piston to translate downward and apply a tension load to the specimen attached above. The flow rate of the fluid in the lower chamber into the expansion tank is controlled by an adjustable orifice and is the main variable in changing the loading rate (i.e., strain rate, applied to the test specimen).

Table 3 shows the 200-kip loader operating parameters used for the four different dynamic strain rates tested. Dynamic Rate 4 was the maximum strain rate achievable by the test apparatus, when the orifice was completely opened.

Table 3. The 200-kip operating parameters for the dynamic tensile test experiments.

Strain Rate (s^{-1})	Orifice Size (in.)	Fluid Pressure (top chamber) (psi)
DR1: 2E-3	1/16	2,290
DR2: 5E-2	3/16	1,650
DR3: 2E-1	1 5/16	2,290
DR4: 2E0	4 1/2	4,575

Figure 5. Schematic of 200-kip loader chambers. (Image reproduced from Huff 1969. Public domain.)

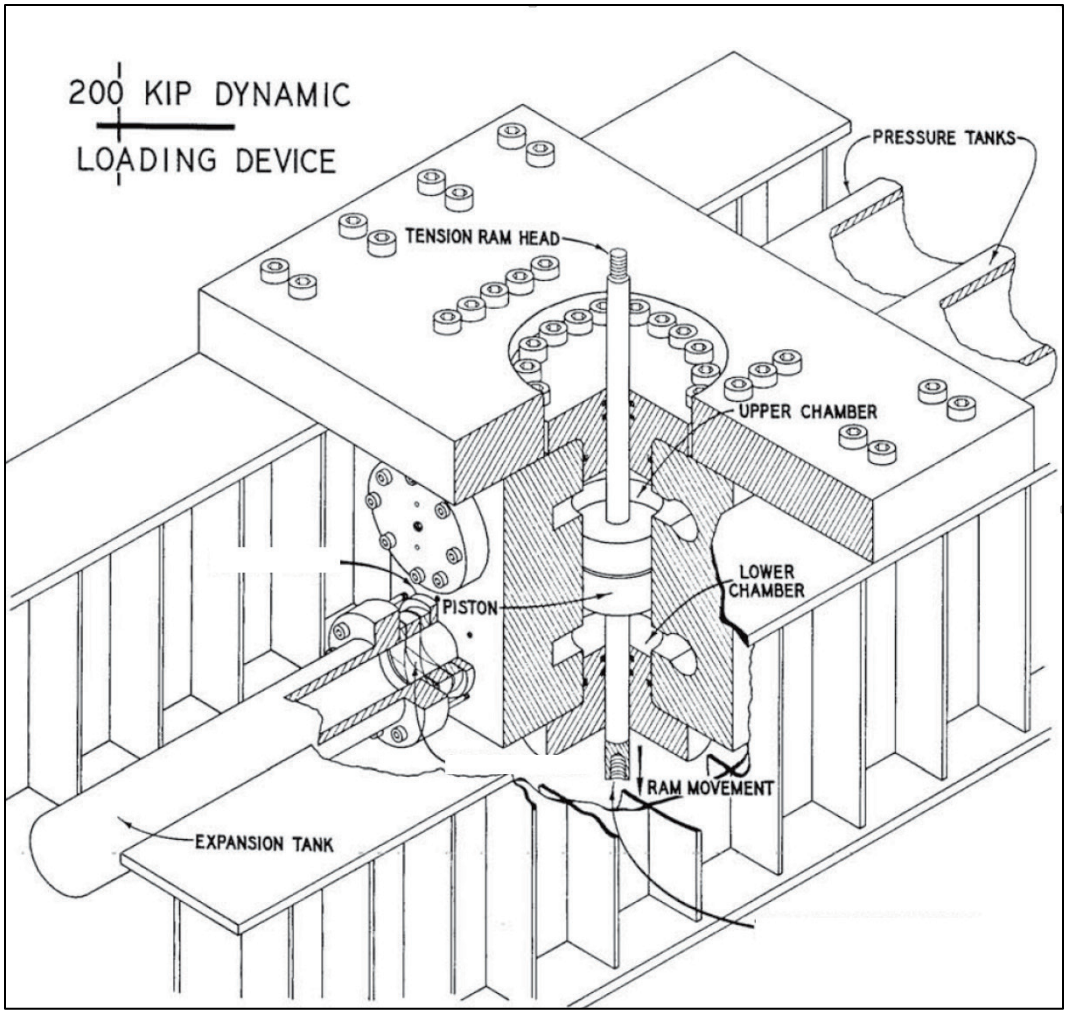

Figure 6. The US Army Engineer Research and Development Center 200-kip hydraulic dynamic loading machine. (Image reproduced from Rowell and Grey 2009. Public domain.)

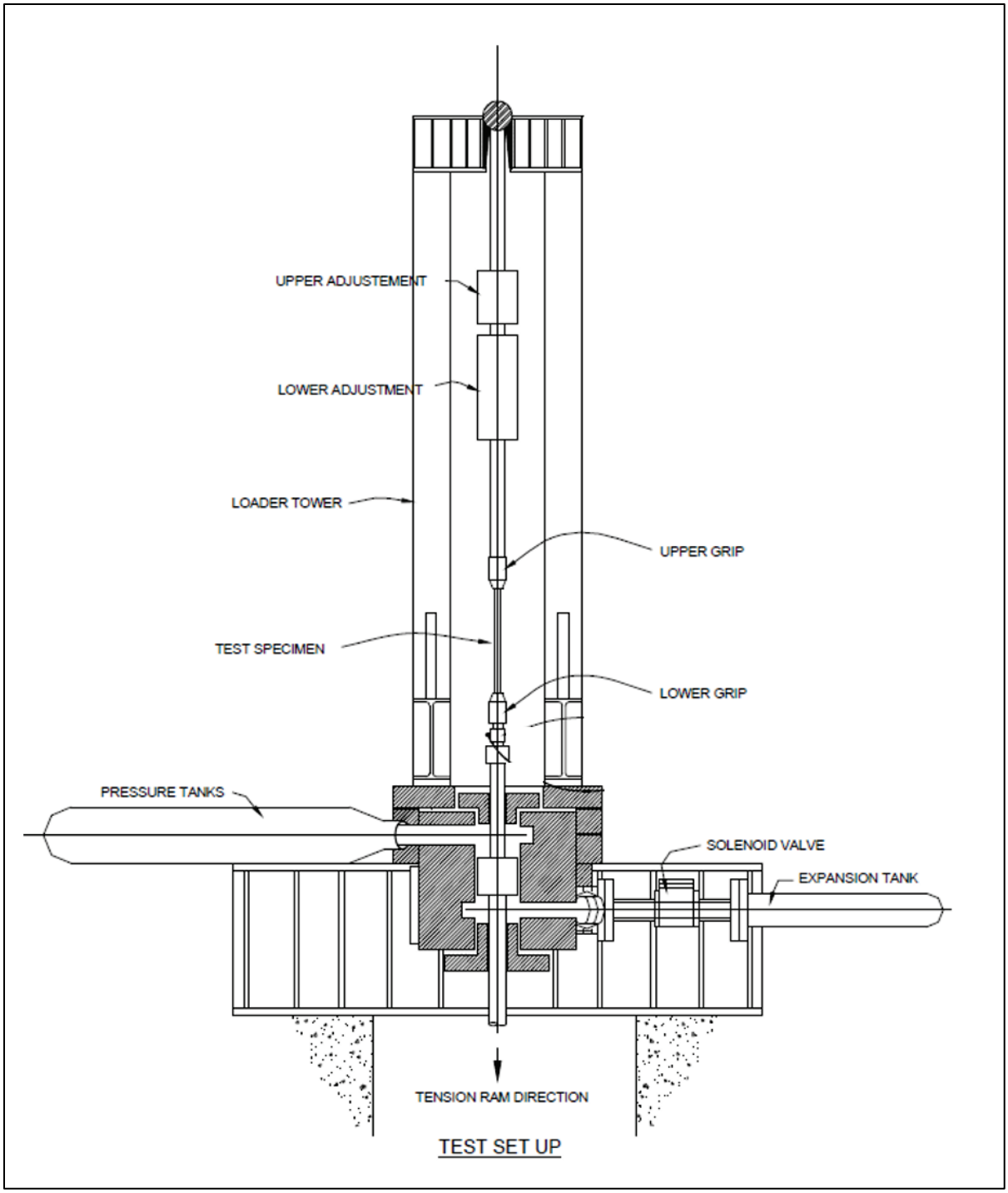

Figure 7. Schematic of test assembly (*left*) and specimen loaded into grips (*right*).

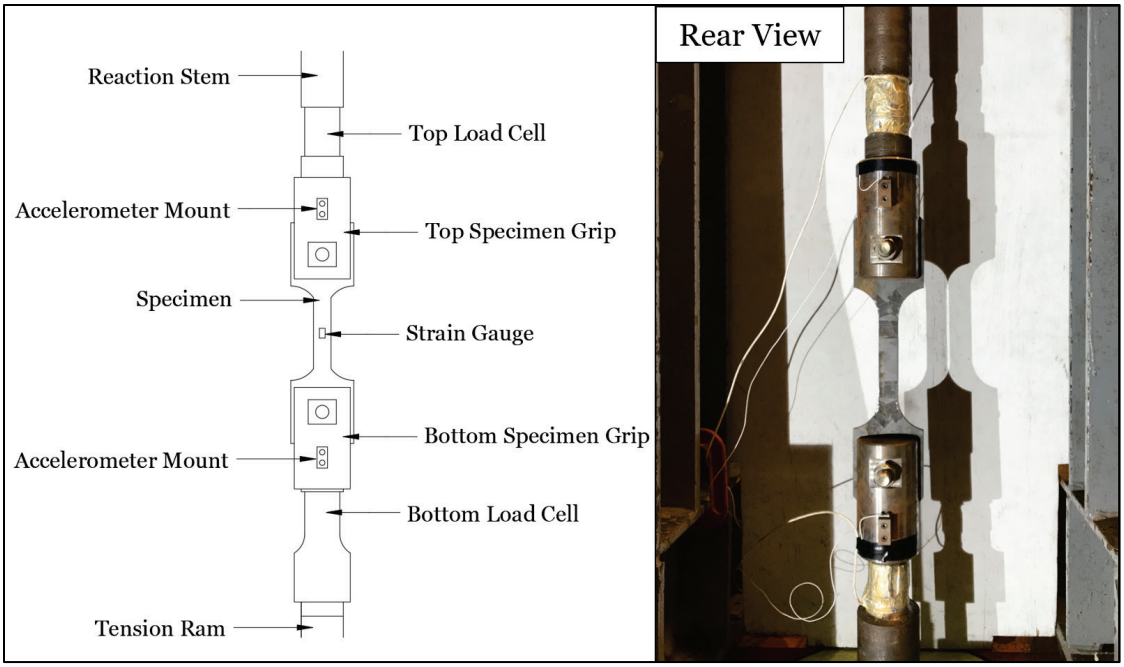

2.5 Instrumentation (Dynamic Testing)

Load, acceleration, and strain gauge data were recorded using a Hi-Techniques Echelon, Model EM-HS Data Acquisition System (Hi-Techniques; Madison, Wisconsin). The sections below explain the instrumentation hardware, application, and analysis. Table 4 lists the different instrumentation and the sampling frequencies for the strain rates tested.

Table 4. Instrumentation utilized for dynamic increase factor (DIF) experiments at the tested rates.

Strain Rate	Load	Acceleration	Deformation	Strain	Sample Frequency
SR: 2E-5 s^{-1}	Integrated top and bottom load cell	—	Integrated optical extensometer	—	10 Hz
DR1: 2E-3 s^{-1}	Top and bottom load cell	—	High-speed camera (120 frames per second [fps])	—	1 kHz
DR2: 5E-2 s^{-1}	Top and bottom load cell	Top and bottom accelerometer	High-speed camera (1,500 fps)	—	10 kHz
DR3: 2E-1 s^{-1}	Top and bottom load cell	Top and bottom accelerometer	High speed camera (13,000 fps)	—	50 kHz
DR4: 2 E0 s^{-1}	Top and bottom load cell	Top and bottom accelerometer	High-speed camera (13,000 fps)	Strain gauge	1,000 kHz

2.5.1 Strain

Axial deformation was measured using a Miro 320S high-speed (HS) camera (Phantom; Wayne, New Jersey). The HS camera recorded locations of the gauge marks from time zero (trigger) through fracture of the specimen. The video was uploaded into Track Eye Motion Analysis (TEMA) 2D software (Image Systems AB; Linkoping, Sweden) (Figure 8), which incorporated an optical extensometer feature that tracked each gauge mark location, represented by a single pixel, frame by frame throughout the length of the video recording. The software then output the distance between gauge marks (elongation) with respect to time.

Figure 8. Track Eye Motion Analysis (TEMA) software interface used to track gauge mark locations over time.

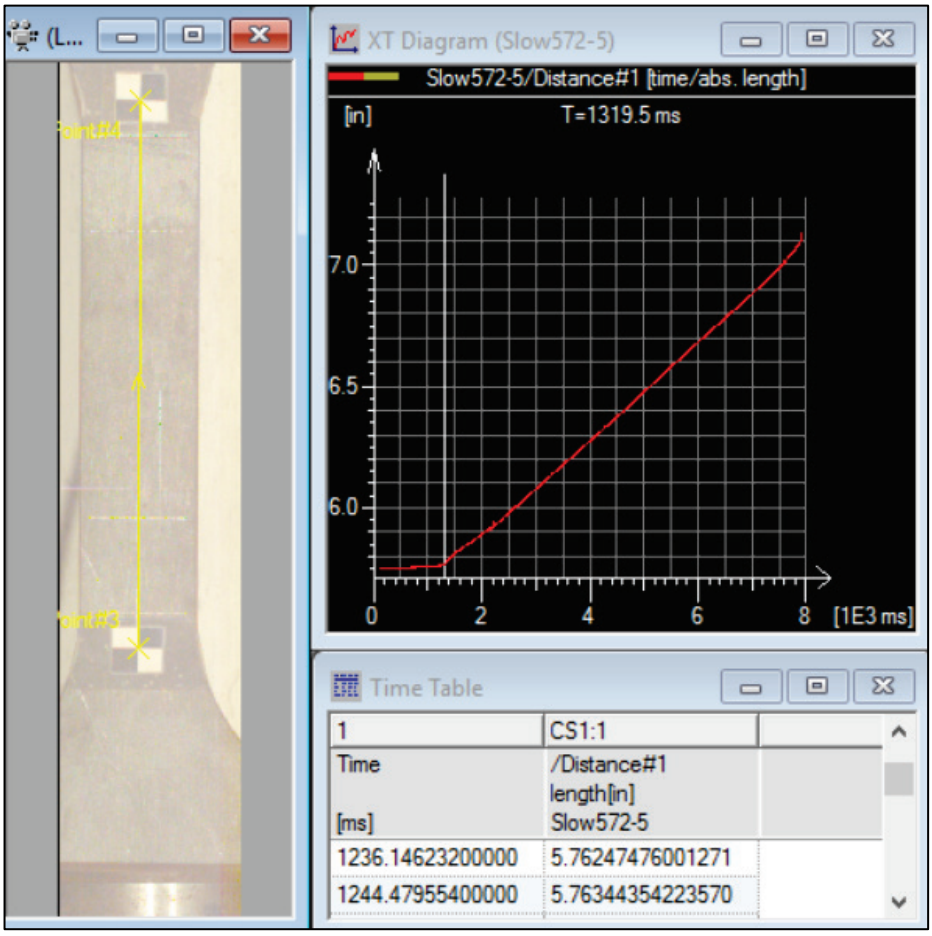

Strain with respect to time was then calculated by importing elongation with respect to time into Excel and using the average axial strain equation from mechanics of materials, Equation (1) (Hibbeler 2014). Average strain rate was determined by calculating the slope of the strain-time data in the elastic deformation region.

$$e = \frac{L - L_0}{L_0}, \quad (1)$$

where

e = axial engineering strain (in./in.).
L = length output from TEMA (in.), and
L_o = original gauge length (in.).

Quadrant markers were added to the specimen to enhance the tracking capabilities of the TEMA software (Figure 9). As stated previously, the software tracked single points, the upper and lower quadrant crosses, as they moved from pixel to pixel. The pixel length was set by the vertical resolution of the HS camera recording and the distance between the tracked points.

The HS camera software was calibrated to remove error due to lens distortion using the prescribed TEMA lens calibration guidelines (Image Systems AB 2015).

The dynamic specimens for Dynamic Rate (DR) 4 yielded within approximately 1 ms. Strain gauges were implemented at this rate to obtain high-resolution strain data before yield because the HS camera could not capture enough frames to ensure capture of yield strain in such a short duration. Strain gauges were applied to specimens used for strain-rate calibration and the specimens tested at DR4.

For these specimens, the mill scale had to be removed from the parent material. Approximately 0.006 in. (less than 2% of thickness) of material was removed by machining across the entire gauge region (Figure 10), which allowed application of the strain gauge to the exposed steel at the center of the gauge region.

Figure 9. An A572 specimen with strain gauge and quadrant markers.

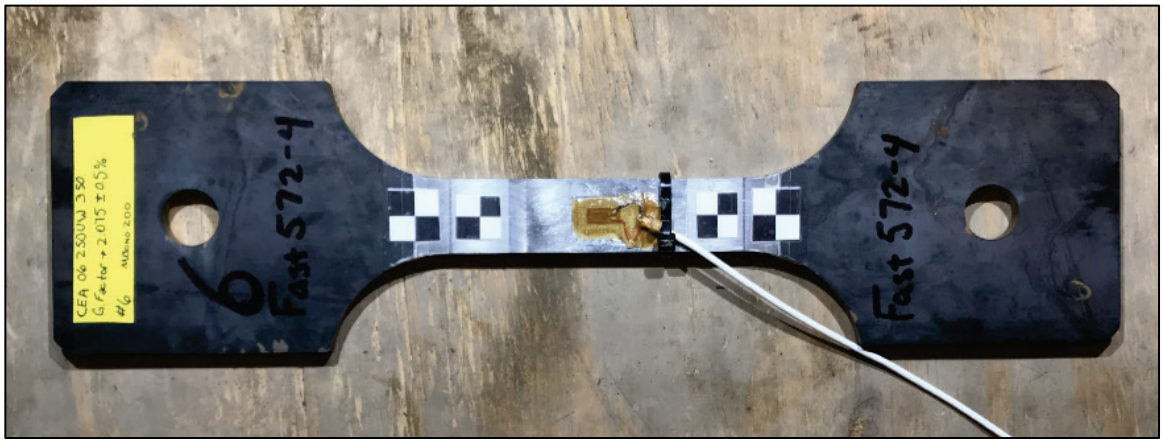

Figure 10. An A572 specimen with machined gauge region to allow application of strain gauge.

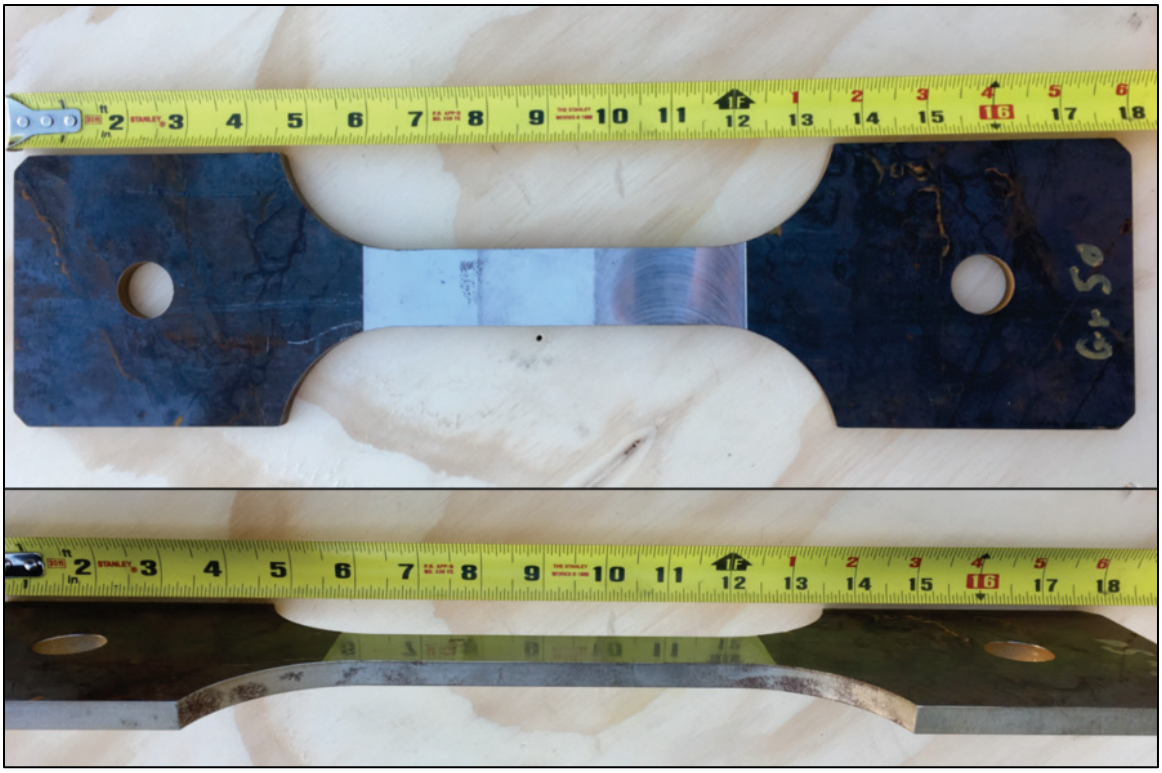

2.5.2 Load

Load was measured using two load cells in series with the 200-kip loader ram. The load cells were made from AISI 4130 quenched and tempered steel with a minimum yield strength of 100 ksi. The bridge network used on the load consisted of eight strain gauges installed in pairs on the quarter points, midway in the necked-down portion of the load cell (Figure 11 and Figure 12). One gauge measured axial strain, and the other measured Poisson's effect. The bridge was wired in such a way as to electrically subtract any radial bending. The output sensitivity transfer function is as follows:

$$\frac{E_0}{E_{in}} = eG(1-\nu)/(2+eG(1-\nu)) \,, \tag{2}$$

where

E_o = output signal (V),
E_{in} = input excitation (V),
G = gauge factor ($\Delta R/Re$),
e = axial engineering strain (in./in.), and
ν = Poisson's ratio.

Figure 11. Wheatstone bridge configuration used for 200-kip load cells.

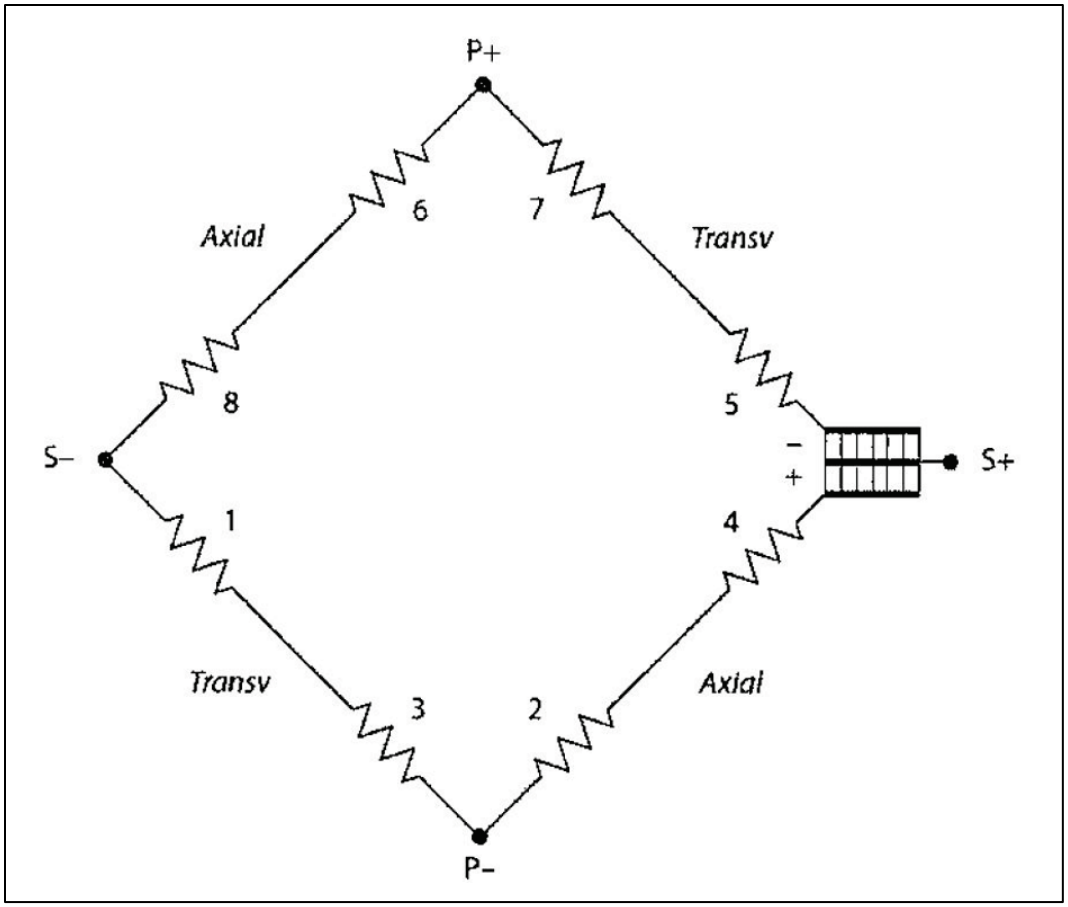

Figure 12. Strain-gauge circuitry configuration for 200-kip load cells.

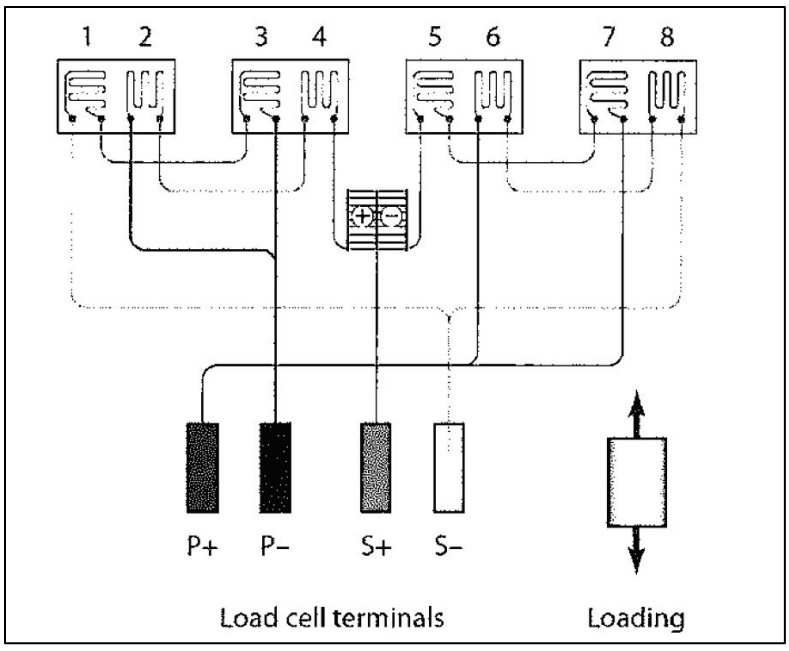

Calibration of the load cells was conducted by placing both in series with a precalibrated, manufactured load cell as shown in Figure 13. The load cells were statically calibrated to a maximum load of 200 kip.

Figure 13. Load cell before instrumentation (*left*) and load cell calibration configuration (*right*).

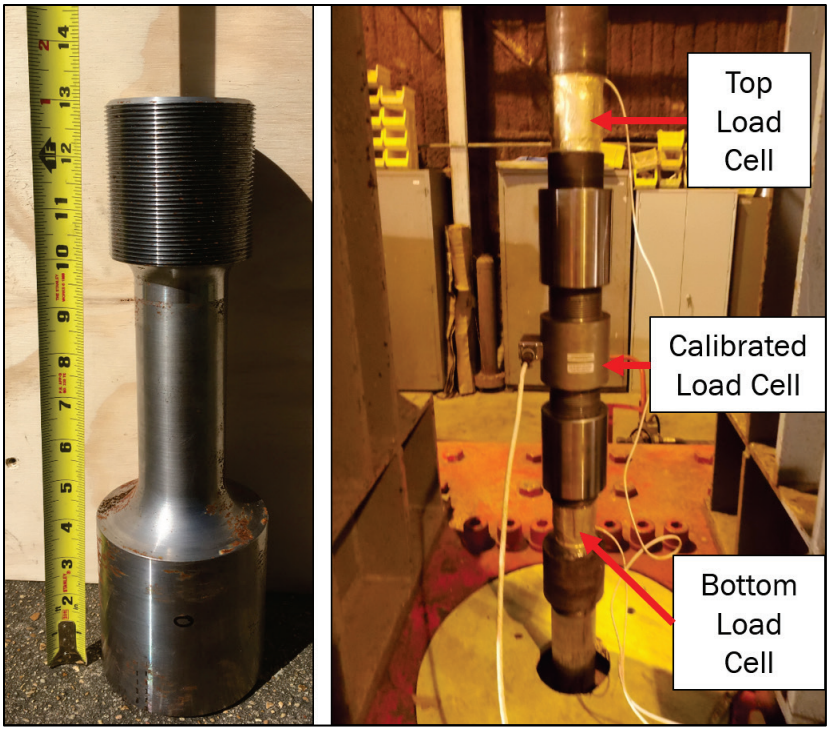

2.5.3 Acceleration

Two accelerometers were used to record acceleration during the higher-rate experiments (5E-2 s^{-1} and higher). The data recorded from these devices allowed inertial load effects to be determined and removed from the load versus time history (Section 2.6.1). Special care was taken to choose accelerometers rated to withstand the large magnitude accelerations that occurred after rupture of the specimen but not so high as to lose accuracy and resolution of the data during the initial loading (Table 5). For example, the accelerations after fracture during the DR4 experiments reached values as high as 15,000 g, but the loading accelerations required for inertial load correction typically measured less than 2,000 g. The accelerometers were mounted in an orientation that measured positive acceleration in the upward direction (Figure 14).

Table 5. Accelerometer information for dynamic tensile tests.

Strain Rate	Accelerometer Model	Maximum Rated Acceleration
SR: 2E-5 s^{-1}	—	—
DR1: 2E-3 s^{-1}	—	—
DR2: 5E-2 s^{-1}	Meggit 7280A-6k	6,000 g
DR3: 2E-1 s^{-1}	Meggit 7280A-20k	20,000 g
DR4: 2E0 s^{-1}	Meggit 7280A-20k	20,000 g

Figure 14. Accelerometer mounted onto the top specimen grip.

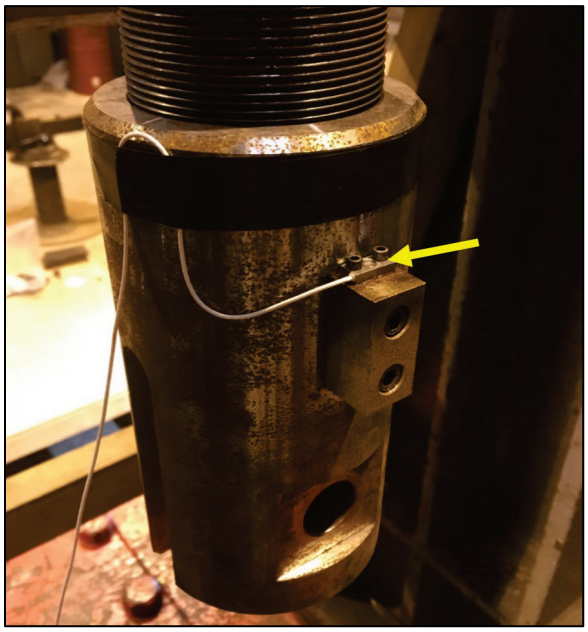

2.6 Load Analysis and Data Reduction

2.6.1 Inertial Force Correction

Newton's second law explains that when force is applied to objects with mass, inertial forces develop to resist the impending motion. If the objects have a large mass or if the accelerations are high, these inertial forces become quite significant. When the tension ram of the testing machine began to first apply rapid load onto the specimen through the lower grip, the mass of the grip and specimen resisted the downward acceleration. Increased load had to be applied to overcome this inertial resistance to begin pulling the lower grip and half of the specimen downward to apply tension within the gauge region of the specimen. The lower load cell would record both the applied load to the specimen and the inertial load. Inertial force was removed from the bottom load cell record to form a corrected load applied to the specimen. Contrarily, the inertial force was added to the top load cell record to form the corrected load on the specimen. An uncoupled (mass)

spring-mass model was used to develop the required load correction equations (Figure 15). Equilibrium equations (Equations 3–5) were developed to solve for the corrected load applied to the specimen.

Figure 15. Diagram of the uncoupled spring-mass model used for load correction.

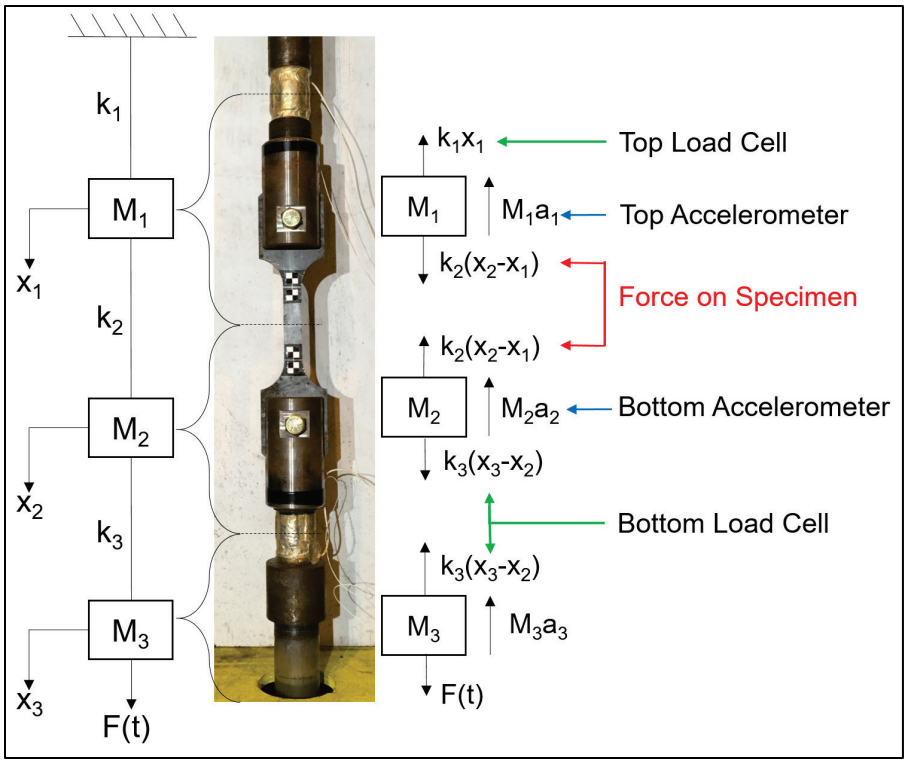

$$k_2(x_2 - x_1) = M_1 a_1 + k_1 x_1, \tag{3}$$

$$k_3(x_3 - x_2) = M_2 a_2 + k_2(x_2 - x_1), \tag{4}$$

$$F(t) = M_3 a_3 + k_3(x_3 - x_2). \tag{5}$$

Equation (3) represents the corrected load on the specimen using the top load cell and acceleration data. Equation (4) was solved to determine the corrected load using the bottom load cell and acceleration data (Equation 6).

$$k_2(x_2 - x_1) = k_3(x_3 - x_2) - M_2 a_2 \tag{6}$$

Since the accelerometers were mounted in an orientation that recorded positive acceleration in the upward direction, the acceleration in Equation (3) and Equation (6) were corrected by switching the signs of a_1 and a_2 to form Equation (7) and Equation (8), respectively. Substitution allowed for Equation (9) to be derived, which states that the corrected load using the top data records (load and acceleration) should theoretically be equal to the corrected load using the bottom

data records. For Static Rate (SR) and DR1, the loading rate produced accelerations of insignificant magnitudes and were therefore neglected.

$$k_2(x_2 - x_1) = k_1 x_1 - M_1 a_1, \tag{7}$$

$$k_2(x_2 - x_1) = k_3(x_3 - x_2) + M_2 a_2, \tag{8}$$

$$k_1 x_1 - M_1 a_1 = k_3(x_3 - x_2) + M_2 a_2, \tag{9}$$

where

$F(t)$ = Applied force as function of time (lbf),
M_1 = Mass of top specimen grip and half of the test specimen (lbm),
M_2 = Mass of bottom specimen grip and half of test specimen (lbm),
M_3 = Mass of tension ram and piston (lbm),
k_1 = Spring constant of upper reaction member (lbf/in.),
k_2 = Spring constant of test specimen (lbf/in.),
k_3 = Spring constant of tension ram and piston (lbf/in.),
a_1 = Acceleration of M_1 (g),
a_2 = Acceleration of M_2 (g),
a_3 = Acceleration of M_3 (g),
x_1 = Displacement of M_1 (in.),
x_2 = Displacement of M_2 (in.), and
x_3 = Displacement of M_3 (in.).

Figure 16 through Figure 18 show an example of inertial force correction for both the top and bottom load cell data for the highest strain rate experiments (DR4). The bottom load cell, attached to the tension ram of the loader, experiences up to four times the acceleration of the upper; therefore, the inertial load correction is much more significant on the bottom load cell data. The average of the corrected top and corrected bottom load versus time histories are used for the calculation of stress.

Figure 16. Correction of top load cell data using top accelerometer.

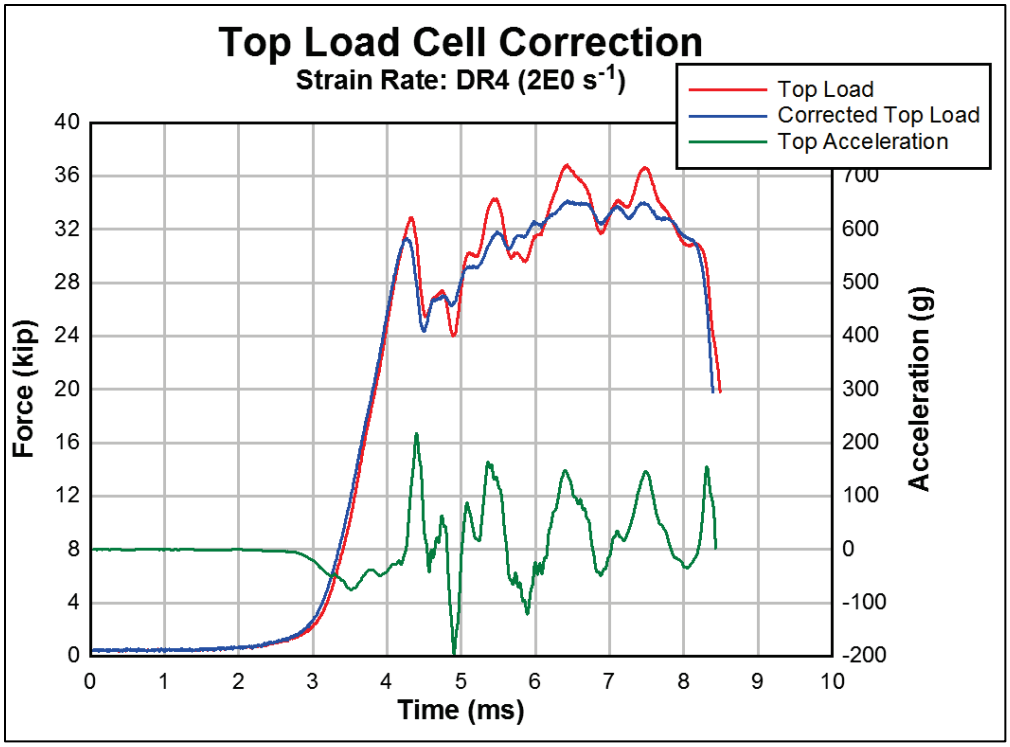

Figure 17. Correction of bottom load cell data using bottom acceleration.

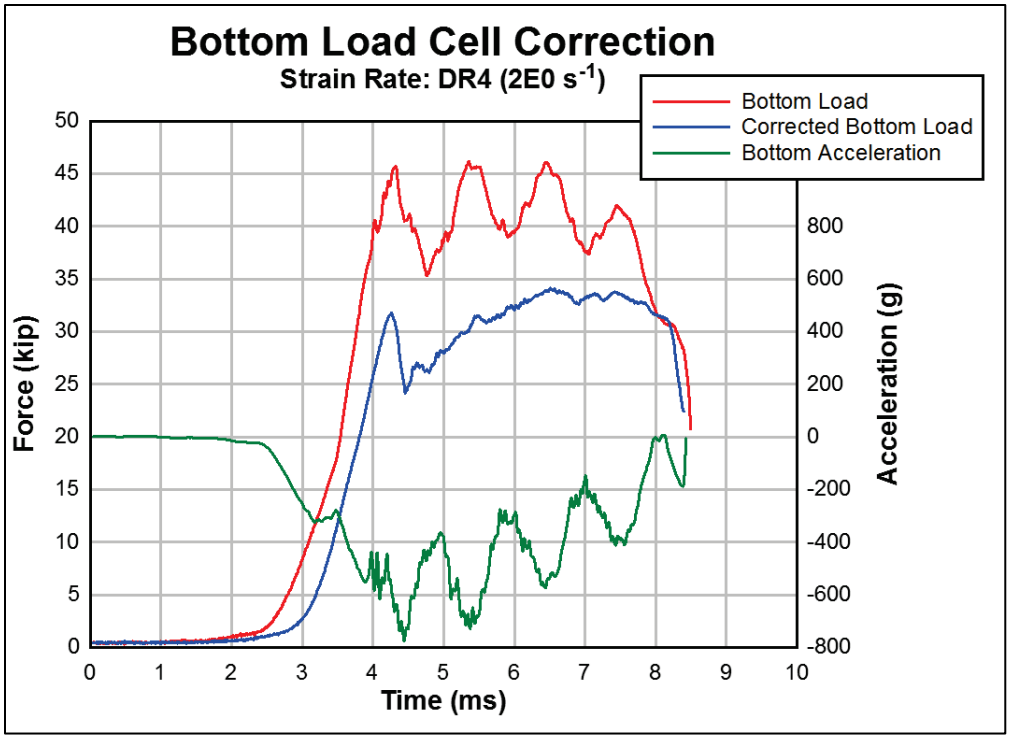

Figure 18. Load correction of both top and bottom load cell data.

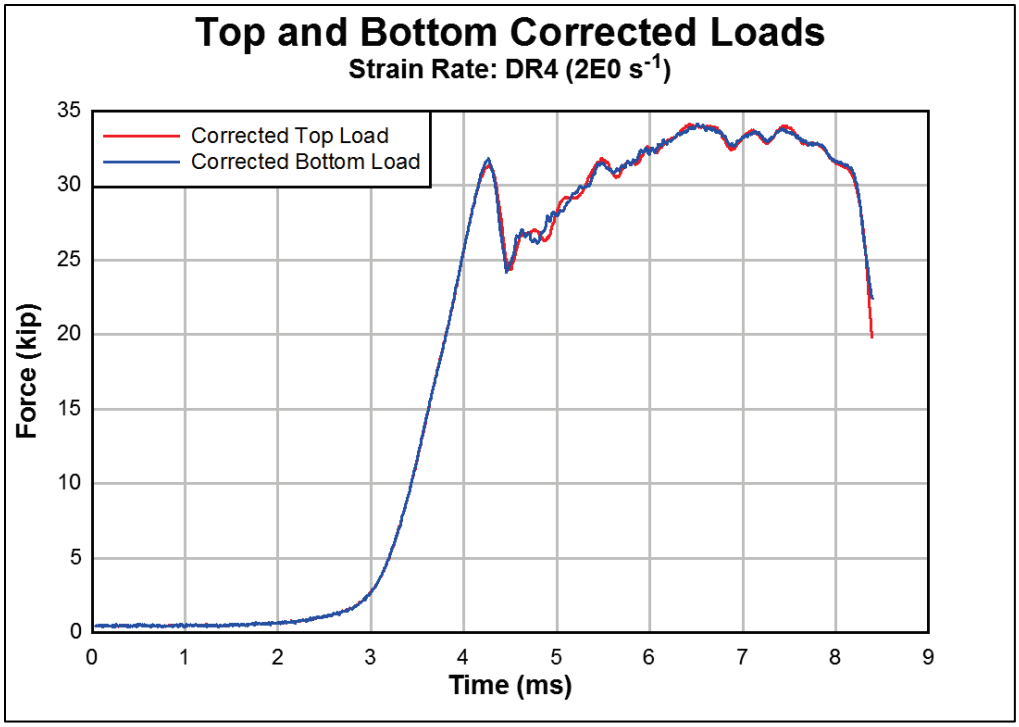

2.6.2 Stress-Strain Diagrams

The average corrected load was divided by the original cross section of the test specimen to calculate engineering stress. Strain was determined from the elongation data as described in Section 2.5.1. Stress was plotted as a function of strain to develop the stress-strain diagram for each test. The upper yield strength was determined as the stress corresponding to the maximum force at the onset of discontinuous yielding as prescribed in E8-7.7.3 (ASTM 2016). The lower yield strength was determined using the minimum stress observed during discontinuous yielding as prescribed in E8-7.7.3. Ultimate tensile strength was calculated by dividing the maximum force applied to the specimen during the test by the original cross-sectional area of the specimen (E8-7.10). The strength properties were rounded to the nearest 0.1 ksi.

2.6.3 Dynamic Increase Factors

The ratio of dynamic-to-static yield stress is defined as the DIF at a specified strain rate. The tested A572 and A992 specimens exhibited discontinuous yielding. ASTM classifies minimum yield stress values for these steels based on the yield point; therefore, the yield point (upper yield strength) was used in determining DIF_y using Equation (10). Figure 19 indicates the values used in the equations below on a static and dynamic stress-strain diagrams.

$$DIF_y = \frac{f_{dy}}{f_y}, \tag{10}$$

$$DIF_u = \frac{f_{du}}{f_u}, \tag{11}$$

where

DIF_y = dynamic increase factor for yield stress for a particular strain-rate,
DIF_u = dynamic increase factor for ultimate tensile stress for a particular strain rate,
f_{dy} = dynamic yield stress at a particular strain rate above static (ksi),
f_{du} = dynamic ultimate tensile stress at a particular strain rate above static (ksi),
f_y = average yield stress measured during static testing (ksi), and
f_u = average ultimate tensile stress measured during static testing (ksi).

Figure 19. Stress-strain diagram showing terms of Equations (10)–(11).

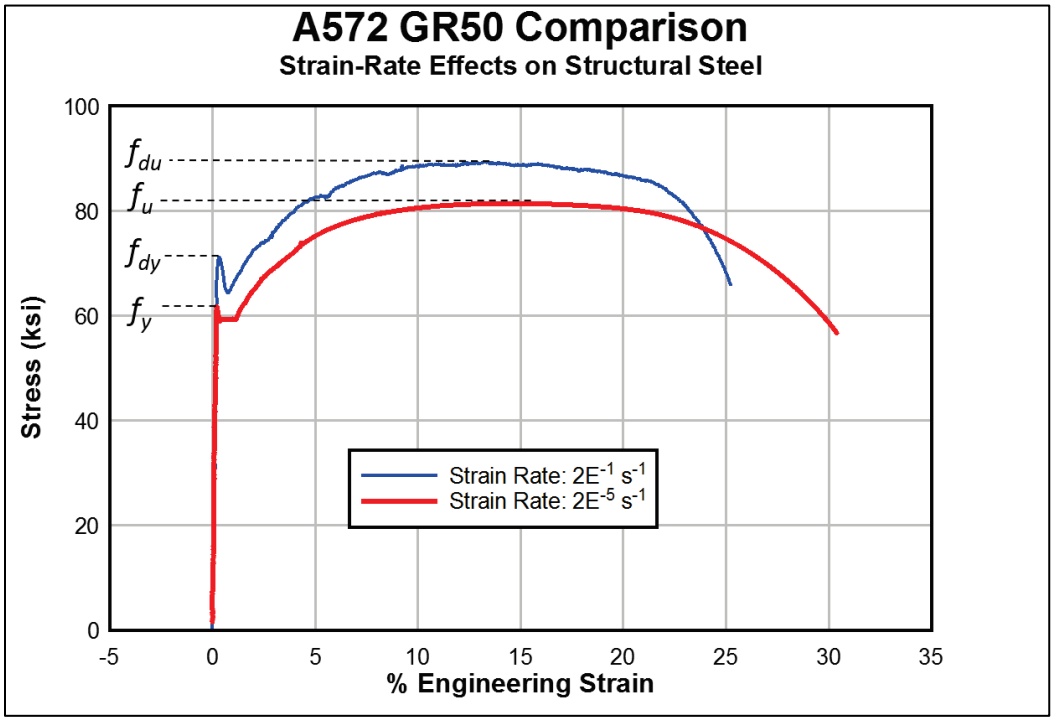

3 Results

The digital records for each of the experiments were analyzed using the procedures described in Section 2. From these data, Table 6 through Table 8 were produced to include upper and lower yield strength, ultimate tensile strength, percent elongation after failure, percent reduction of area, and average strain rate. Slope was calculated from the strain-time data in the elastic deformation region to determine the average strain rate. The upper yield strength, lower yield strength, and ultimate tensile strength were determined as mentioned in Section 2.6.2. Elongation (after fracture) and reduction of area were measured according to E8 specifications and rounded to the nearest 0.1%. Stress-strain diagrams for the A572 experiments are shown in Appendix A, and the A992 diagrams are shown in Appendix B.

Dynamic experiments DR2-572-1 and DR2-572-2 did not fracture the specimen; however, after the stress-strain data were analyzed, it was found that loading past ultimate stress had been obtained. Dynamic strengths of these specimens were included in the DIF results. Caution should be taken when analyzing elongation and reduction values from specimens that fractured on gauge marks as the values may be uncharacteristically low and unrepresentative of the material.

Baseline yield (f_y) and ultimate (f_u) strengths were determined by averaging values obtained from static testing of each material. Yield and ultimate DIF for each test were then determined with Equation (10) and Equation (11) and listed in Table 9 through Table 11. Red text indicates data captured form specimen that fractured along gauge marks.

The yield and ultimate DIF values for each experiment were plotted in DPlot Version 2.3.5.4 software (Hydesoft Computing, LLC 2018). Analysis of the data lead to formulation of a bilinear least-squares regression curve fit on a log-linear DIF versus strain-rate plot. The individual values for each experiment and the developed design curves are shown in Figure 20 (DIF_y) and Figure 21 (DIF_u).

Table 6. Baseline material strengths from static tension tests.

Experiment #	Average Strain Rate (s^{-1})	Upper Yield Strength (ksi)	Lower Yield Strength (ksi)	Ultimate Tensile Strength (ksi)	Elongation	Reduction of Area
SR-572-1	1.88E-05	61.7	58.9	81.4	30.5%	65.4%
SR-572-2	2.01E-05	61.8	58.6	79.7	31.0%	67.8%
SR-572-3	2.21E-05	61.7	59.0	81.8	29.2%	63.2%
SR-572-4	1.86E-05	61.6	58.3	82.0	27.1%	65.1%
SR-572-5	2.21E-05	61.2	58.6	81.8	26.2%	63.9%
SR-572-6	2.29E-05	61.1	58.4	81.8	26.5%	65.1%
SR-572-7	2.57E-05	61.5	59.2	81.6	25.7%	64.5%
SR-572-8	2.08E-05	61.2	58.5	84.9	26.0%	65.6%
Static Average (A572)	**2.14E-05**	**61.5**	**58.7**	**81.9**	**27.8%**	**65.1%**
SR-992-1	1.89E-05	54.6	51.7	69.2	34.0%	69.2%
SR-992-2	1.98E-05	52.4	50.8	68.0	32.0%	72.1%
SR-992-3	2.10E-05	54.6	51.1	69.1	32.9%	67.1%
SR-992-4	1.75E-05	54.4	51.9	69.3	32.7%	71.7%
SR-992-5	2.31E-05	54.1	51.2	69.2	31.5%	70.0%
SR-992-6	3.22E-05	54.8	50.9	69.5	32.0%	67.4%
SR-992-7	2.30E-05	54.4	51.2	69.3	31.0%	69.5%
SR-992-8	2.08E-05	57.6	52.2	69.5	30.4%	68.1%
SR-992-9	2.28E-05	53.1	50.4	68.5	34.0%	71.3%
SR-992-10	2.46E-05	52.6	50.0	68.5	33.5%	69.6%
SR-992-11	2.37E-05	54.8	51.0	68.3	32.7%	69.1%
SR-992-12	2.41E-05	52.4	50.6	68.7	32.3%	67.5%
SR-992-13	3.16E-05	52.3	50.5	68.6	32.5%	67.1%
SR-992-14	3.54E-05	53.2	51.0	68.5	33.1%	67.1%
Static Average (A992)	**2.42E-05**	**54.0**	**51.0**	**68.9**	**32.0%**	**69.1%**

Table 7. Dynamic material strengths from dynamic testing A572.

Experiment #	Average Strain Rate (s^{-})	Upper Yield Strength (ksi)	Lower Yield Strength (ksi)	Ultimate Tensile Strength (ksi)	Elongation	Reduction of Area
DR1-572-1	2.67E-03	66.5	62.7	85.6	27.1%	58.0%
DR1-572-2	2.61E-03	65.1	61.2	85.8	26.2%	51.5%
DR1-572-3	2.67E-03	67.7	61.8	85.0	29.3%	53.2%
DR1-572-4	2.72E-03	64.2	61.9	85.1	26.4%	49.8%
DR1-572-5	2.86E-03	65.2	61.5	85.7	26.1%	56.1%
DR2-572-1*	4.64E-02	70.0	64.5	86.7	—	—
DR2-572-2*	4.50E-02	70.6	64.8	87.5	—	—
DR2-572-3	5.16E-02	70.3	64.9	87.6	27.6%	55.7%
DR2-572-4**	5.64E-02	69.5	65.4	88.1	24.0%	40.5%
DR2-572-5	5.38E-02	69.6	64.1	87.9	26.3%	56.8%
DR2-572-6	5.88E-02	71.7	65.7	87.4	26.6%	51.9%
DR2-572-7	6.24E-02	69.5	64.8	87.7	27.3%	53.3%
DR2-572-8	5.34E-02	67.5	65.0	87.4	26.6%	52.9%
DR3-572-1	1.96E-01	69.8	65.4	89.2	28.4%	57.4%
DR3-572-2	2.02E-01	71.2	64.3	89.4	29.7%	55.6%
DR3-572-3	2.26E-01	72.7	67.8	90.6	27.4%	56.3%
DR3-572-4	2.40E-01	71.9	66.9	90.0	26.8%	59.6%
DR3-572-5	2.42E-01	72.8	67.6	90.0	27.1%	55.8%
DR4-572-1	2.60E+00	83.3	67.4	97.5	36.3%	62.9%
DR4-572-2	2.91E+00	83.5	69.5	98.0	32.0%	62.3%
DR4-572-3	2.41E+00	84.7	69.0	99.0	36.1%	65.1%
DR4-572-4**	2.61E+00	82.8	67.4	98.3	33.1%	51.0%
DR4-572-5	2.67E+00	84.3	68.6	96.4	32.4%	62.2%
DR4-572-6	2.46E+00	82.5	68.2	98.4	34.1%	63.7%

* Specimen loaded past ultimate tensile strength but not until fracture.

** Specimen fractured on gauge mark.

Table 8. Dynamic material strengths from dynamic testing A992.

Experiment #	Average Strain Rate (s^{-1})	Upper Yield Strength (ksi)	Lower Yield Strength (ksi)	Ultimate Tensile Strength (ksi)	Elongation	Reduction of Area
DR1-992-1	2.06E-03	60.6	53.5	71.3	27.6%	56%
DR1-992-2	2.45E-03	61.7	55.6	72.4	29.4%	57%
DR1-992-3	2.07E-03	60.8	54.2	72.0	30.0%	56%
DR1-992-4	2.00E-03	58.9	52.3	71.3	27.8%	54%
DR1-992-5	2.01E-03	59.4	54.1	71.2	28.4%	58%
DR2-992-1	4.18E-02	64.5	55.8	74.0	27.2%	55%
DR2-992-2	3.75E-02	63.6	57.8	74.2	32.8%	62%
DR2-992-3	4.47E-02	65.7	58.1	74.2	32.1%	58%
DR2-992-4	4.25E-02	62.9	56.9	73.6	31.9%	63%
DR2-992-5	4.95E-02	65.6	55.5	74.0	29.3%	58%
DR2-992-6**	4.72E-02	65.0	56.3	73.9	27.4%	39%
DR2-992-7	4.39E-02	62.9	57.5	73.5	29.5%	59%
DR3-992-1	2.72E-01	66.5	60.3	76.0	32.7%	60%
DR3-992-2	2.77E-01	68.3	61.3	76.1	33.7%	65%
DR3-992-3	2.45E-01	67.9	59.7	76.4	31.7%	59%
DR3-992-4	2.46E-01	68.0	60.0	76.3	32.0%	64%
DR3-992-5	2.75E-01	67.4	61.0	76.0	31.8%	64%
DR4-992-1	1.86E+00	78.9	64.0	82.9	40.8%	62%
DR4-992-2	1.75E+00	78.3	61.0	83.7	38.0%	64%
DR4-992-3	1.98E+00	79.0	59.8	83.7	42.2%	64%
DR4-992-4**	2.63E+00	78.4	59.9	84.0	36.6%	52%
DR4-992-5	1.97E+00	77.4	57.4	83.5	38.8%	68%
DR4-992-6**	1.97E+00	78.7	61.2	83.5	38.7%	62%
DR4-992-7	2.34E+00	76.2	59.9	82.7	43.6%	70%
DR4-992-8**	2.61E+00	79.4	61.0	83.2	35.1%	51%
DR4-992-9	2.41E+00	77.3	57.7	83.4	36.4%	62%
DR4-992-10**	2.17E+00	77.3	56.8	83.4	36.8%	46%

** Specimen fractured on gauge mark.

Table 9. Static DIF values with respect to the average static strengths.

Experiment #	Average Strain Rate (s^{-1})	DIF_y	DIF_u
SR-572-1	1.88E-05	1.004	0.994
SR-572-2	2.01E-05	1.005	0.973
SR-572-3	2.21E-05	1.004	0.999
SR-572-4	1.86E-05	1.002	1.002
SR-572-5	2.21E-05	0.996	0.999
SR-572-6	2.29E-05	0.994	0.999
SR-572-7	2.57E-05	1.000	0.997
SR-572-8	2.08E-05	0.996	1.037
Static Average (A572)	**2.14E-05**	**1**	**1**
SR-992-1	1.89E-05	1.012	1.005
SR-992-2	1.98E-05	0.971	0.987
SR-992-3	2.10E-05	1.012	1.003
SR-992-4	1.75E-05	1.008	1.006
SR-992-5	2.31E-05	1.003	1.005
SR-992-6	3.22E-05	1.016	1.009
SR-992-7	2.30E-05	1.008	1.006
SR-992-8	2.08E-05	1.068	1.009
SR-992-9	2.28E-05	0.984	0.995
SR-992-10	2.46E-05	0.975	0.995
SR-992-11	2.37E-05	1.016	0.992
SR-992-12	2.41E-05	0.971	0.998
SR-992-13	3.16E-05	0.969	0.996
SR-992-14	3.54E-05	0.986	0.995
Static Average (A992)	**2.42E-05**	**1**	**1**

Table 10. DIF experimental values for A572.

Experiment #	Average Strain Rate (s^{-1})	DIF_y	DIF_u
DR1-572-1	2.67E-03	1.082	1.045
DR1-572-2	2.61E-03	1.059	1.048
DR1-572-3	2.67E-03	1.101	1.038
DR1-572-4	2.72E-03	1.044	1.039
DR1-572-5	2.86E-03	1.061	1.047
DR2-572-1*	4.64E-02	1.139	1.059
DR2-572-2*	4.50E-02	1.148	1.069
DR2-572-3	5.16E-02	1.144	1.070
DR2-572-4**	5.64E-02	1.131	1.076
DR2-572-5	5.38E-02	1.132	1.074
DR2-572-6	5.88E-02	1.166	1.067
DR2-572-7	6.24E-02	1.131	1.071
DR2-572-8	5.34E-02	1.098	1.067
DR3-572-1	1.96E-01	1.135	1.089
DR3-572-2	2.02E-01	1.158	1.092
DR3-572-3	2.26E-01	1.183	1.107
DR3-572-4	2.40E-01	1.170	1.099
DR3-572-5	2.42E-01	1.184	1.099
DR4-572-1	2.60E+00	1.355	1.191
DR4-572-2	2.91E+00	1.358	1.197
DR4-572-3	2.41E+00	1.378	1.209
DR4-572-4	2.61E+00	1.347	1.201
DR4-572-5	2.67E+00	1.371	1.177
DR4-572-6	2.46E+00	1.342	1.202

* Specimen loaded past ultimate tensile strength but not until fracture.

** Specimen fractured on gauge mark.

Table 11. DIF experimental values for A992.

Experiment #	Average Strain Rate (s^{-1})	DIF_y	DIF_u
DR1-992-1	2.06E-03	1.123	1.035
DR1-992-2	2.45E-03	1.144	1.051
DR1-992-3	2.07E-03	1.127	1.045
DR1-992-4	2.00E-03	1.092	1.035
DR1-992-5	2.01E-03	1.101	1.034
DR2-992-1	4.18E-02	1.196	1.074
DR2-992-2	3.75E-02	1.179	1.077
DR2-992-3	4.47E-02	1.218	1.077
DR2-992-4	4.25E-02	1.166	1.069
DR2-992-5	4.95E-02	1.216	1.074
DR2-992-6**	4.72E-02	1.205	1.073
DR2-992-7	4.39E-02	1.166	1.067
DR3-992-1	2.72E-01	1.233	1.104
DR3-992-2	2.77E-01	1.266	1.105
DR3-992-3	2.45E-01	1.259	1.109
DR3-992-4	2.46E-01	1.260	1.108
DR3-992-5	2.75E-01	1.249	1.104
DR4-992-1	1.86E+00	1.462	1.204
DR4-992-2	1.75E+00	1.451	1.215
DR4-992-3	1.98E+00	1.464	1.215
DR4-992-4**	2.63E+00	1.453	1.220
DR4-992-5	1.97E+00	1.435	1.212
DR4-992-6**	1.97E+00	1.459	1.212
DR4-992-7	2.34E+00	1.412	1.201
DR4-992-8**	2.61E+00	1.472	1.208
DR4-992-9	2.41E+00	1.433	1.211
DR4-992-10**	2.17E+00	1.433	1.211

** Specimen fractured on gauge mark.

Figure 20. Experimental yield strength DIF values for A572 and A992.

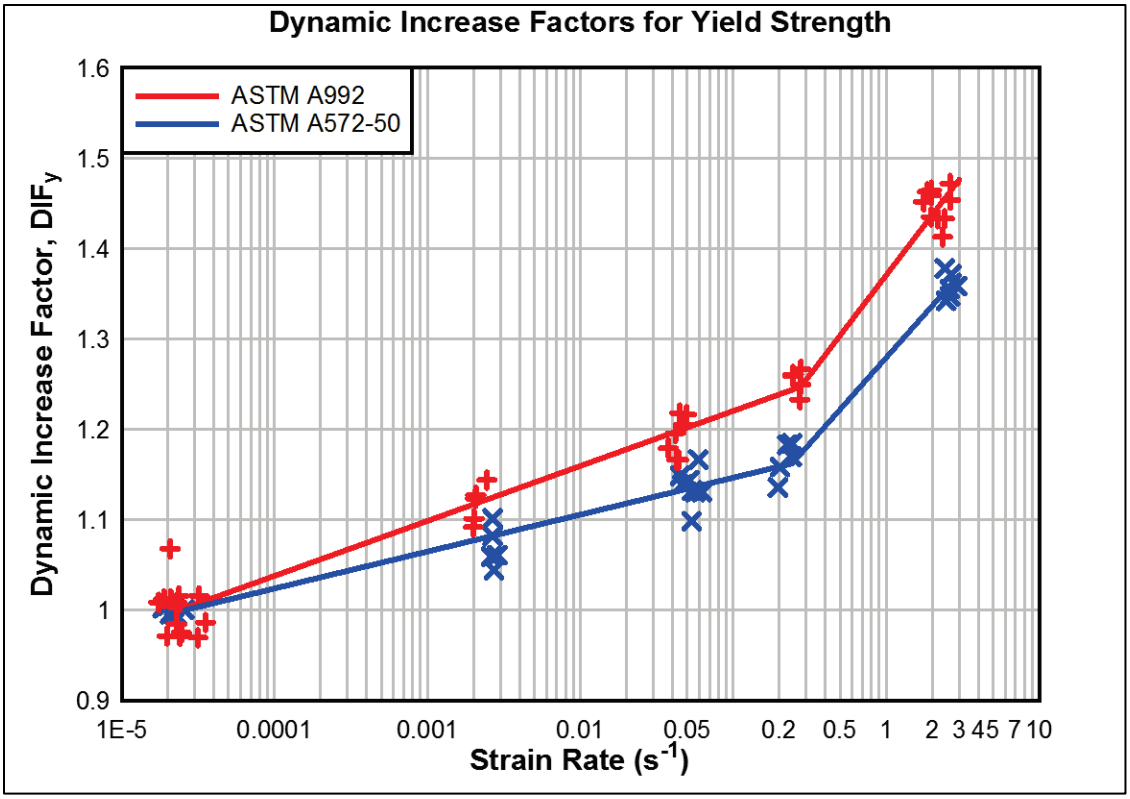

Figure 21. Experimental ultimate tensile strength DIF values for A572 and A992.

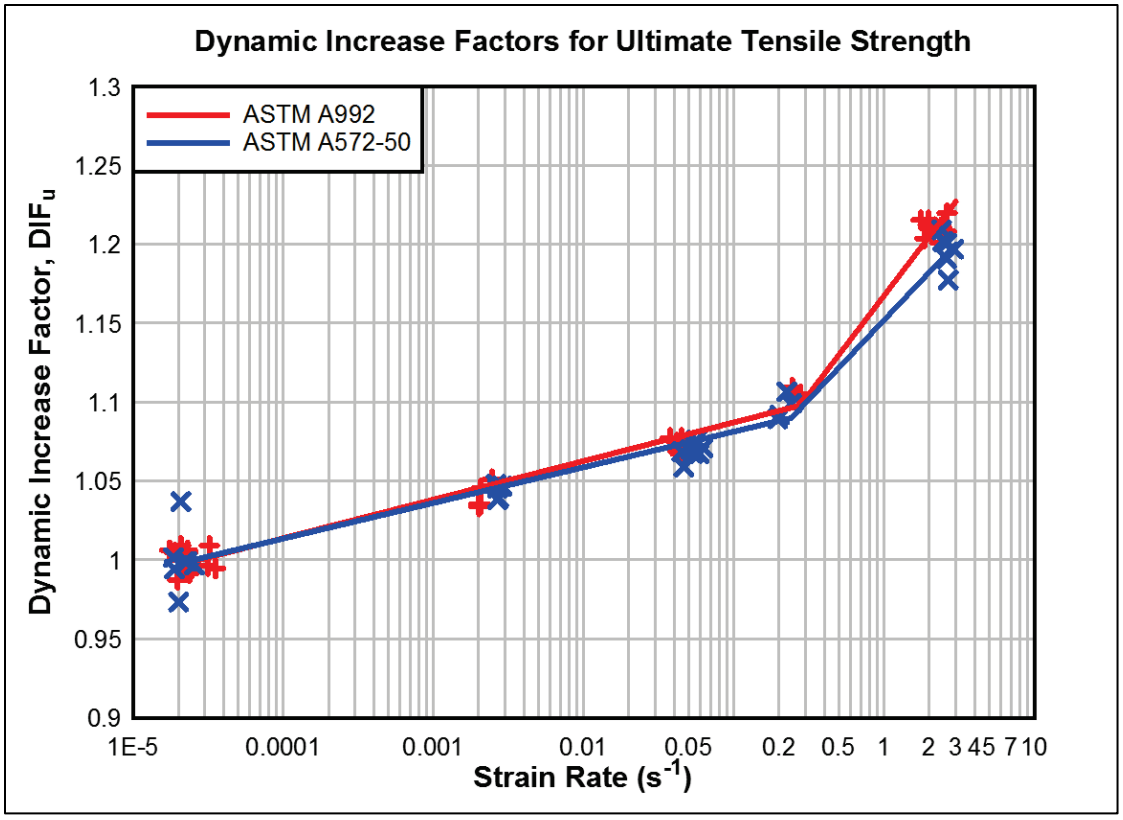

4 Discussion of Results

Accelerometers, load cells, strain gauges, and the HS camera performed properly throughout all reported experiments. Advances in measurement instrumentation and techniques have allowed for greater resolution in the capturing of material strength properties of these steels at high strain rates when compared to many of the reports listed in the references section. The load cells were calibrated at the beginning of this experimental series. Recalibration was performed at the midpoint and conclusion of the experiments. No change was observed in signal sensitivity, which indicated that the load cells had maintained calibration throughout all experiments.

The DR4 stress-strain curves for both steels exhibited oscillations after yielding even with inertial load correction, which can be partially attributed to stress wave propagation through the loading ram and specimen after yield. Wave propagation speed, which is neglected in these experiments, starts to play an increased role in recording material response as strain rate increases. There is a slight difference in time between the instantaneous response of the material in the gauge region of the specimen and the measured response captured by the load cells and accelerometers located a finite distance away from the gauge region. The small difference in time contributes to the unsmooth stress-strain curves for the DR4 experiments. The impacts of this phenomena on upper yield strength and ultimate tensile strength at DR4 are negligible; however, the lower yield strength and yield plateau regions of the stress-strain diagrams can be greatly masked by this effect. If DIF data were desired for strain rates greater than tested during this research (>10 s^{-1}), stress wave propagation factors would likely have a much greater influence on the material response and would have to be factored into the measured material response.

The influence of load correction on the stress-strain curves is shown in Figure 22. It is clear from this figure that DIF values will be substantially larger if inertial forces are neglected at higher strain rates. Experimental statistics for the A572 and A992 tests are in Tables 12 and 13, respectively.

Figure 22. Comparison between stress-strain curves with and without correcting for inertial forces.

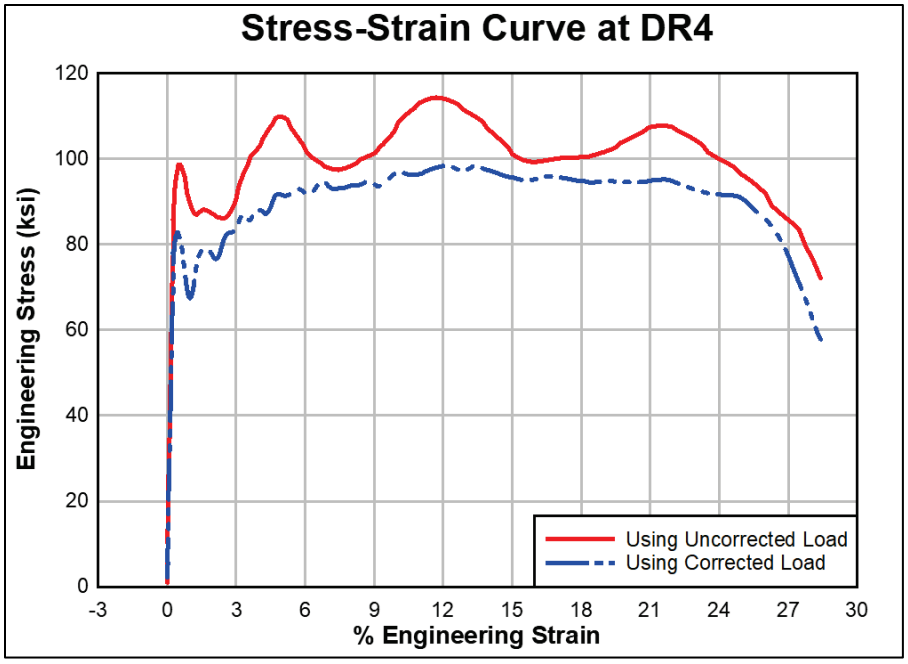

The strain rate corresponding to each targeted rate could not be kept constant between tests; however, the dynamic yield and ultimate tensile strength values were obtained without a substantial amount of distribution when grouped by target strain rate. The highest distribution was evident with the lower yield stress values for the A992 steel at DR4 because of the dynamic phenomena previously discussed.

Table 12. Experimental statistics for A572 tests at each group of strain rates.

Target Strain Rate (s^{-1})	Standard Deviation Strain Rate (s^{-1})	Standard Deviation Upper Yield Strength (ksi)	Standard Deviation Lower Yield Strength (ksi)	Standard Deviation Ultimate Tensile Strength (UTS) (ksi)
2.00E-05 (Static)	2.3E-06	0.27	0.31	1.43
2.00E-03 (DR1)	9.4E-05	1.37	0.56	0.36
5.00E-02 (DR2)	5.9E-03	1.20	0.50	0.42
2.00E-01 (DR3)	2.1E-02	1.24	1.50	0.55
2.00E+00 (DR4)	1.8E-01	0.85	0.85	0.90

Table 13. Experimental statistics for A992 tests at each group of strain rates.

Target Strain Rate (s^{-1})	Standard Deviation Strain rate (s^{-1})	Standard Deviation Upper Yield Strength (ksi)	Standard Deviation Lower Yield Strength (ksi)	Standard Deviation UTS (ksi)
2.00E-05 (Static)	5.3E-06	1.38	0.58	0.48
2.00E-03 (DR1)	1.9E-04	1.13	1.20	0.53
5.00E-02 (DR2)	3.9E-03	1.20	1.01	0.27
2.00E-01 (DR3)	1.6E-02	0.70	0.67	0.18
2.00E+00 (DR4)	3.1E-01	1.00	2.15	0.39

Caution should be taken when analyzing stress and strain at rupture for the DR4 experiments. Acceleration near impending failure increased dramatically, creating inertial forces that could not be accurately corrected. The inertial forces masked the rapid decrease in load that would typically indicate failure of the specimen on a load-versus-time plot. Strain at failure was also difficult to analyze from the strain-versus-time data because the strain rate was very high in the plastic region (1E3 s^{-1}). Determination of fracture was made with the HS camera footage. Each frame corresponded to a 0.07 ms increment in time, and early fracture initiation was sometimes difficult to identify; therefore, it is highly probable that the stress and strain *at fracture* are not represented accurately in the stress-strain plots for the DR4 experiments. Elongation *after* fracture data (Table 7 and Table 8) should be considered instead of elongation *at* fracture when considering the ductility properties of the steels at this strain rate.

Experimental data for both (the yield and ultimate DIF values) exhibited bilinear trends with a transition in slope between rates of 0.2 and 2 s^{-1}. Change in strain rate sensitivity, represented by the change in slope of the DIF curves, has been documented for many materials (Manjoine 1944; Flathau 1971; Soohoo et al. 1974; Hong and Kang 2016; Lindholm and Bessey 1969; Mocko and Kruszka 2013) and is associated with different regions of strain-rate sensitivity. Figure 23 depicts an example of yield-strength sensitivity regions with respect to strain rate and temperature for steels (Soohoo et al. 1974). Transition from one region of rate-sensitivity region to another is material specific and often difficult to quantify. Acquisition of additional DIF data between DR3, DR4, and beyond would provide information on the strain rate sensitivity in the transformation region of A572-50 and A992 steels.

Figure 23. General regions for yield strength sensitivity of steel to strain rate and temperature. (Image reproduced from Soohoo et al. 1974. Public domain.)

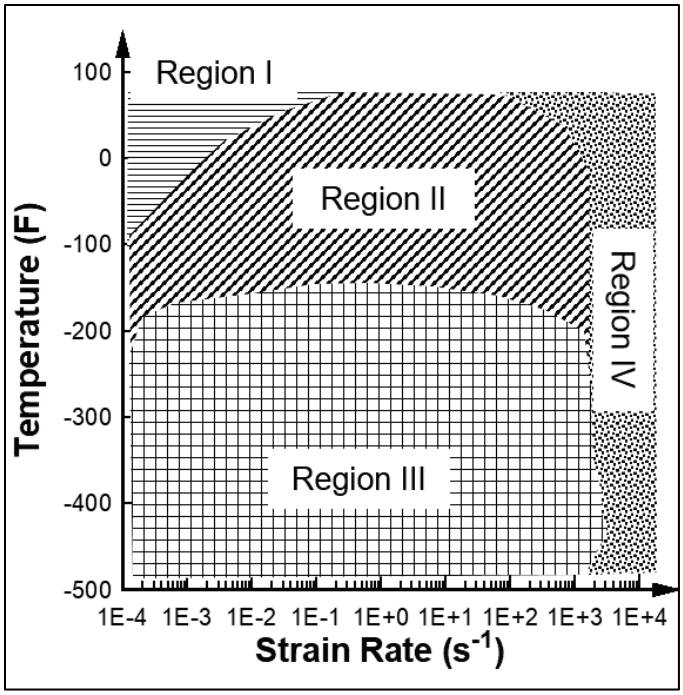

Extrapolation of the empirically derived DIF curves for either of these steels is *highly* discouraged. Review of previous research on dynamic material properties indicated that rate sensitivities could often drastically change with little increase or decrease in strain rate. Lindholm and Bessey (1969) made the following statement on the subject of extrapolation after conducting a large survey of strain rate and temperature effects on material properties of metals, with which the authors of this report strongly agree.

A final observation is that extrapolation of the available data beyond the range of strain rate or of temperature at which the tests were performed is not recommended. The detailed mechanisms controlling the plastic flow of metals are very complex and there is no assurance, and indeed little likelihood, that the same mechanisms are operative over the whole range of conditions encountered (Lindholm and Bessey 1969).

The static yield strength of the A572 (61.5 ksi) was substantially greater than that of the A992 (54 ksi), even though both steels are specified 50 ksi. The difference in static yield strength likely explains why the A992 DIF_y experimental values were higher, as previous research has shown an inverse relation between DIF_y and static yield strength (Malvar 1998; Hong et al. 2016). Malvar (1998) documented how the DIF_y values for reinforcing steel are highly related to static

yield strength values and established an empirical formula to approximate the DIF values of different grade reinforcing steel based on static yield stress values alone. The DIF_y results for the structural steels were compared to Malvar's approximation formula for reinforcing steel in Figure 24. Differences between the experimental results and Malvar's approximation equation can most likely be attributed to the difference in chemical composition between structural and reinforcing steels.

Figure 24. Comparison of experimental DIF_y data of structural steel and Malvar's approximation formula for reinforcing steel.

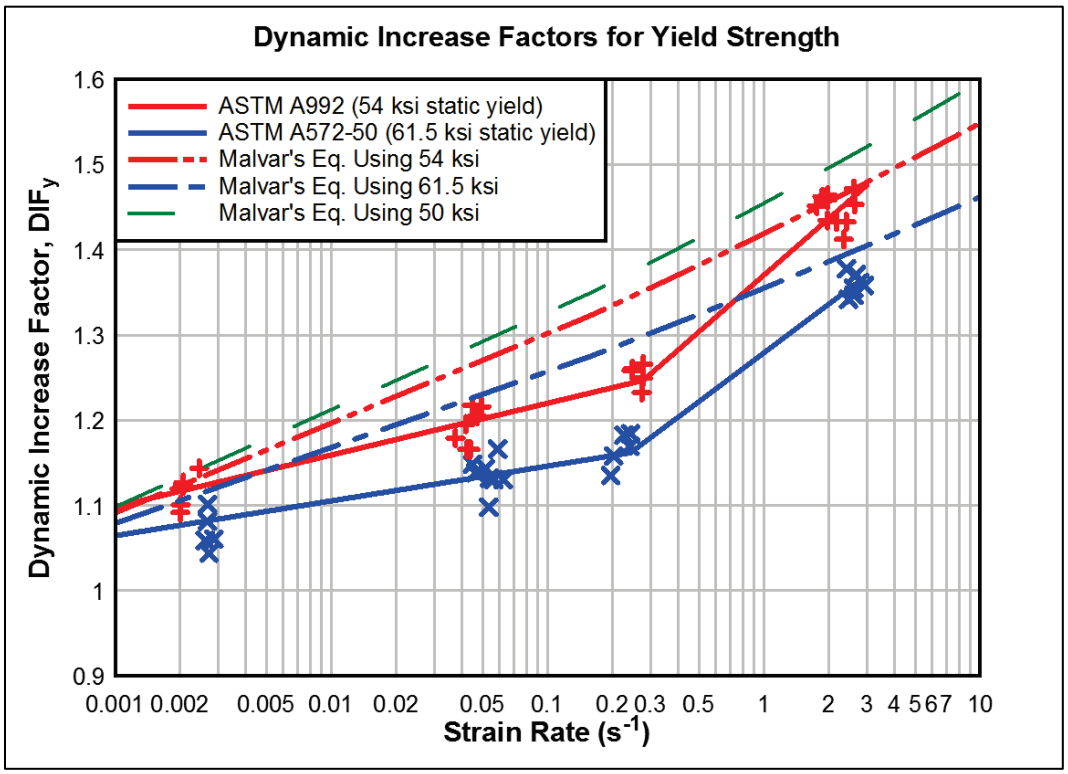

The DIF_y curves developed from the experiments were added to Figure 5-2 of the UFC and shown in Figure 25. It is uncertain how the A36 and A514 DIF_y curves were formulated, as the source of data for these steels has eluded the authors. It is logical that the DIF curves for A992 and A572 would lay between those of A36 and A514 because of the difference in static yield stress values. Without the report(s) that detail the A36 data, it is difficult to determine why the DIF_y values for A992 and A572 are above A36 for strain rates under 2E-2 s^{-1}.

Figure 25. Comparison of experimental results to Unified Facilities Criteria (UFC) values of A36 and A514.

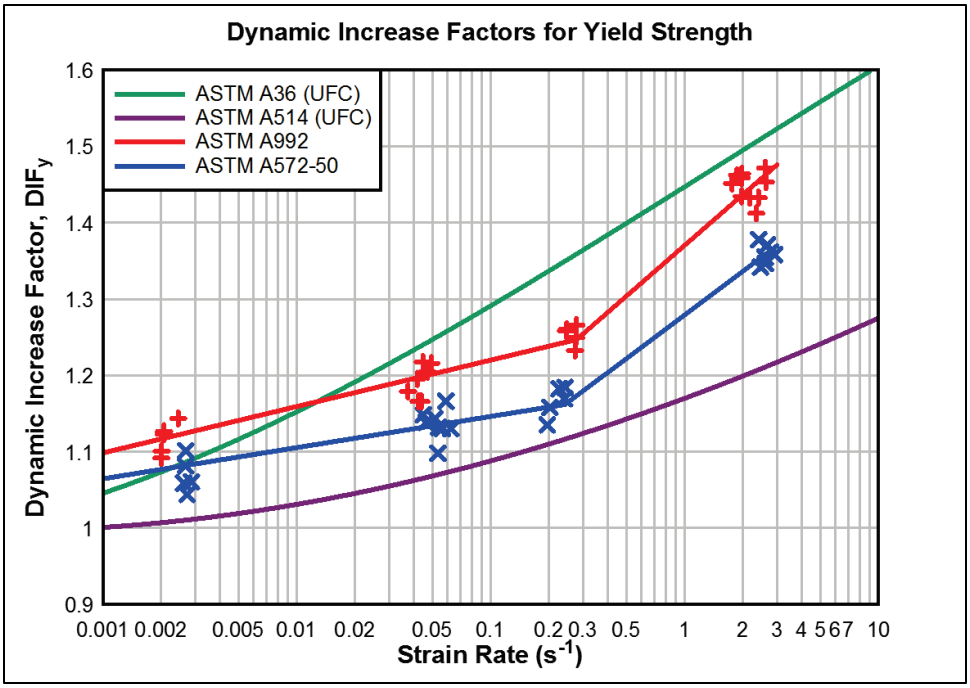

Figure 27 compares the A36 DIF_y values obtained by Cowell (1969) and the current UFC DIF_y values. It is unknown why Cowell used the lower yield strength values to calculate the DIF for yield in these steels; however, it is clear that the values obtained using Cowell's testing machine and instrumentation were much higher than would be expected. Further review of Cowell's reports and TR-331 (Cowell and Keeton 1962; Cowell 1963, 1969), which detailed the testing machine and data collected for those experiments, indicated that acceleration was not recorded during the experiments. There was also no mention of inertial load correction, which would require acceleration data. The lack of inertial load correction would generate errors in load (stress) values that increased with strain rate and is the most probable reason that Cowell's DIF_y values are larger than both the published values of the UFC for A36 and the experimental values of A572 from this research. A second look at Figure 22 indicates how the lower yield strength values for an uncorrected stress-strain curve could match closely to the upper yield strength value for a corrected stress-strain curve through coincidence alone. This could also explain why the lower yield strength DIF values in Figure 26 were closer than the upper yield strength DIF values when compared to the results of this research.

It is interesting to note how closely the UFC A36 DIF_y curve follows the least-squares curve fit of Cowell's A36 data. The *dashed line* in Figure 27 was generated by reducing a curve fit of Cowell's data by 5%.

Figure 26. Comparison of experimental results of A572 and Ex-Ten.

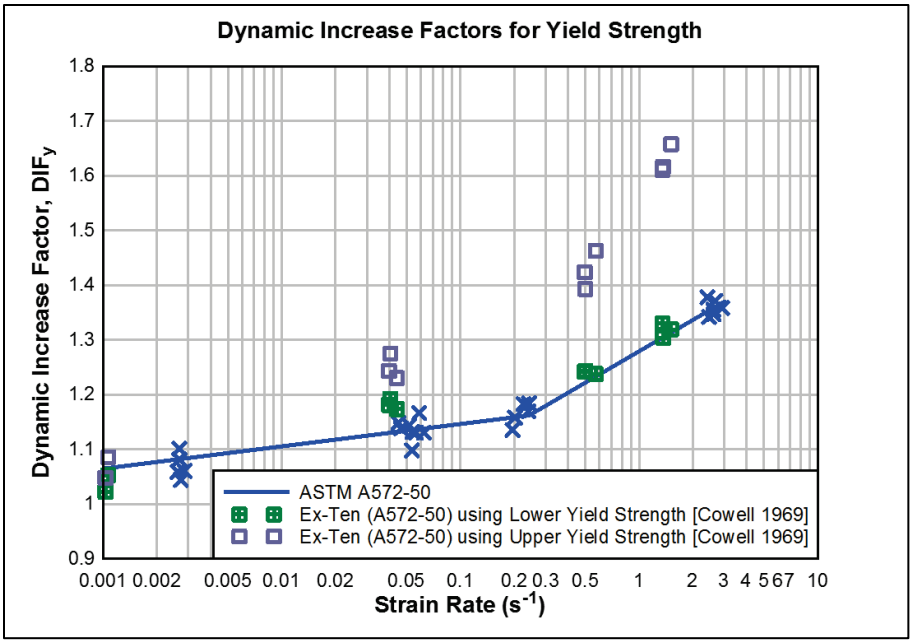

Figure 27. Comparison of *DIFy* of A36 between Cowell's data and the UFC.

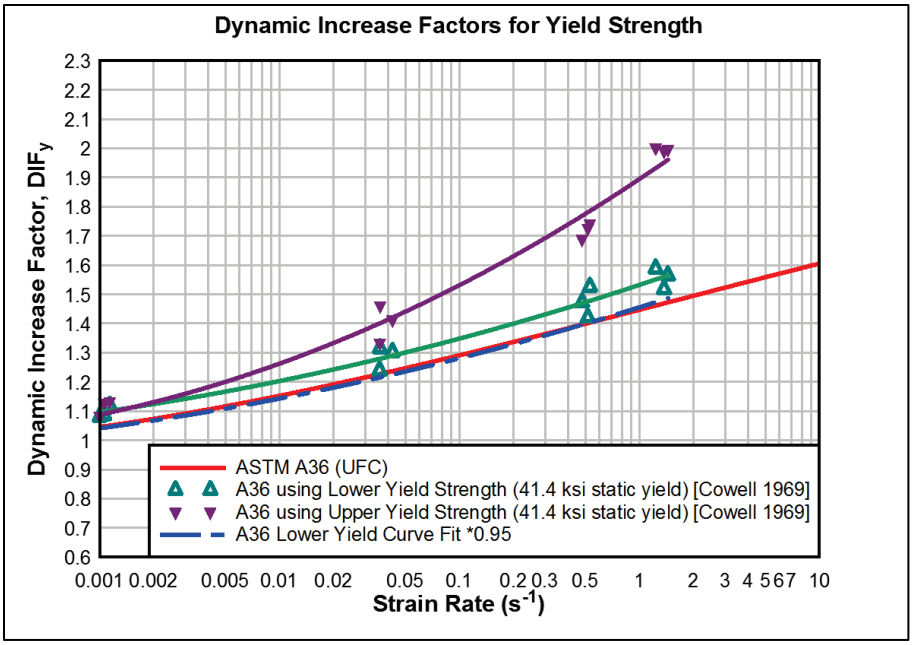

The percent elongation after fracture and percent reduction of area are shown in Figure 28. Both ductility properties increased slightly with strain rate. Comparisons between the static and dynamic ductility properties cannot be accurately made because of the difference in specimen geometry for the different types of tests.

Figure 28. Dynamic ductility properties of A572 and A992 steels for tested rates.

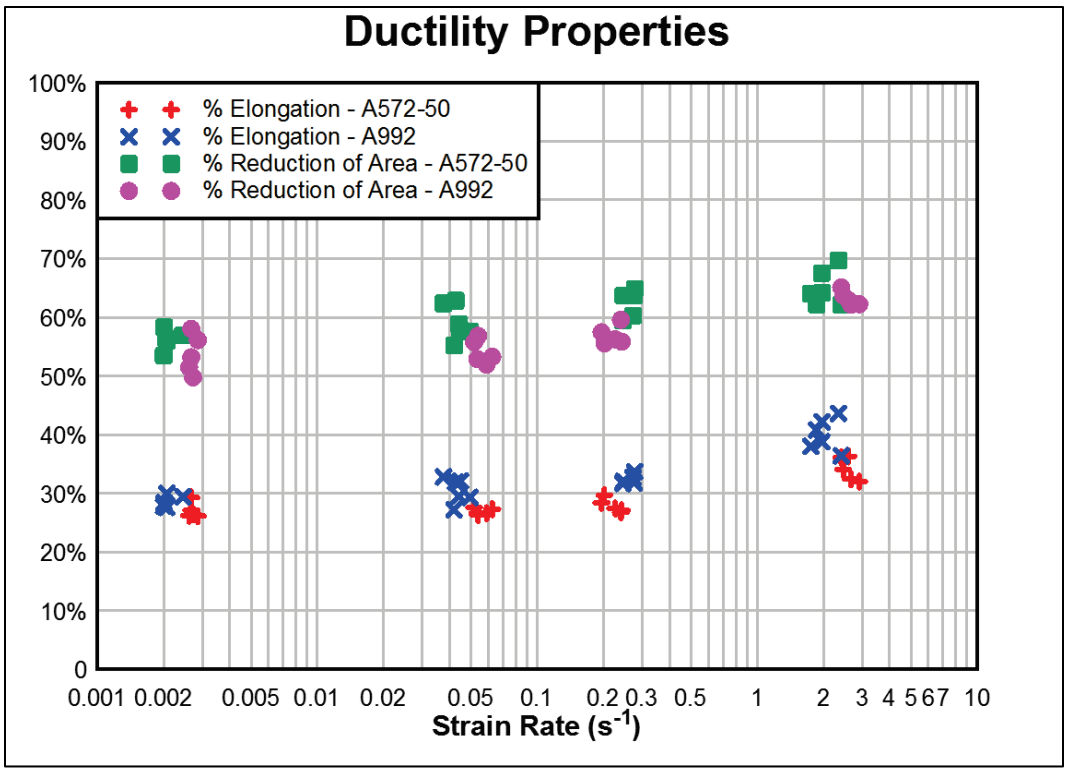

5 Summary of Experimental Results, Conclusions, and Recommendations

5.1 Summary of Results

The results of the research reported herein are summarized as follows and are applicable for the range of strain rates tested.

- The yield strength of both A572-50 and A992 steels increased appreciably as the loading rate, or strain rate, application was increased. A992 steel displayed a slightly higher strain-rate sensitivity than A572-50 (Table 14).
- The ultimate tensile strength of both steels increased with strain rate but to a lesser degree than yield strength. A992 exhibited a very slightly higher strain rate sensitivity than A572-50 (Table 15).
- Percent elongation after failure and percent reduction of area increased slightly with an increase in strain rate (Table 16), which is highly beneficial with regards to plastic design.
- Inertial effects created by the rapid application of load must be considered for strain rates of 5E-2 and higher when determining the true load applied to a specimen.

Table 14. Average yield strength DIF for the strain rate ranges tested.

Approximate Strain Rate (s^{-1})	A572-50 Average DIF_y	A992 Average DIF_y	Difference
2E-3	1.07	1.12	4.6%
5E-2	1.14	1.19	4.3%
2E-1	1.16	1.25	7.5%
2E0	1.36	1.45	6.4%

Table 15. Average ultimate tensile strength DIF for strain rate ranges tested.

Approximate Strain Rate (s^{-1})	A572-50 Average DIF_u	A992 Average DIF_u	Difference
2E-3	1.04	1.04	0%
5E-2	1.07	1.07	0%
2E-1	1.10	1.11	0.9%
2E0	1.20	1.21	0.8%

Table 16. Average percent elongation after fracture and percent reduction of area for strain rate ranges tested.

Approximate Strain Rate (s^{-1})	A572-50 Average % Elongation After Fracture	A992 Average % Elongation After Fracture	Difference	A572-50 Average % Reduction of Area	A572-50 Average % Reduction of Area	Difference
2E-3	27.0	28.6	5.8%	53.7	56.2	4.5%
5E-2	26.9	30.5	12.5%	54.1	59.1	8.8%
2E-1	27.9	32.4	14.9%	56.9	62.4	9.2%
2E0	34.2	40.0	15.6%	63.2	64.9	2.7%

5.2 Conclusions

The following conclusions were made based on the results of this research and are applicable for the range of strain rates tested.

- The load-carrying capacity for both A572-50 and A992 structural steels will increase with strain rate.
- The difference in strain rate sensitivity between the two tested steels can most likely be attributed to the moderate difference in static yield strength.
- The strain rate sensitivity for yield and ultimate tensile strength are inversely related to static yield strength.
- Strain rate sensitivity for yield and ultimate tensile strength change with increased strain rates, which is represented by the change in slope of the DIF curves between the rates of 2E-1 and 2E0 s-1.
- The 200-kip hydraulic testing apparatus and instrumentation used in these experiments proved adequate in obtaining accurate material strength properties of steel from approximately 1E-3 to 3E0 s^{-1}.

5.3 Recommendations

Also based on the results of this research, the following recommendations are made.

- Extrapolation of DIF values, ductility properties, or the conclusions regarding either, outside of the rates tested is highly discouraged.
- Similar experiments should be conducted with specimen of increasing cross-sectional areas (e.g., 0.75, 1.5, and 3 $in.^2$) to determine if strain-rate sensitivity will change with respect to structural-member thickness. A new test configuration will have to be implemented to develop the required strain rates for significantly larger cross sections. The cross sections of the specimens for this research were approximately 0.5 $in.^2$ and required less than 50 kip of

force to fracture at the highest rate. It may be required to implement a three-point bending test to achieve similar rates of strain for much larger cross sections.

- Both steels tested were produced domestically. It is highly recommended that additional testing on foreign-produced A572-50- and A992-specified steel be conducted to ensure that strain-rate sensitivity values match those of domestic steel.

Bibliography

Cited References

ASTM. 2014. *Standard Specification for Carbon Structural Steel*. ASTM A36/A36M-14. West Conshohocken, PA: ASTM International.

ASTM. 2015. *Standard Specification for High-Strength Low-Alloy Columbium-Vanadium Structural Steel*. ASTM A572/A572M-15. West Conshohocken, PA: ASTM International.

ASTM. 2017a. *Standard Specification for General Requirements for Rolled Structural Steel Bars, Plates, Shapes, and Sheet Piling*. ASTM A6/A6M-17. West Conshohocken, PA: ASTM International.

ASTM. 2017b. *Standard Specification for Structural Steel for Bridges*. ASTM A709/709M -17. West Conshohocken, PA: ASTM International.

ASTM. 2011. *Standard Specification for Structural Steel Shapes*. ASTM A992/A992M-11. West Conshohocken, PA: ASTM International.

ASTM. 2016. *Standard Test Methods for Tension Testing of Metallic Materials*. ASTM E8/E8M-16a. West Conshohocken, PA: ASTM International.

Cowell, W. L. 1963. *NCEL Dynamic Testing Machine*. Technical Report TR-331. Port Hueneme, CA: US Naval Civil Engineering Laboratory.

Cowell, W. L. 1969. *Dynamic Tests on Selected Structural Steels*. Technical Report R-642. Port Hueneme, CA: US Naval Civil Engineering Laboratory.

Cowell, W. L., and J. R. Keeton. 1962. *Dynamic Tests on High Strength Steel*. Technical Note N-427. Port Hueneme, CA: US Naval Civil Engineering Laboratory.

DoD (Department of Defense). 2014. *Structures to Resist the Effects of Accidental Explosions*. UFC 3-340-02. Washington, DC: US Army Corps of Engineers, Naval Facilities Engineering Command, Air Force Civil Engineer Support Agency.

Flathau, W. J. 1971. *Dynamic Tests of Large Reinforcing Bar Splices*. Vicksburg, MS: US Army Engineer Waterways Experiment Station.

Hibbeler, R. C. 2014. *Mechanics of Materials*. Boston, MA: Prentice Hall.

Hong, S., and T. Kang. 2016. "Dynamic Strength Properties of Concrete and Reinforcing Steel Subjected to Extreme Loads." *ACI Structural Journal* 113 (5): 983–995.

Huff, W. L. 1969. *Test Devices: Blast Load Generator Building*. Vicksburg, MS: US Army Engineer Waterways Experiment Station.

Hydesoft Computing, LLC. 2018. *DPlot*. Version 2.3.5.4. Vicksburg, MS: Hydesoft Computing. http://www.dplot.com/index.htm.

Image Systems AB. 2015. *TEMA User's Guide*. Linköping, Sweden: Image Systems AB.

Lindholm, U. S., and R. L. Bessey. 1969. *A Survey of Rate Dependent Strength Properties of Metals*. Technical Report AFML-TR-69-119. Wright-Patterson Air Force Base, Ohio: Air Force Materials Laboratory, Air Force Systems Command.

Malvar, J. L. 1998. "Review of Static and Dynamic Properties of Steel Reinforcing Bars." *ACI Materials Journal* 95 (5): 609–614.

Manjoine, M. J. 1944. "Influence of Rate of Strain and Temperature on Yield Stresses of Mild Steel." *Journal of Applied Mechanics* 11 (4): 211–218.

Mocko, W., and L. Kruszka. 2013. "Results of Strain Rate and Temperature on Mechanical Properties of Selected Structural Steels." In *11th International Conference on Modern Building Materials, Structures and Techniques, MBMST 2013,* Elsevier, Ltd., 789–797.

Rowell, S. P., and C. E. Grey, S. C. Woodson, and K. P. Hager. 2009. *High Strain-Rate Testing of Mechanical Couplers*. Vicksburg, MS: US Army Engineering Research and Development Center. https://apps.dtic.mil/sti/citations/ADA508609.

Soohoo, P., C. W. Jiang, and M. M. Chen. 1974. *Dynamic Properties of Steels*. AMMRC CTR 74-24. Watertown, Massachusetts: Army Materials and Mechanics Research Center.

Weathersby, J. H. 2003. *Investigation of Bond Slip Between Concrete and Steel Reinforcement Under Dynamic Loading Conditions*. PhD Diss. Louisiana State University.

Uncited References

Asay, J. R., and G. I. Kerley. 1987. "The Response of Materials to Dynamic Loading." *International Journal of Impact Engineering* 5 (1–4): 69–99.

Desai, S. 1969. *Mechanical Properties of ASTM A572 Grade 65 Steel*. Paper 371, Fritz Laboratory Reports. Bethlehem, PA: Fritz Engineering Laboratory, Dept. of Civil Engineering, Lehigh University.

Elam, C. F. 1938. "The Influence of Rate of Deformation on the Tensile Test with Special Reference to the Yield Point in Iron and Steel." In *Proceedings of the Royal Society of London. Series A, Mathematical and Physical Sciences,* 568–592.

Eleiche, Abdel-Salam M. 1972. *A Literature Survey of the Combined Effects of Strain Rate and Elevated Temperature on the Mechanical Properties of Metals*. Technical Report AFML-TR-72-125. Write-Patterson Air Force Base, OH: Air Force Materials Laboratory.

Eleiche, A. M., and J. D. Campbell. 1975. *The Influence of Strain-Rate History and Temperature on the Shear Strength of Copper, Titanium, and Mild Steel*. AFML-TR-76-90. Wright-Patterson AFB, OH: Air Force Material Laboratory.

El-Magd, E. 1994. "Mechanical Properties at High Strain Rates." *Journal de Physique IV Colloque* 04 (C8): 149–170.

Hackett, E. M. 1989. *Effects of High Rate Shear on the Microstructure and Deformation and Fracture Behavior of Two High Strength Steels*. TTRC/SME-89/27. Bethesda, MD: David Taylor Research Center.

Healey, J., A. Ammar, J. Vellozzi, G. Pecone, S. Weissman, and N. Dobbs. 1975. *Design of Steel Structures to Resist the Effects of HE Explosions*. Dover, NJ: Picatinny Arsenal.

Inhaber, H. 1967. "Variation of Yield Stress With Strain and Strain Rate in Mild Steel." *Journal of Engineering for Industry* 89 (3): 478–481.

Johnson, P. C., B. A. Stein, and R. S. Davis. 1962. *Basic Parameters of Metal Behavior Under High Rate Forming*. Technical Report No. WAL TR 111.2/20-6. Watertown, MA: US Army Materials Research Agency.

Keenan, W. A., and A. Feldman. 1960. *The Yield Strength of Intermediate Grade Reinforcing Bars Under Rapid Loading*. Civil Engineering Studies, Structural Research Series No. 197. Kirtland Air Force Base, NM: Air Force Special Weapons Center, Air Research and Development Command.

Kendall, D. P. 1972. "The Effect of Strain Rate and Temperature on Yielding in Steels." *Jornal of Basic Engineering* 91 (1): 207–212.

Kendall, D. P., and T. E. Davidson. 1966. "The Effect of Strain Rate on Yielding in High Strength Steels." *Journal of Basic Engineering* 88 (1): 37–44.

Lucon, E. 2016. "Experimental Assessment of the Equivalent Strain Rate for an Instrumented Charpy Test." *Journal of Research of the National Institute of Standards and Technology* 121:165–179.

Maiden, C. J., and S. J. Green. 1966. "Compressive Strain-Rate Tests on Six Selected Materials at Strain Rates from 10^-3 to 10^4 in/in/sec." *Journal of Applied Mechanics* 496–504.

Malvar, J. L., and J. E. Crawford. 1998. "Dynamic Increase Factors for Steel Reinforcing Bars." In *Twenty-Eighth DDESB Seminar,* Orlando, FL, 1–17.

Moon, D. P., and J. E. Campbell. 1961. *Effects of Moderatly High Strain Rates on the Tensile Properties of Metals*. DMIC Memorandum 142. Columbus, OH: Defense Metals Information Center, Battelle Memorial Institute.

Nadai, A., and M. J. Manjoine. 1941. "High-Speed Tension Tests at Elevated Temperatures- Parts II and III." *ASTM Journal of Applied Mechanics* 8 (2): 77–91.

NagarajaRao, N., M. Lohrmann, and L. Tall. 1966. "Effect of Strain Rate on the Yield Stress of Structural Steel." *ASTM Journal of Materials* 1 (1).

Ngo, T., P. Mendis, A. Gupta, and J. Ramsay. 2007. "Blast Loading and Blast Effects on Structures—An Overview." *Electronic Journal of Structural Engineering* (1):76–91.

Samanta, S. K. 1968. "Resistance to Dynamic Compression of Low-Carbon Steel and Alloy Steels at Elevated Temperatures and at High Strain Rates." *International Journal of Mechanical Science* 10 (8): 613–636.

Sierakowski, R. L. 1997. *Strain Rate Behavior of Metals and Composites*. Columbus, OH: Ohio State University, Civil and Environmental Engineering and Geodetic Science.

Singh, M., D. Sood, R. K. Gupta, R. Kumar, P. C. Gautam, B. Sewak, A. C. Sharma, and T. Mathew. 2008. "Dynamic Yield Strength of Mild Steel under Impact Loading." *Defence Science Journal* 58 (2): 275–284.

Soroushian, P., and K. Choi. 1987. "Steel Mechanical Properties at Different Strain Rates." *Journal of Structural Engineering* 113 (4): 663–672.

Staffier, S. R., and M. A. Sozen. 1975. *Effect of Strain Rate on Yield Stress of Model Reinforcement*. Structural Research Series No. 415. Urbana, IL: University of Illinois.

Stewart, W. L., P. E. Rowe, and P. J. Pahl. 1965. *Dynamic Tests of Model Steel Structures*. Research Report R65-32. Port Hueneme, CA: Massachusetts Institute of Technology, Naval Civil Engineering, Laboratory.

Stout, M. G., and P. S. Follansbee. 1986. "Strain Rate Sensitivity, Strain Hardening, and Yield Behavior of 304L Stainless Steel." *Journal of Engineering Materials and Technology* 108 (4): 344–353.

USACE (US Army Corps of Engineers). 1957. *The Design of Structures to Resist the Effects of Atomic Weapons, Strength of Materials and Structural Elements*. EM 1110-345-414. Vicksburg, MS: US Army Engineer Waterways Experiment Station.

Vision Research. 2017. *Phantom Camera Control Application Software*. Wayne, NJ: Vision Research.

Whittington, W. R., A. L. Oppedal, S. Turnage, Y. Hammi, H. Rhee, P. G. Allison, C. K. Crane, and M. F. Horstemeyer. 2014. "Capturing the Effect of Temperature, Strain Rate, and Stress State on the Plasticity and Fracture of Rolled Homogeneous Armor (RHA) Steel." *Materials Science & Engineering* 594:82–88.

Work, C. E., and T. J. Dolan. 1953. *The Influence of Temperature and Rate of Strain on the Properties of Metals in Torsion*. WADC Technical Report 53-10. Wright-Patterson Air Force Base, OH: Wright Air Development Center.

Yongning, L., Z. Jinhua, and Z. Huijiu. 1992. "Variation of Yield Stress with Strain Rate for Three Carbon Steels." *Journal of Engineering Materials and Technology* 114 (4): 348–353.

Symbols

Symbol	Meaning
DIF_y	Dynamic Increase Factor for Yield Stress
DIF_u	Dynamic Increase Factor for Ultimate Tensile Stress
E	Signal Excitation (Voltage)
F	Force
G	Gauge Factor
L	Gauge Length
M	Mass
R	Electrical Resistance
a	Acceleration
e	Engineering Strain
f_{dy}	Dynamic Yield Stress
f_{du}	Dynamic Ultimate Tensile Stress
f_y	Static Yield Stress
f_u	Static Ultimate Tensile Stress
K	Spring Constant
lbf	Pound (Force)
lbm	Pound (Mass)
x	Displacement
v	Poisson's Ratio (Greek Letter "Nu")

Appendix A: ASTM A572-50 Stress-Strain Diagrams

The following 32 figures present ASTM A572-50 stress-strain diagrams.

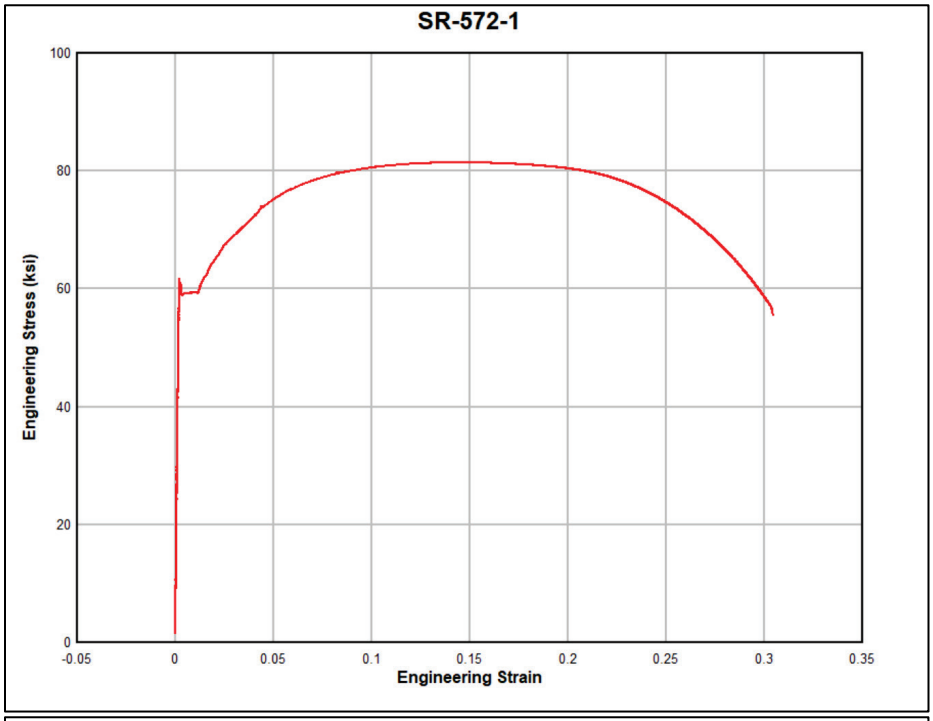

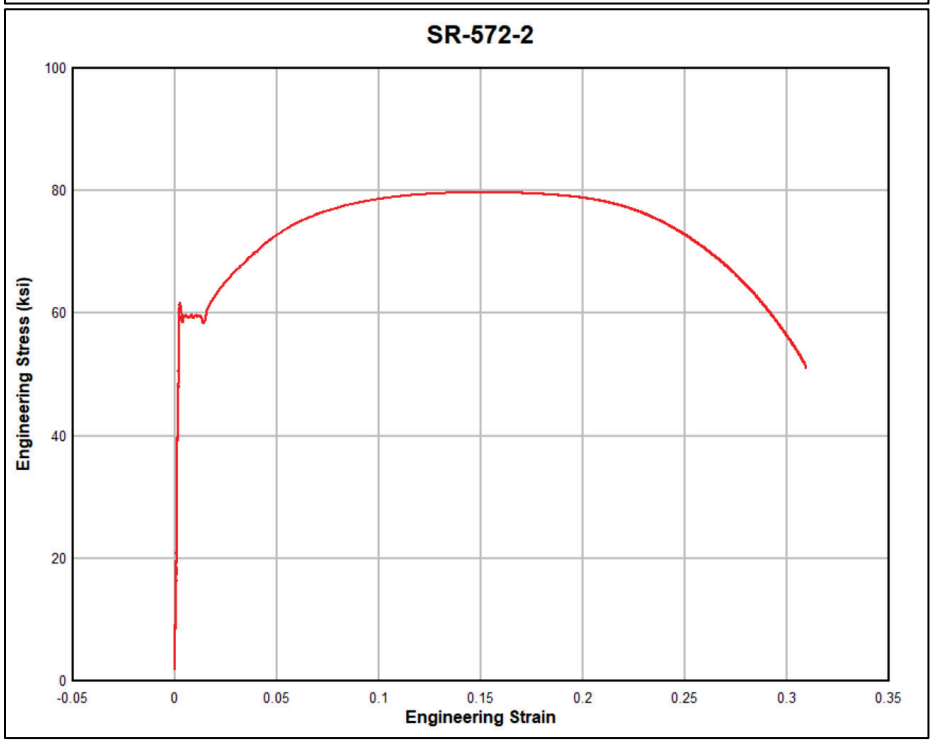

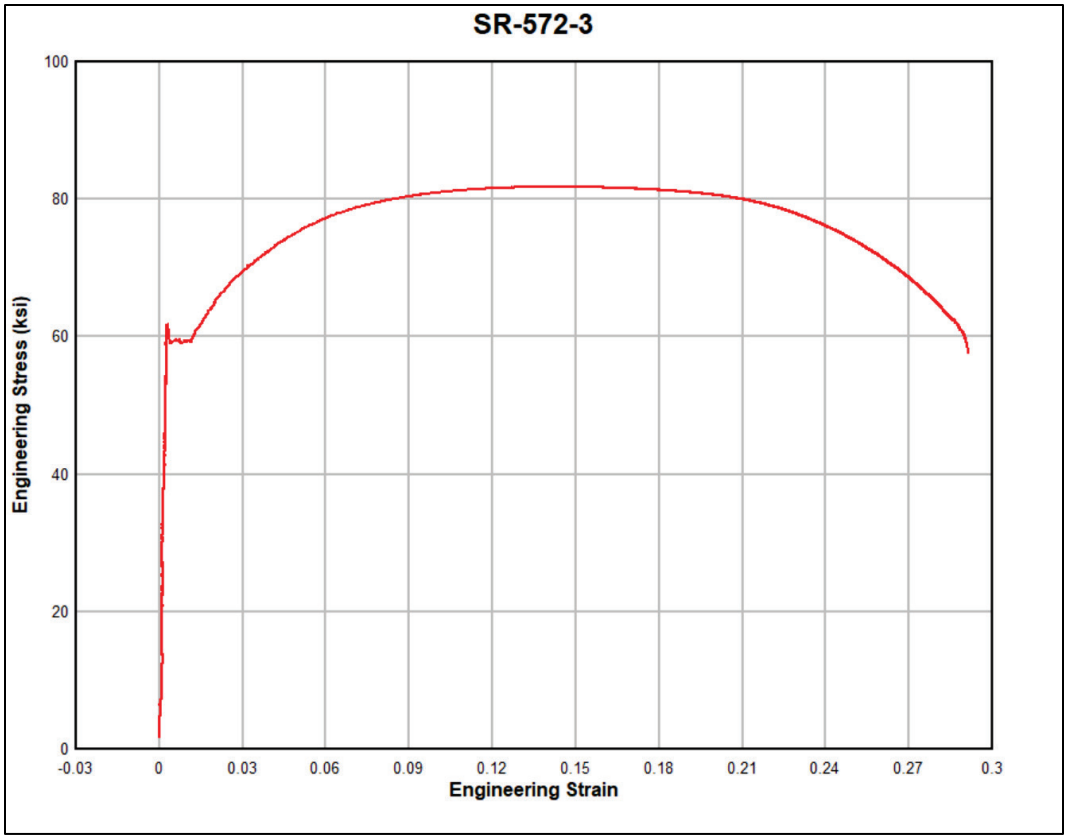
SR-572-3
Engineering Stress (ksi)
100
80
60
40
20
0
-0.03
0
0.03
0.06
0.09
0.12
0.15
0.18
0.21
0.24
0.27
0.3
Engineering Strain

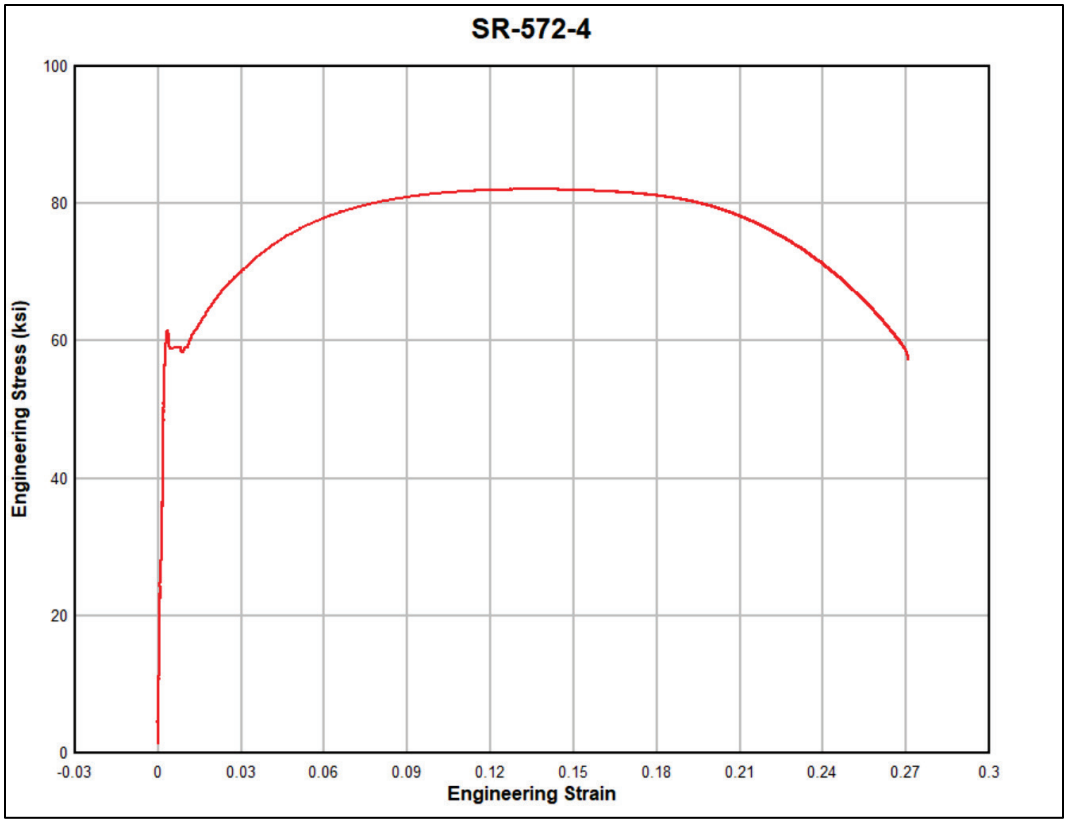
SR-572-4
Engineering Stress (ksi)
100
80
60
40
20
0
-0.03
0
0.03
0.06
0.09
0.12
0.15
0.18
0.21
0.24
0.27
0.3
Engineering Strain

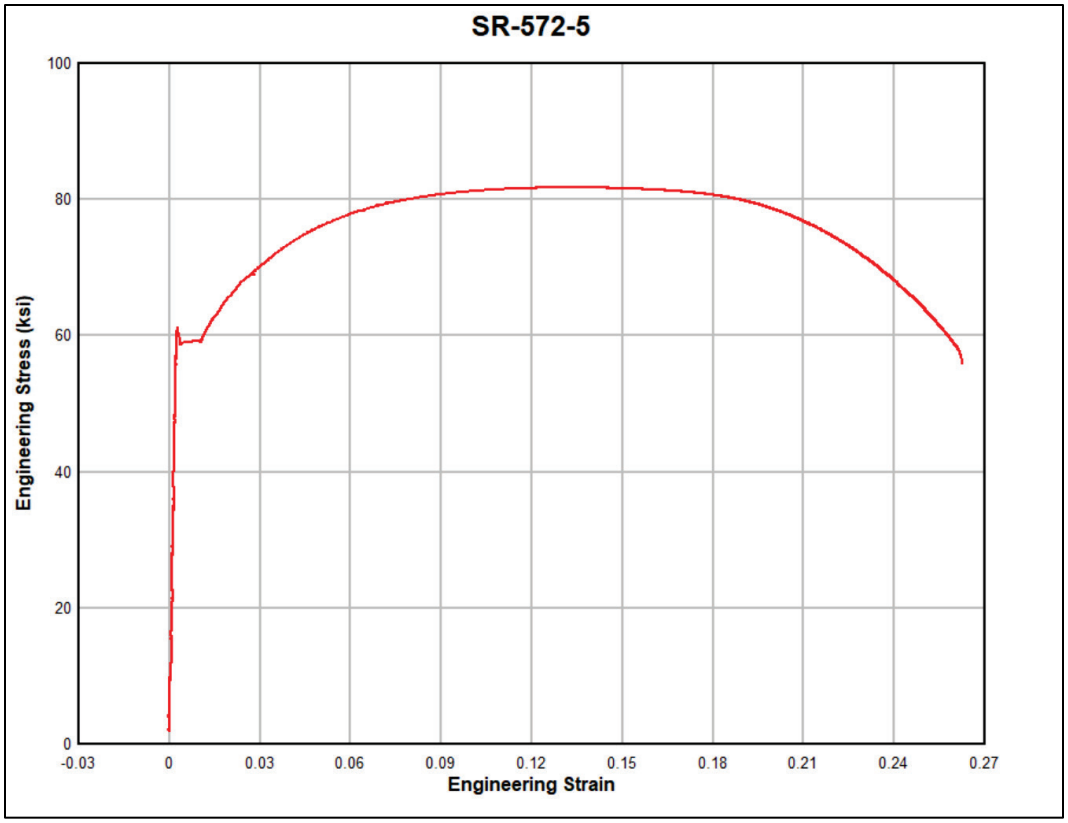
SR-572-5
Engineering Stress (ksi)
100
80
60
40
20
0
-0.03
0
0.03
0.06
0.09
0.12
0.15
0.18
0.21
0.24
0.27
Engineering Strain

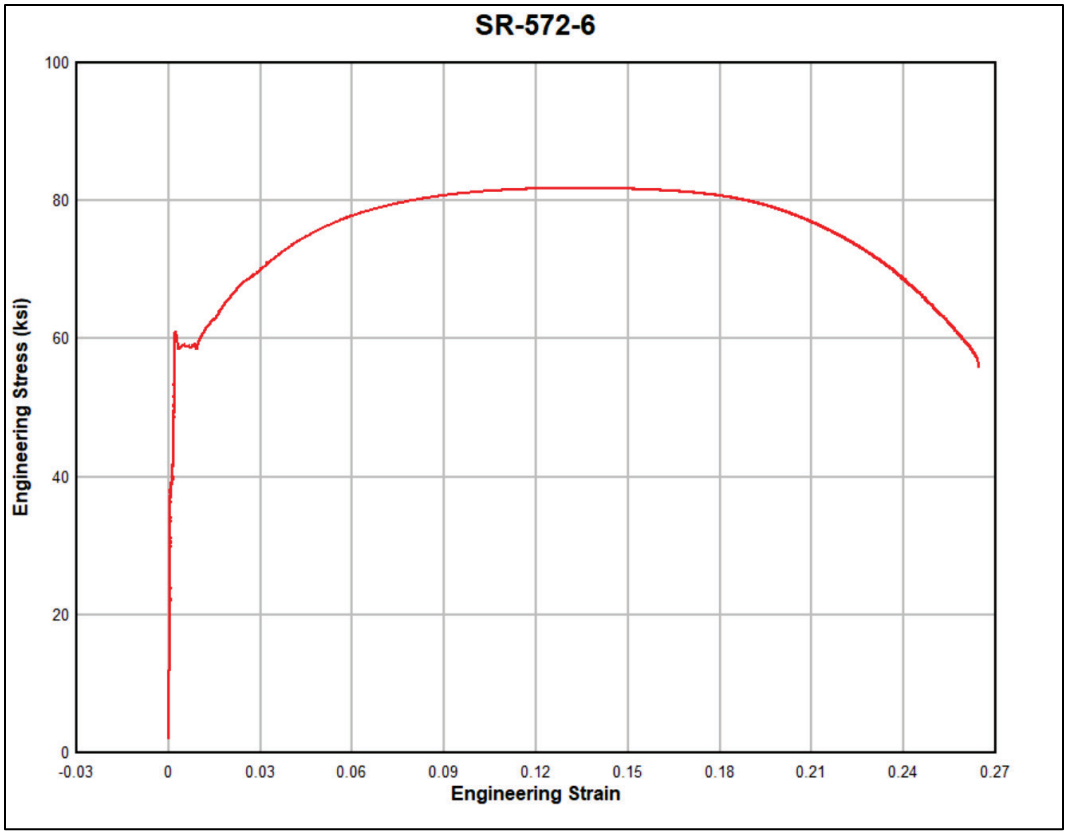
SR-572-6
Engineering Stress (ksi)
100
80
60
40
20
0
-0.03
0
0.03
0.06
0.09
0.12
0.15
0.18
0.21
0.24
0.27
Engineering Strain

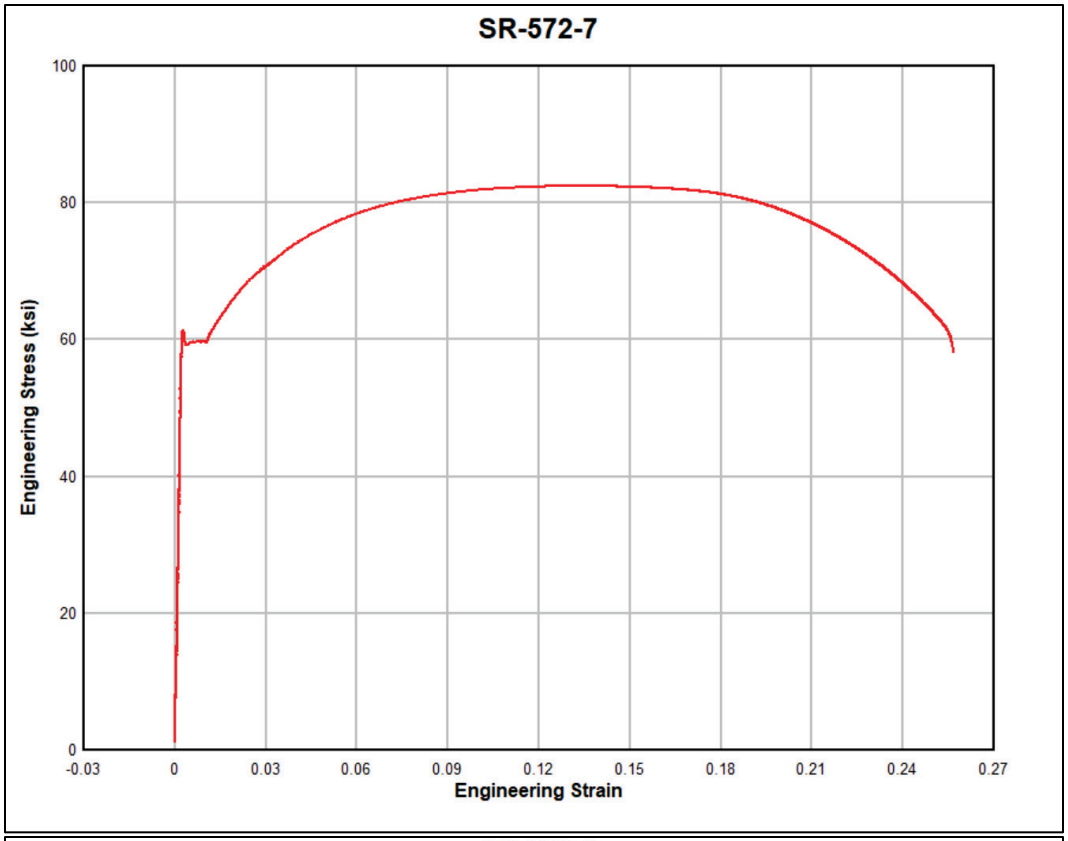
SR-572-7
Engineering Stress (ksi)
100
80
60
40
20
0
-0.03
0
0.03
0.06
0.09
0.12
0.15
0.18
0.21
0.24
0.27
Engineering Strain

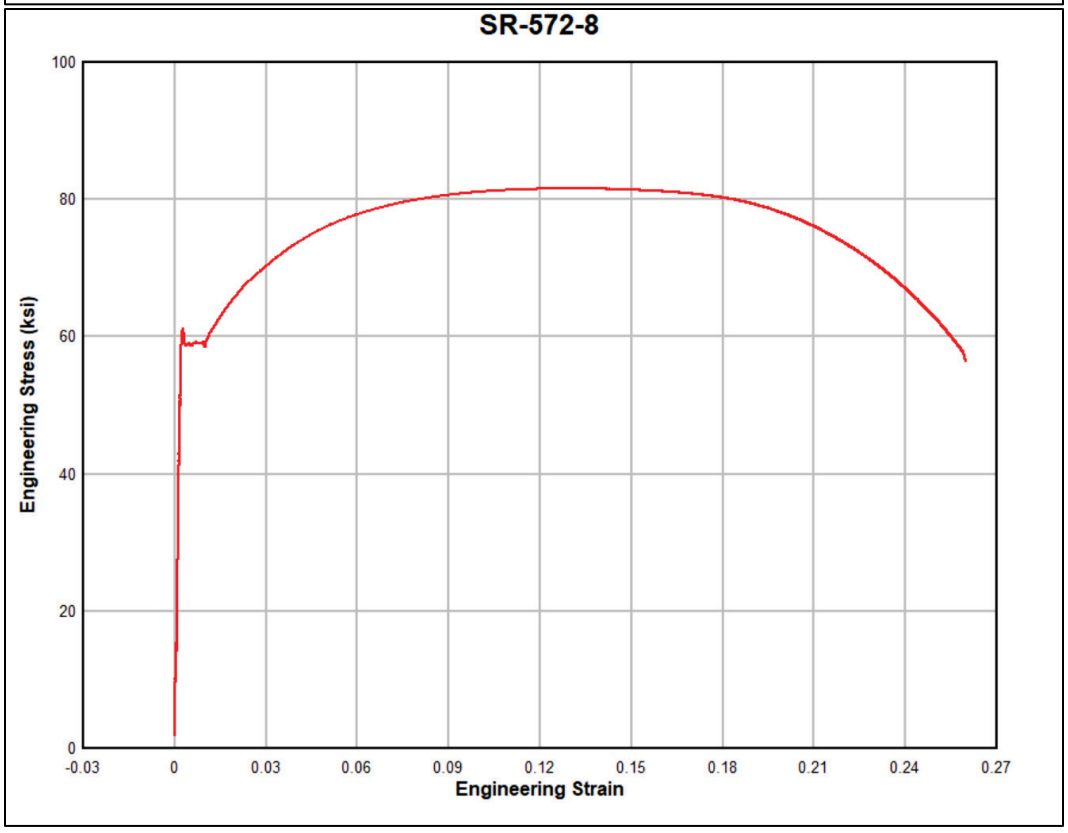
SR-572-8
Engineering Stress (ksi)
100
80
60
40
20
0
-0.03
0
0.03
0.06
0.09
0.12
0.15
0.18
0.21
0.24
0.27
Engineering Strain

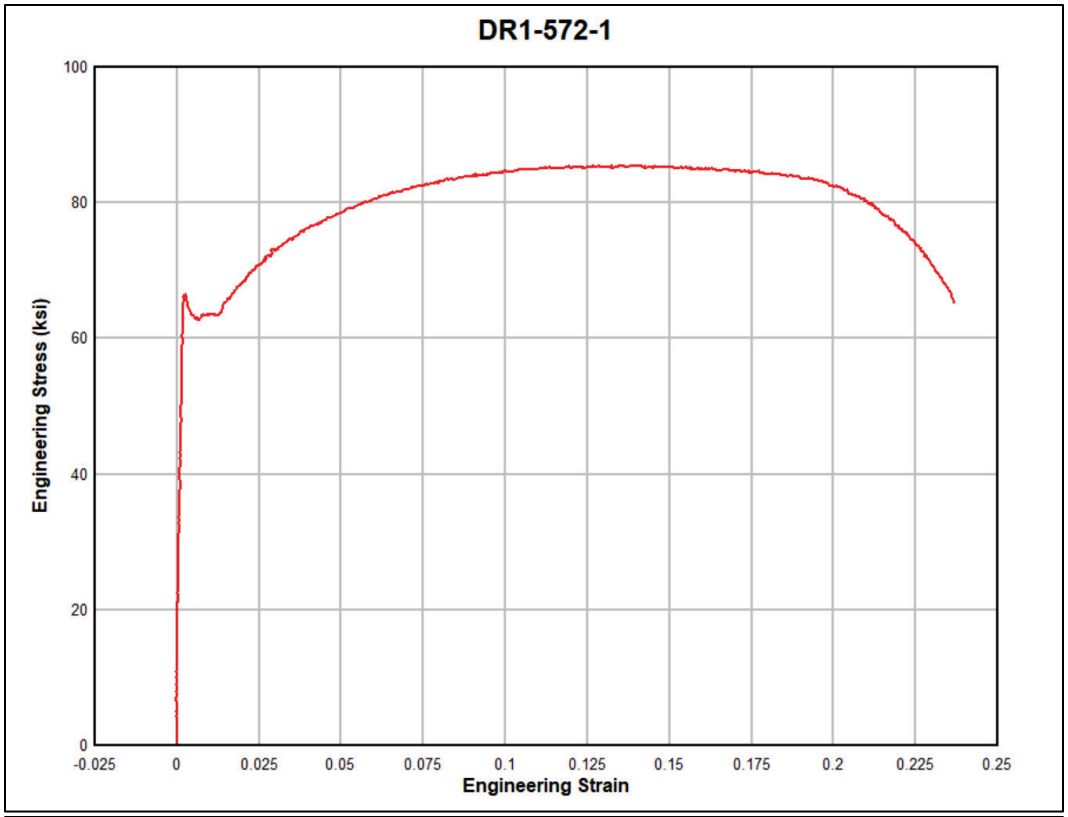
DR1-572-1
Engineering Stress (ksi)
100
80
60
40
20
0
-0.025
0
0.025
0.05
0.075
0.1
0.125
0.15
0.175
0.2
0.225
0.25
Engineering Strain

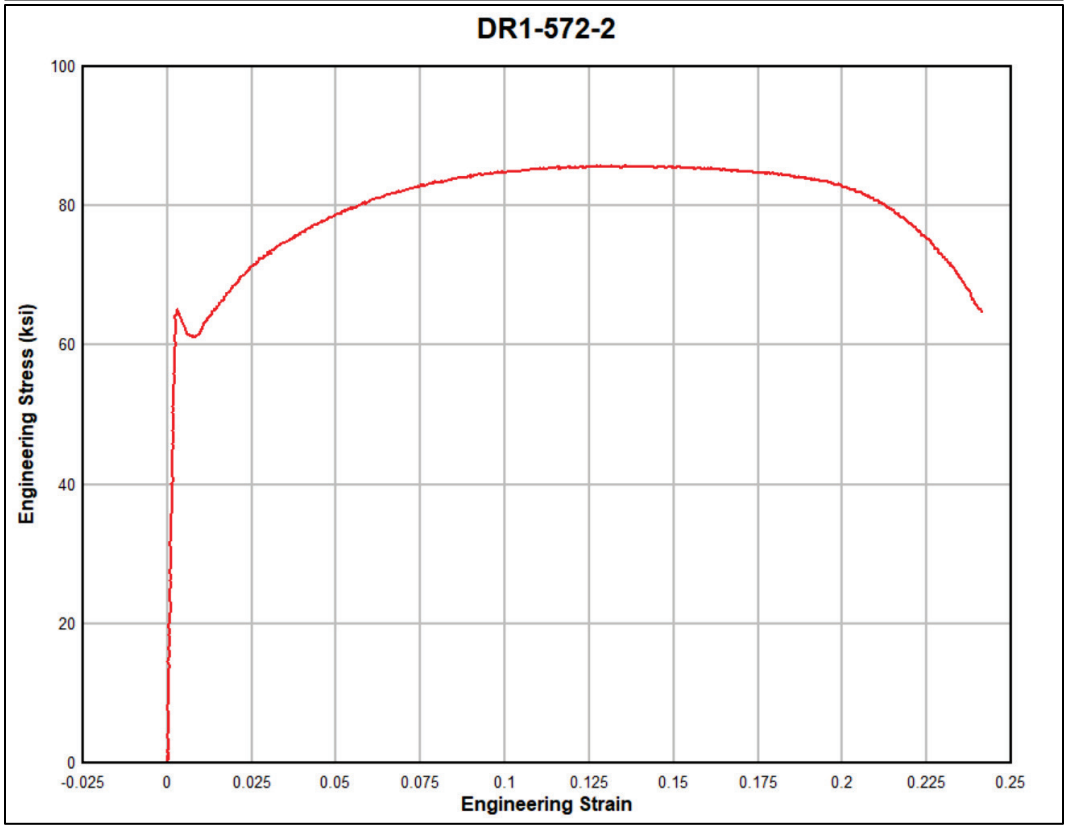
DR1-572-2
Engineering Stress (ksi)
100
80
60
40
20
0
-0.025
0
0.025
0.05
0.075
0.1
0.125
0.15
0.175
0.2
0.225
0.25
Engineering Strain

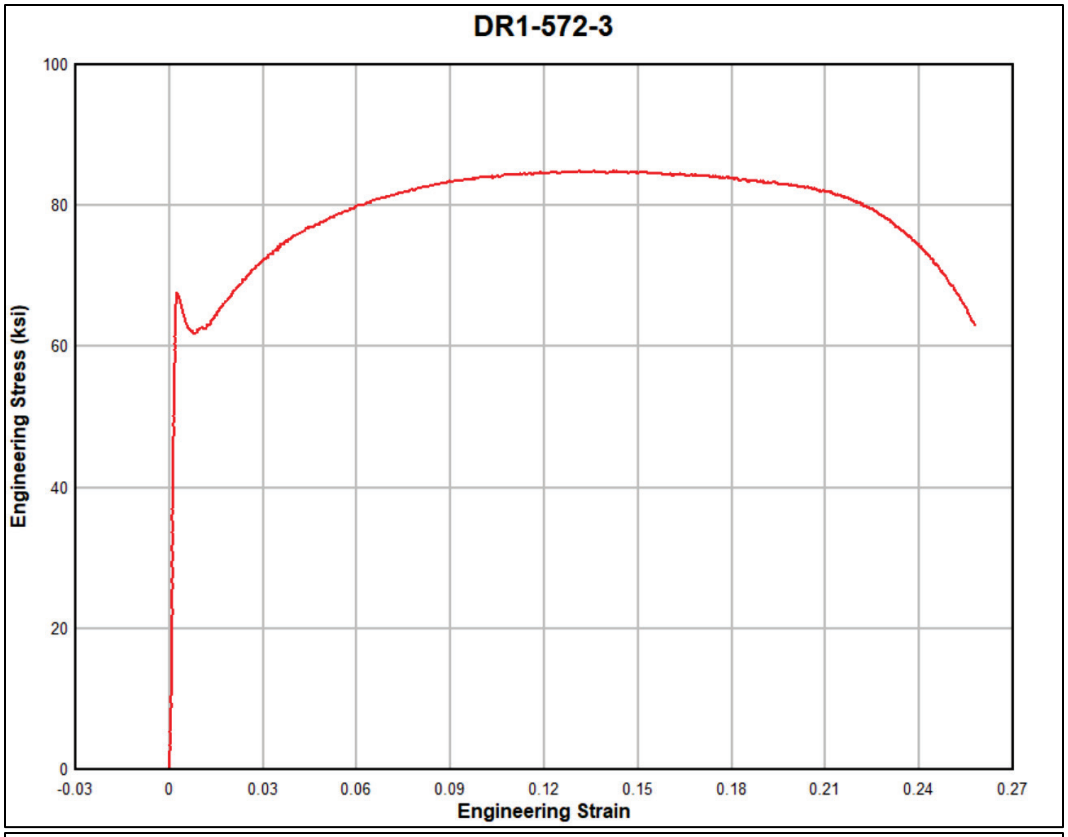
DR1-572-3
Engineering Stress (ksi)
100
80
60
40
20
0
-0.03
0
0.03
0.06
0.09
0.12
0.15
0.18
0.21
0.24
0.27
Engineering Strain

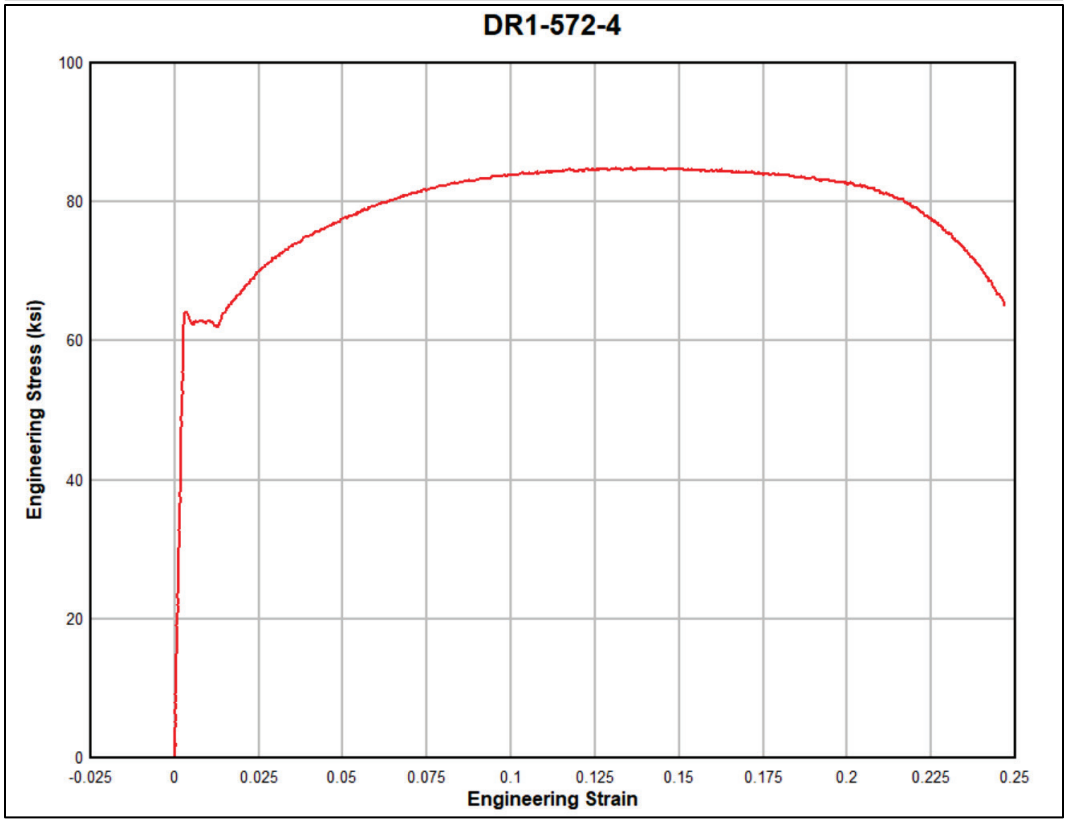
DR1-572-4
Engineering Stress (ksi)
100
80
60
40
20
0
-0.025
0
0.025
0.05
0.075
0.1
0.125
0.15
0.175
0.2
0.225
0.25
Engineering Strain

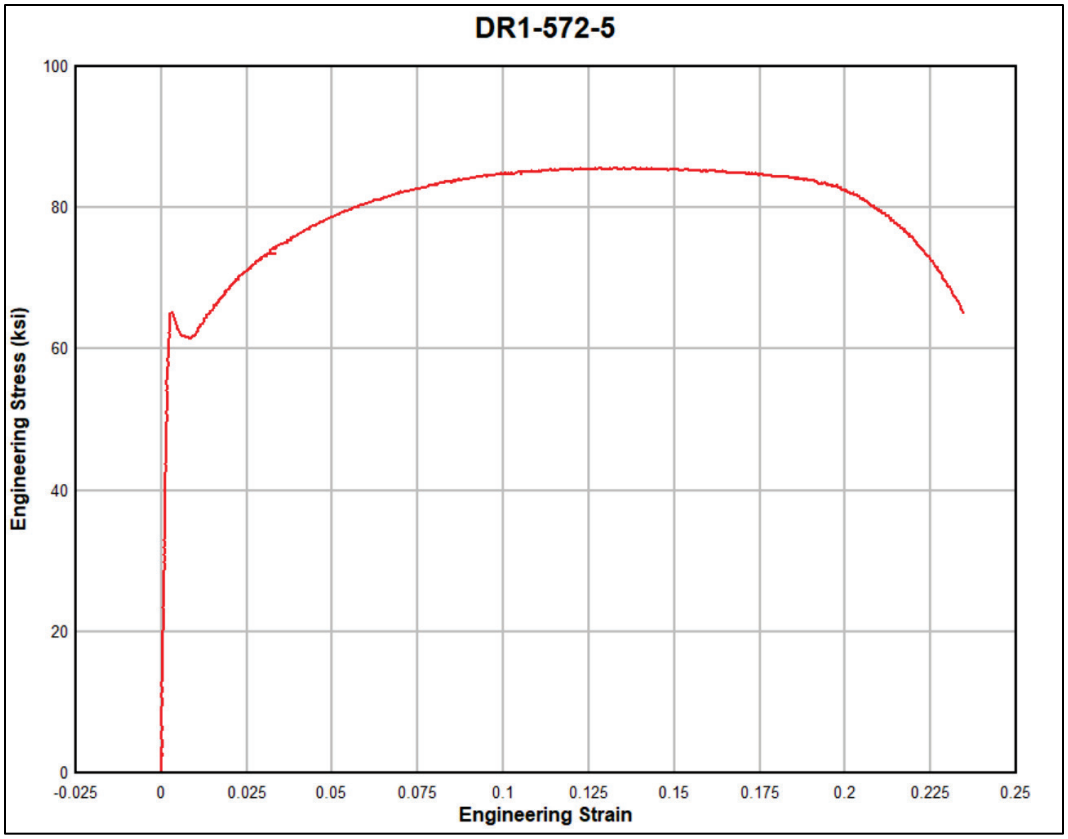
DR1-572-5
Engineering Stress (ksi)
100
80
60
40
20
0
-0.025
0
0.025
0.05
0.075
0.1
0.125
0.15
0.175
0.2
0.225
0.25
Engineering Strain

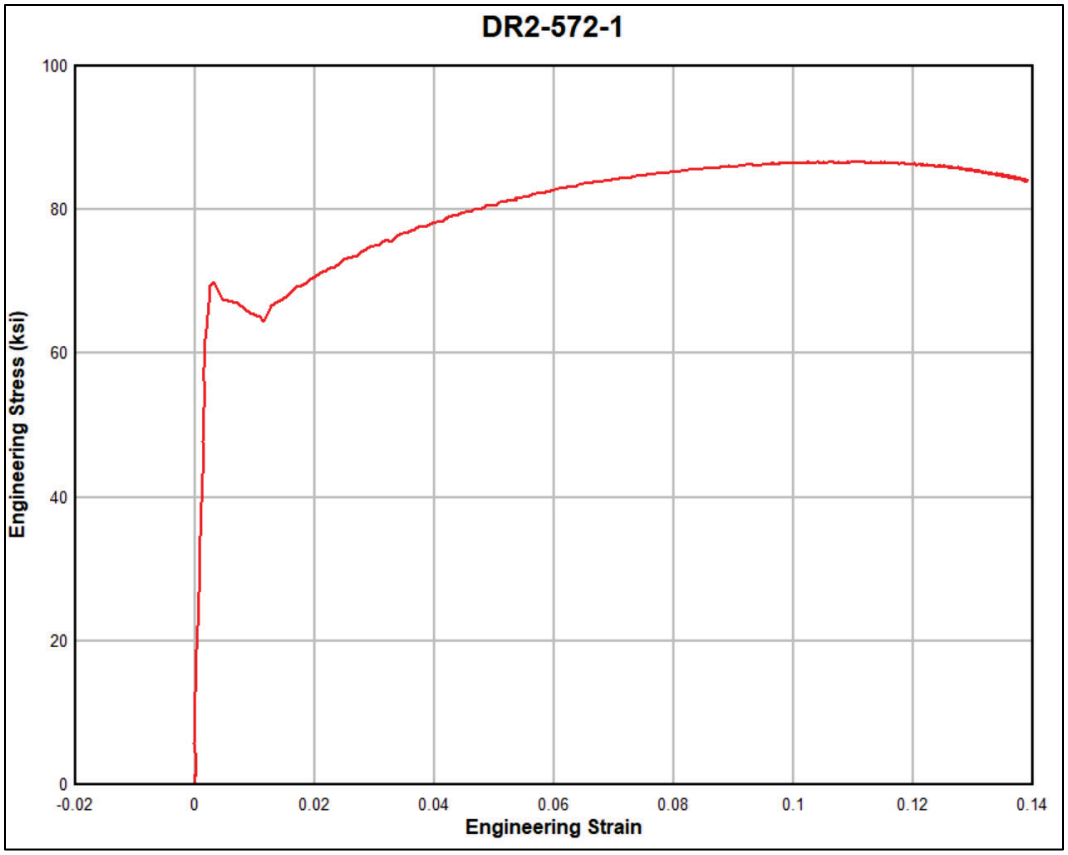
DR2-572-1
Engineering Stress (ksi)
100
80
60
40
20
0
-0.02
0
0.02
0.04
0.06
0.08
0.1
0.12
0.14
Engineering Strain

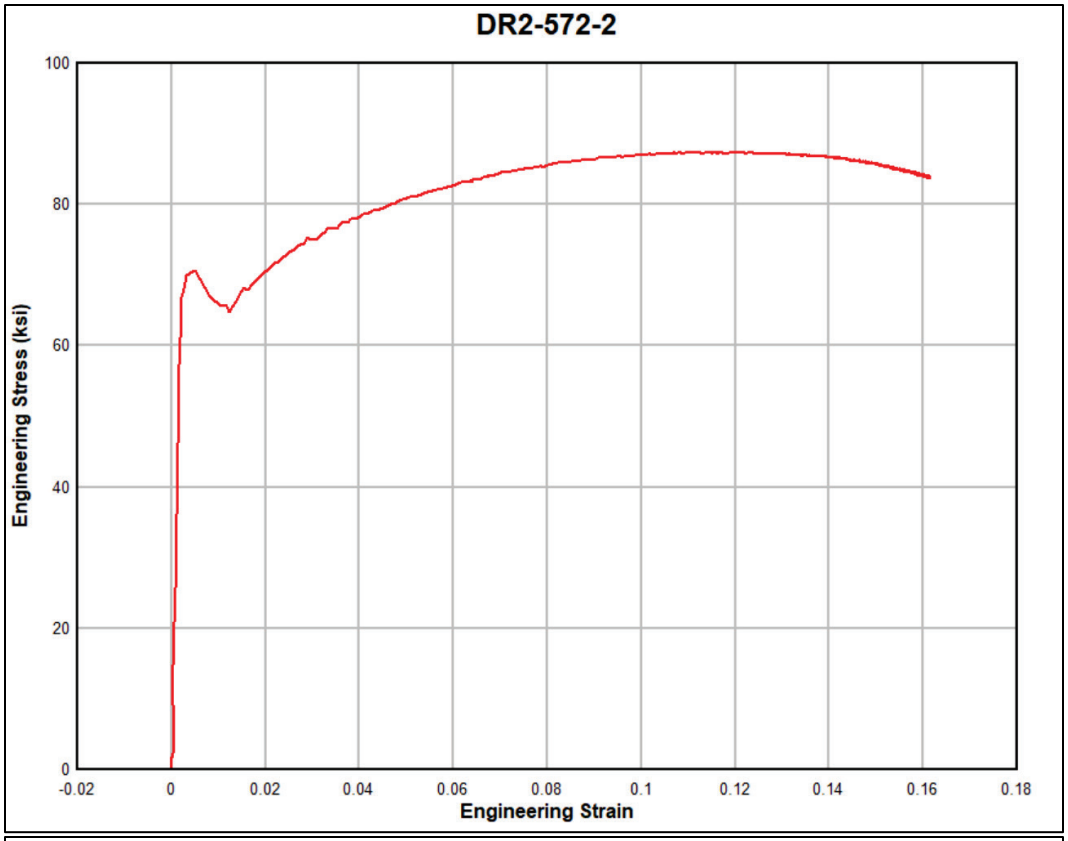
DR2-572-2
Engineering Stress (ksi)
100
80
60
40
20
0
-0.02
0
0.02
0.04
0.06
0.08
0.1
0.12
0.14
0.16
0.18
Engineering Strain

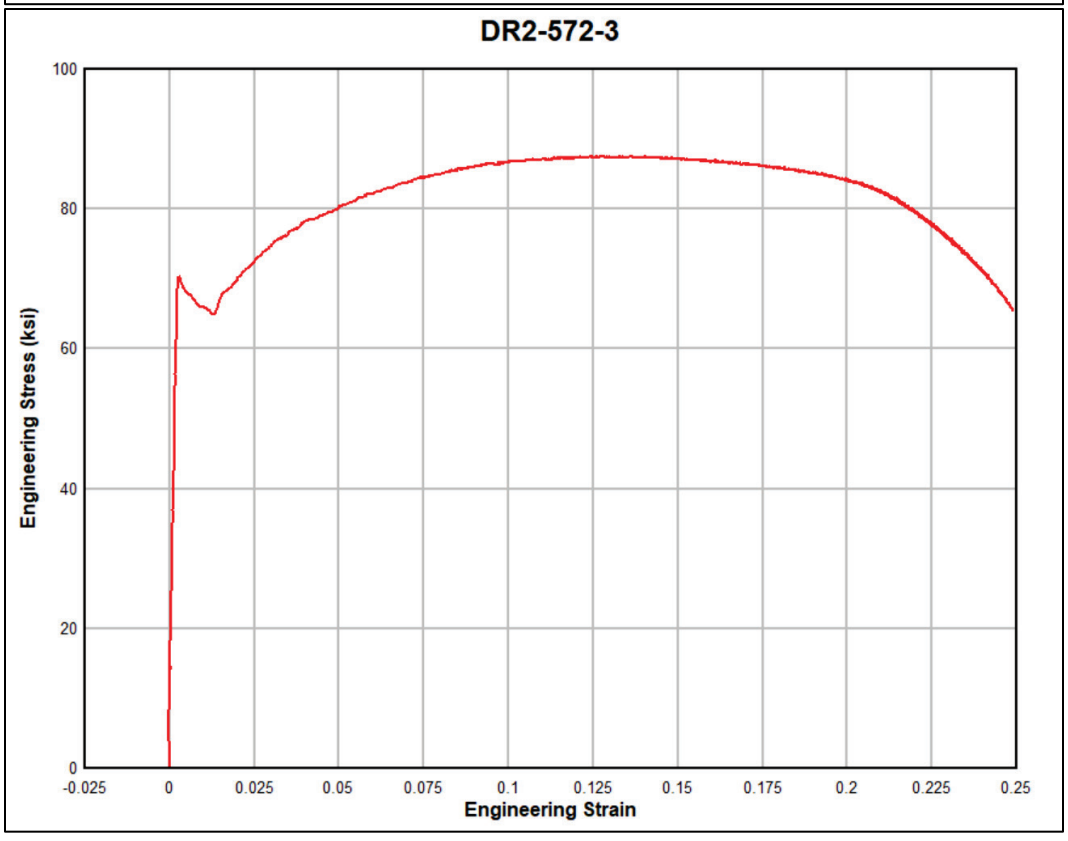
DR2-572-3
Engineering Stress (ksi)
100
80
60
40
20
0
-0.025
0
0.025
0.05
0.075
0.1
0.125
0.15
0.175
0.2
0.225
0.25
Engineering Strain

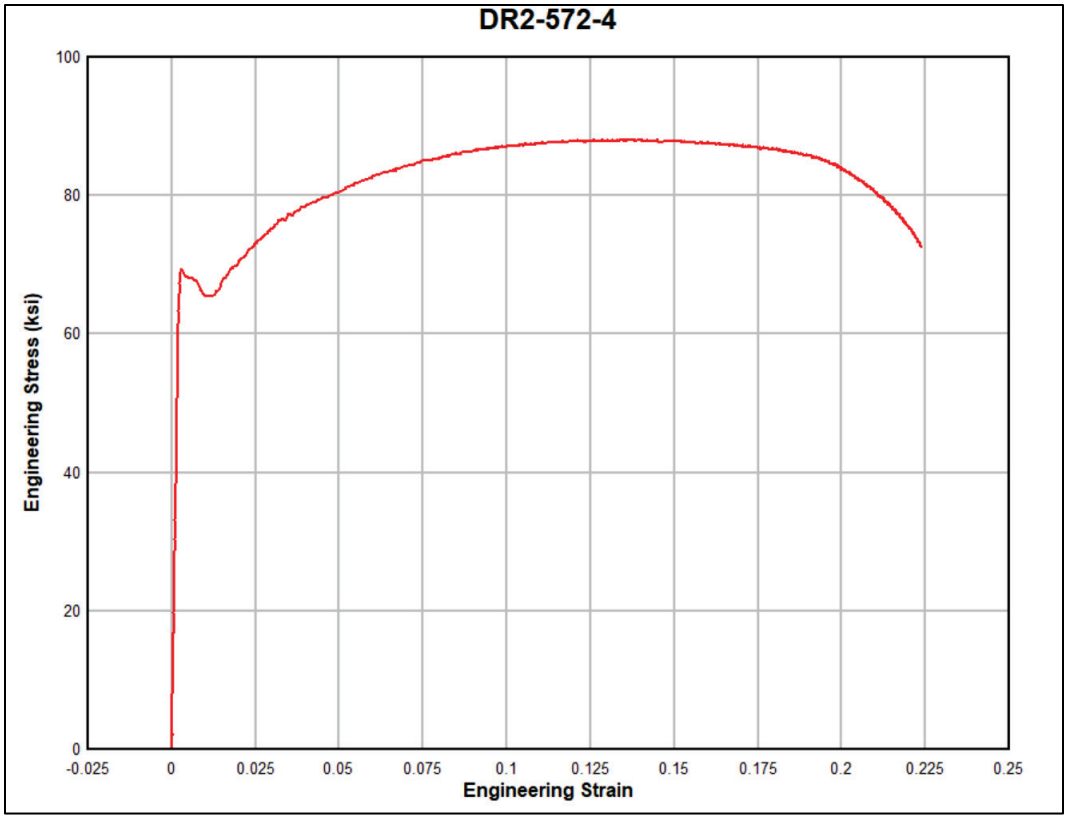
DR2-572-4
Engineering Stress (ksi)
100
80
60
40
20
0
-0.025
0
0.025
0.05
0.075
0.1
0.125
0.15
0.175
0.2
0.225
0.25
Engineering Strain

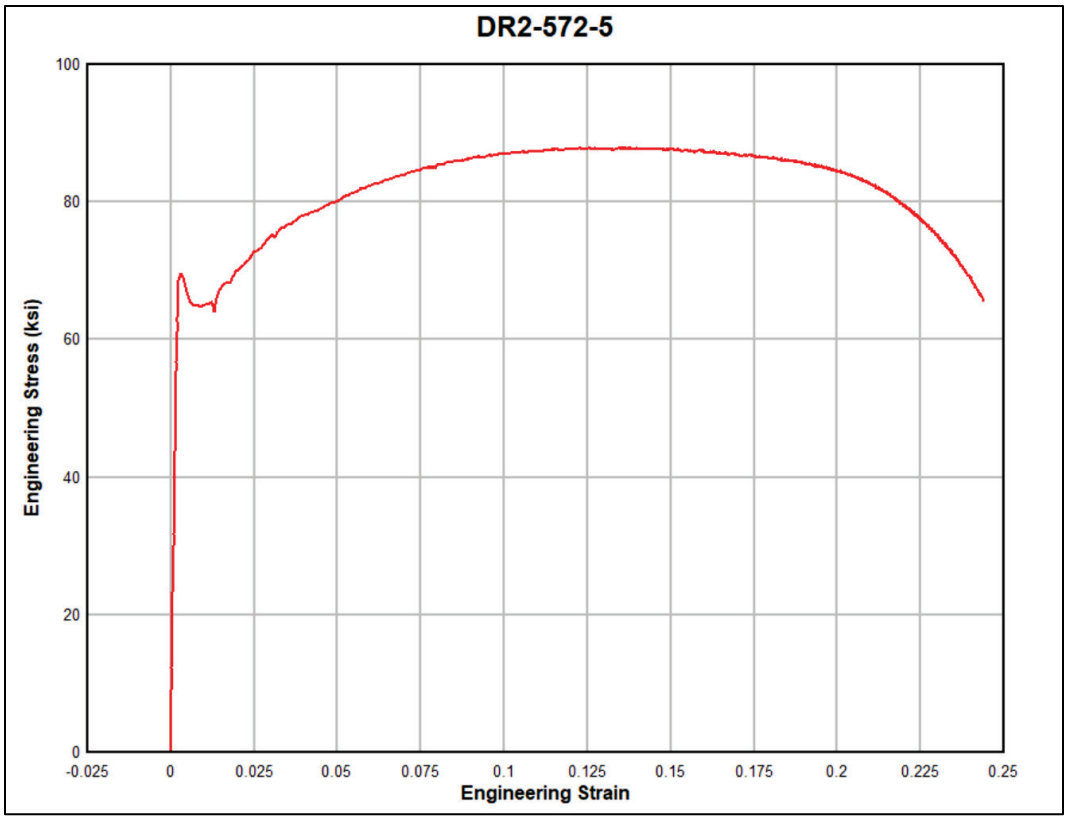
DR2-572-5
Engineering Stress (ksi)
100
80
60
40
20
0
-0.025
0
0.025
0.05
0.075
0.1
0.125
0.15
0.175
0.2
0.225
0.25
Engineering Strain

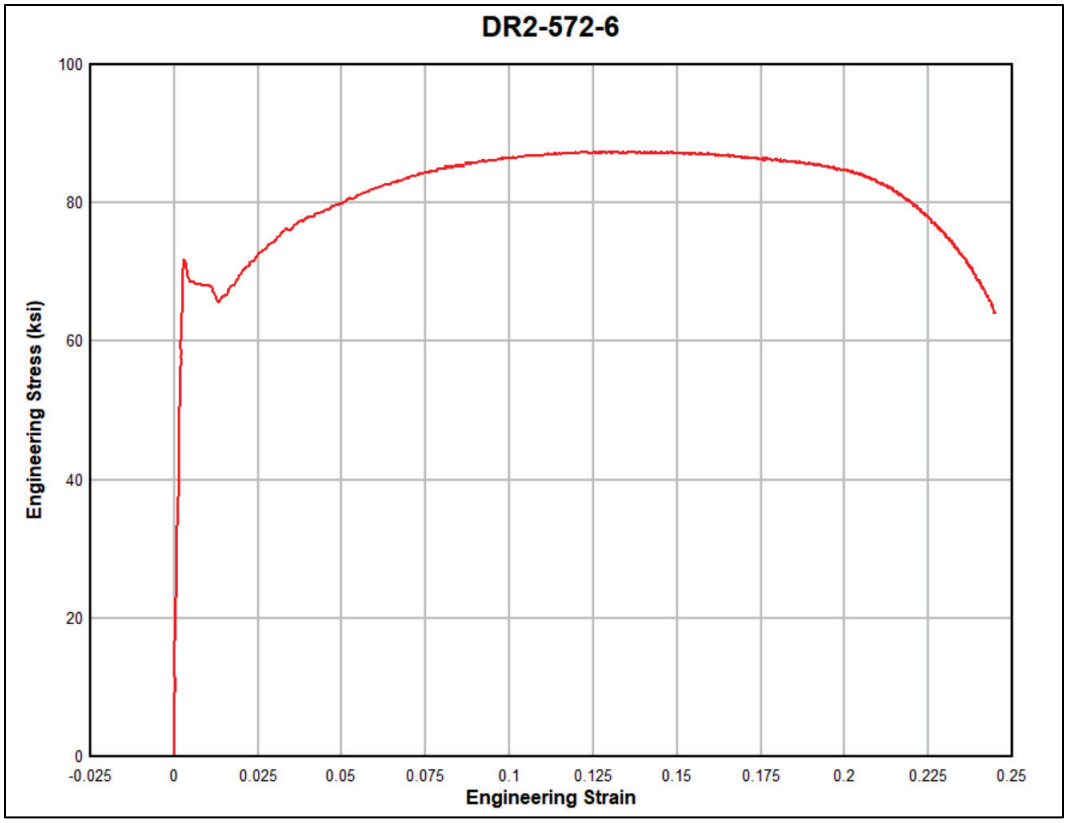
DR2-572-6
Engineering Stress (ksi)
100
80
60
40
20
0
-0.025
0
0.025
0.05
0.075
0.1
0.125
0.15
0.175
0.2
0.225
0.25
Engineering Strain

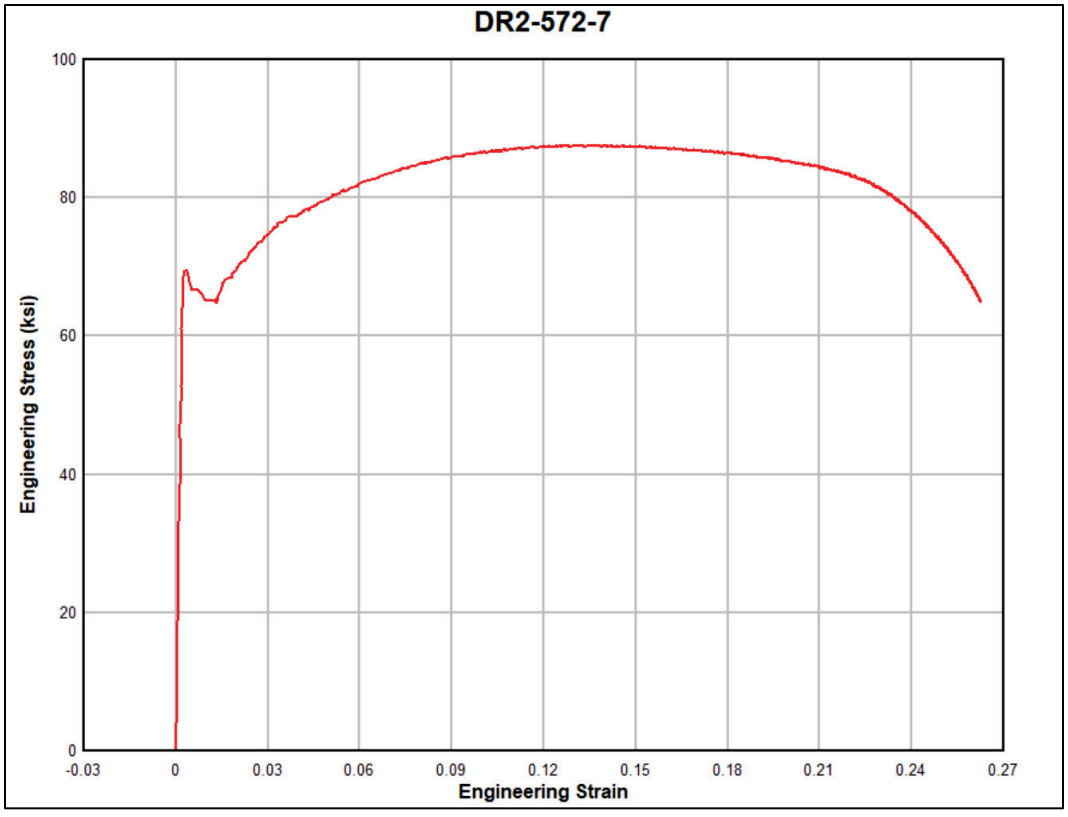
DR2-572-7
Engineering Stress (ksi)
100
80
60
40
20
0
-0.03
0
0.03
0.06
0.09
0.12
0.15
0.18
0.21
0.24
0.27
Engineering Strain

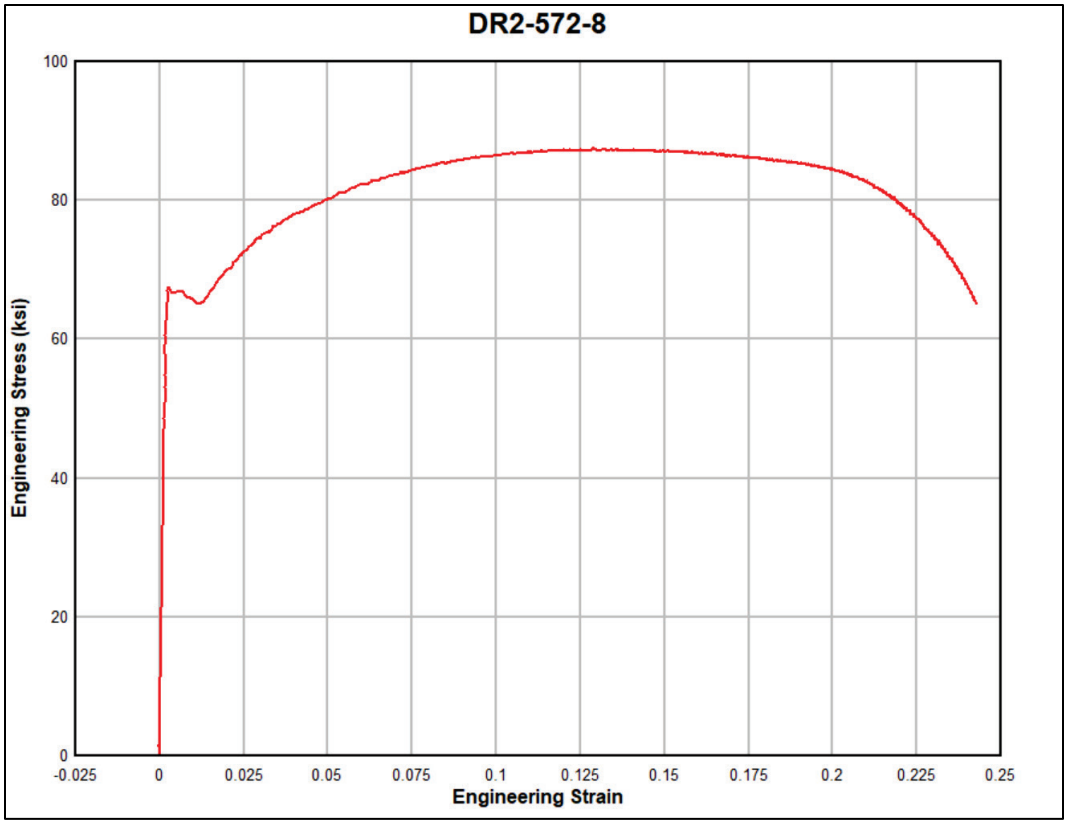
DR2-572-8
Engineering Stress (ksi)
100
80
60
40
20
0
-0.025
0
0.025
0.05
0.075
0.1
0.125
0.15
0.175
0.2
0.225
0.25
Engineering Strain

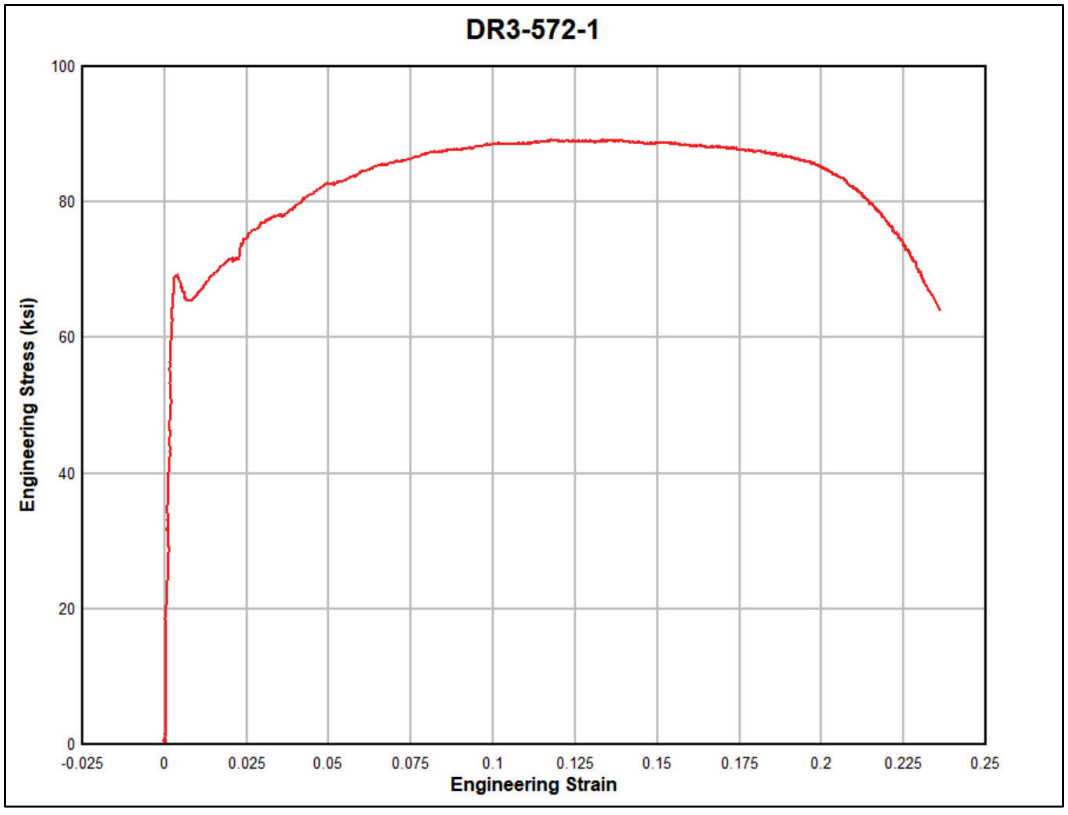
DR3-572-1
Engineering Stress (ksi)
100
80
60
40
20
0
-0.025
0
0.025
0.05
0.075
0.1
0.125
0.15
0.175
0.2
0.225
0.25
Engineering Strain

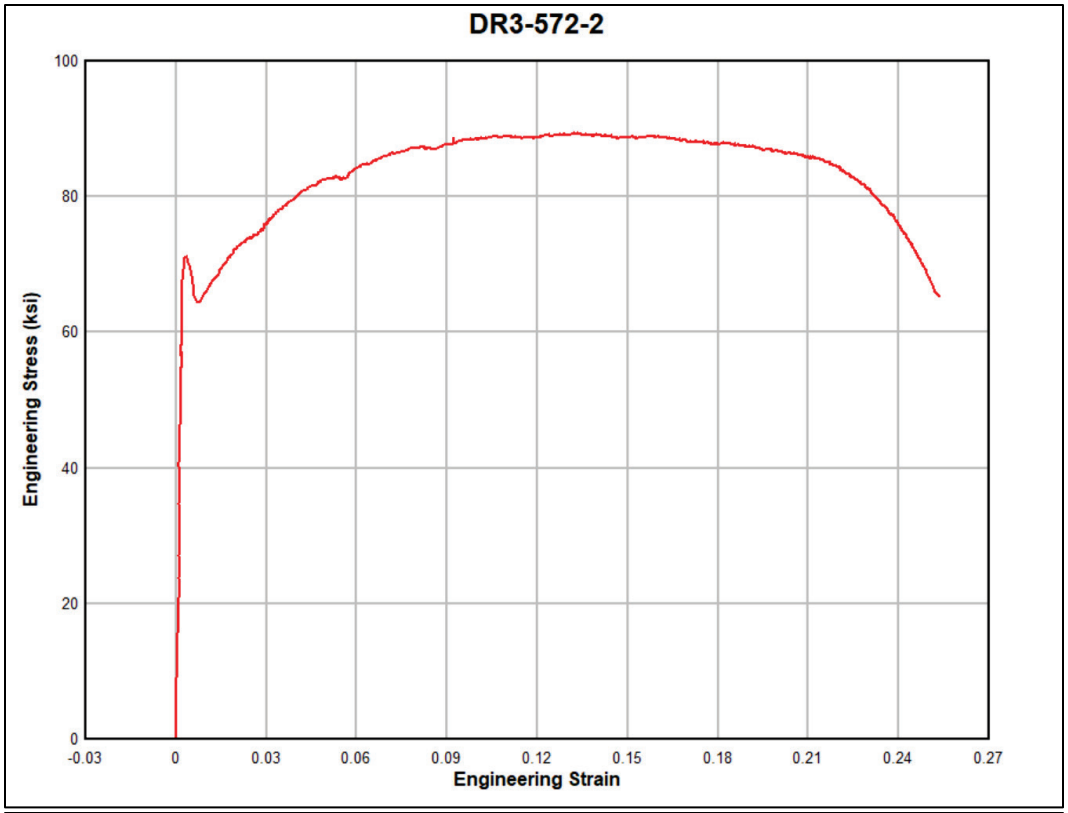
DR3-572-2
Engineering Stress (ksi)
100
80
60
40
20
0
-0.03
0
0.03
0.06
0.09
0.12
0.15
0.18
0.21
0.24
0.27
Engineering Strain

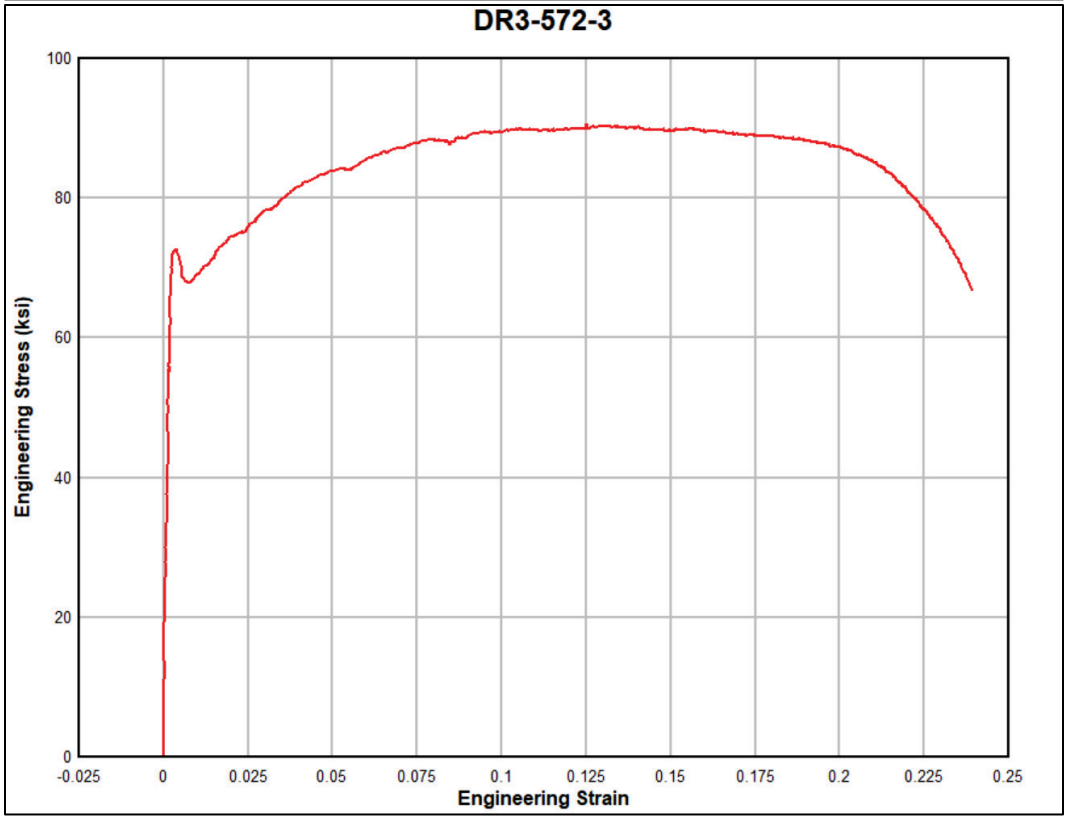
DR3-572-3
Engineering Stress (ksi)
100
80
60
40
20
0
-0.025
0
0.025
0.05
0.075
0.1
0.125
0.15
0.175
0.2
0.225
0.25
Engineering Strain

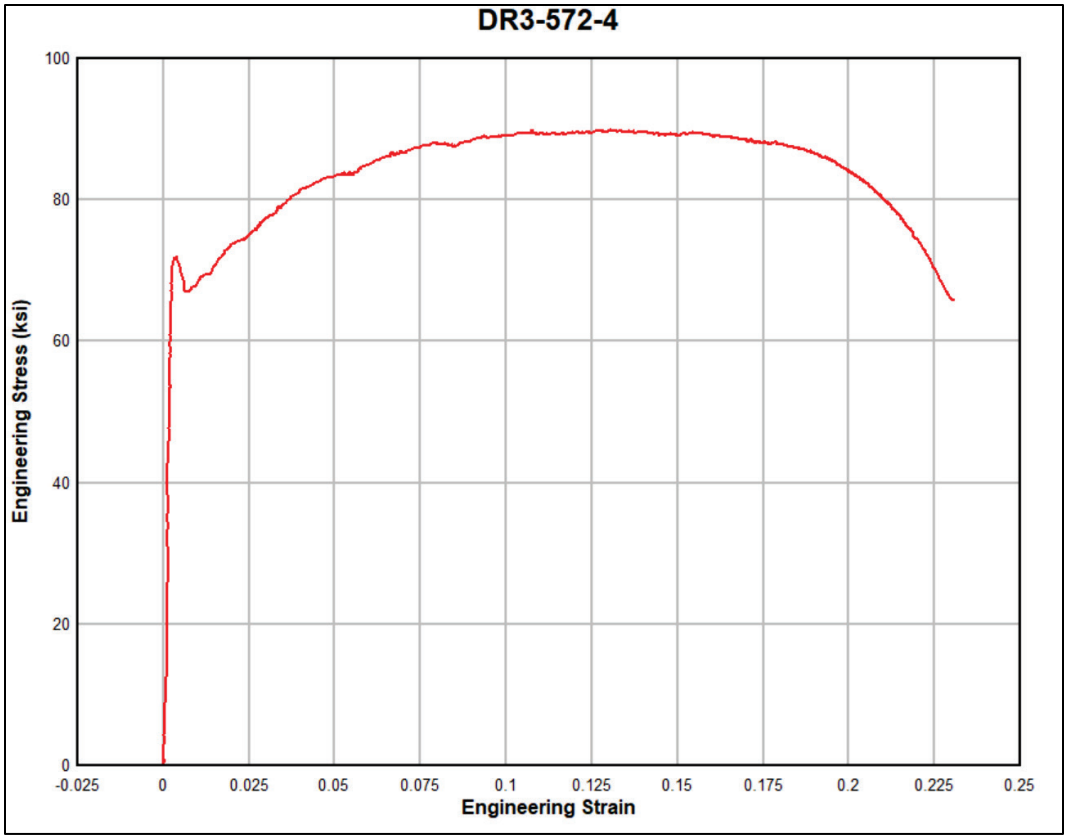
DR3-572-4
Engineering Stress (ksi)
100
80
60
40
20
0
-0.025
0
0.025
0.05
0.075
0.1
0.125
0.15
0.175
0.2
0.225
0.25
Engineering Strain

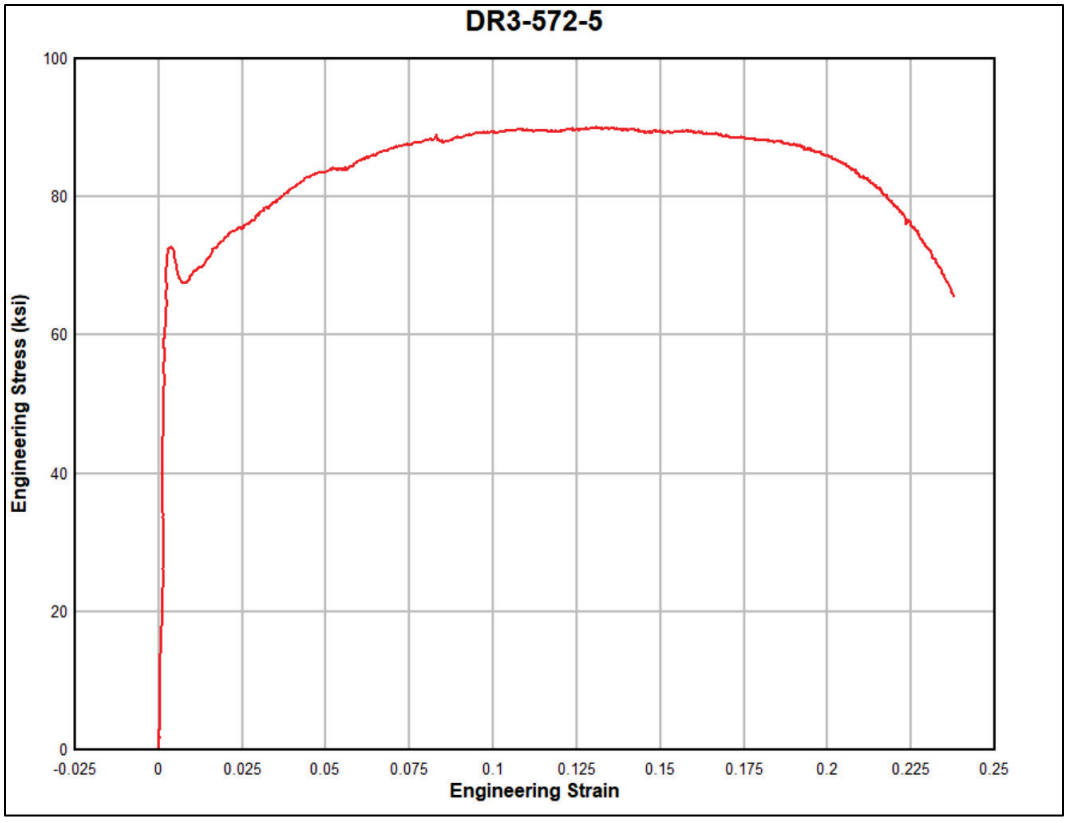
DR3-572-5
Engineering Stress (ksi)
100
80
60
40
20
0
-0.025
0
0.025
0.05
0.075
0.1
0.125
0.15
0.175
0.2
0.225
0.25
Engineering Strain

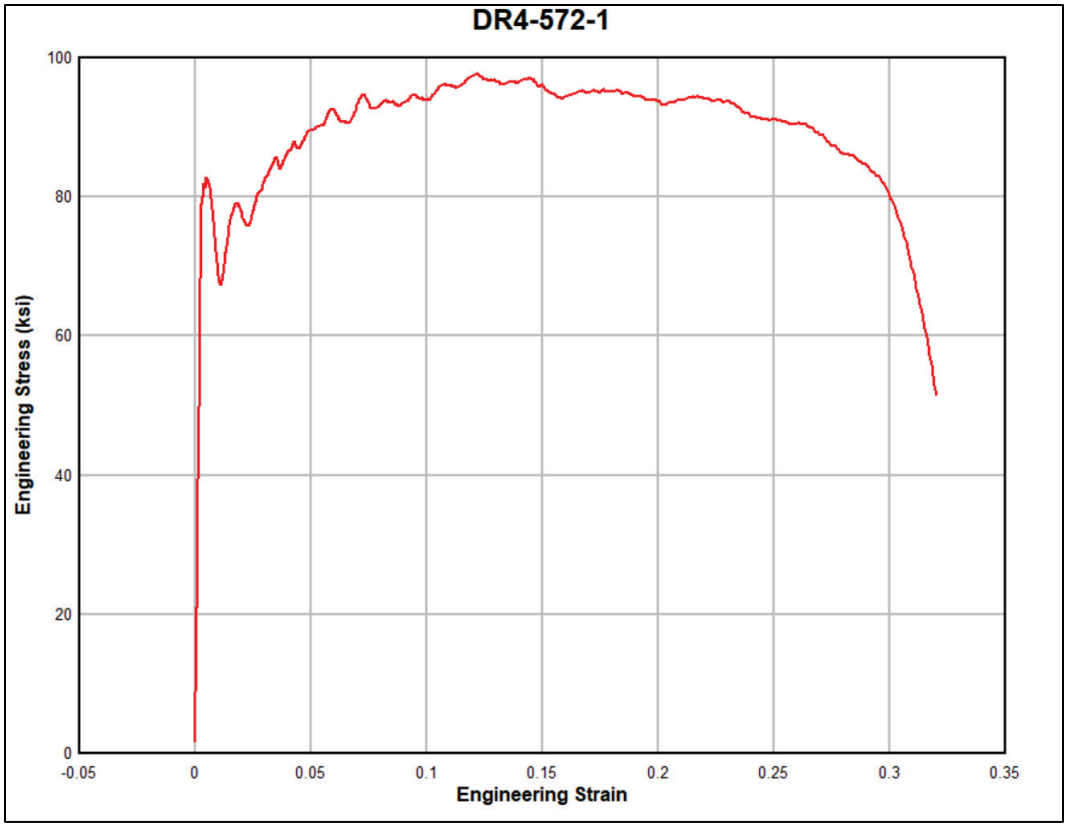
DR4-572-1
Engineering Stress (ksi)
100
80
60
40
20
0
-0.05
0
0.05
0.1
0.15
0.2
0.25
0.3
0.35
Engineering Strain

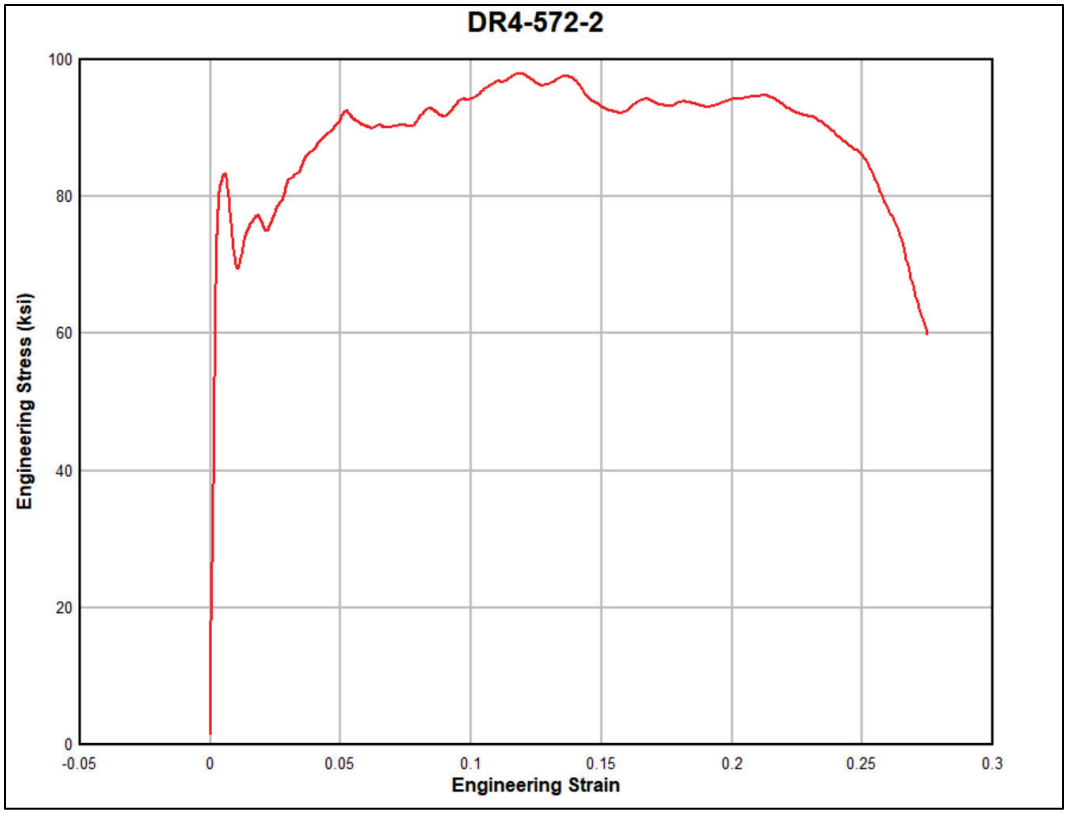
DR4-572-2
Engineering Stress (ksi)
100
80
60
40
20
0
-0.05
0
0.05
0.1
0.15
0.2
0.25
0.3
Engineering Strain

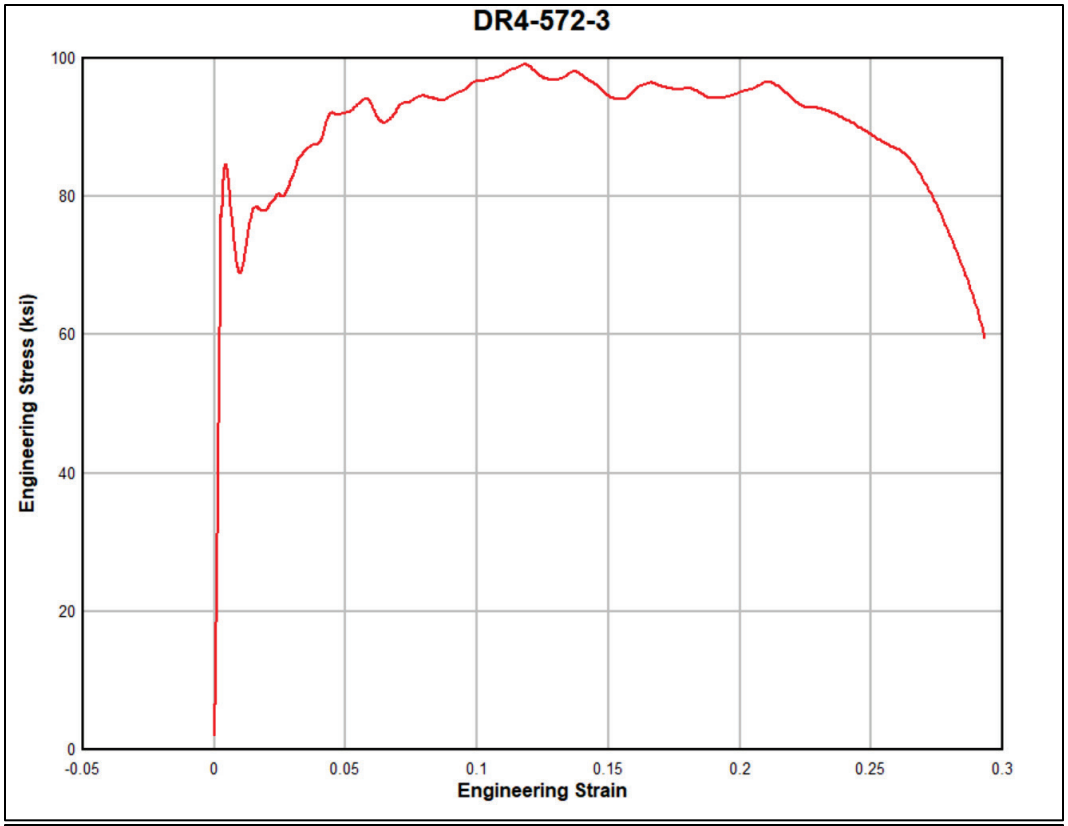
DR4-572-3
Engineering Stress (ksi)
100
80
60
40
20
0
-0.05
0
0.05
0.1
0.15
0.2
0.25
0.3
Engineering Strain

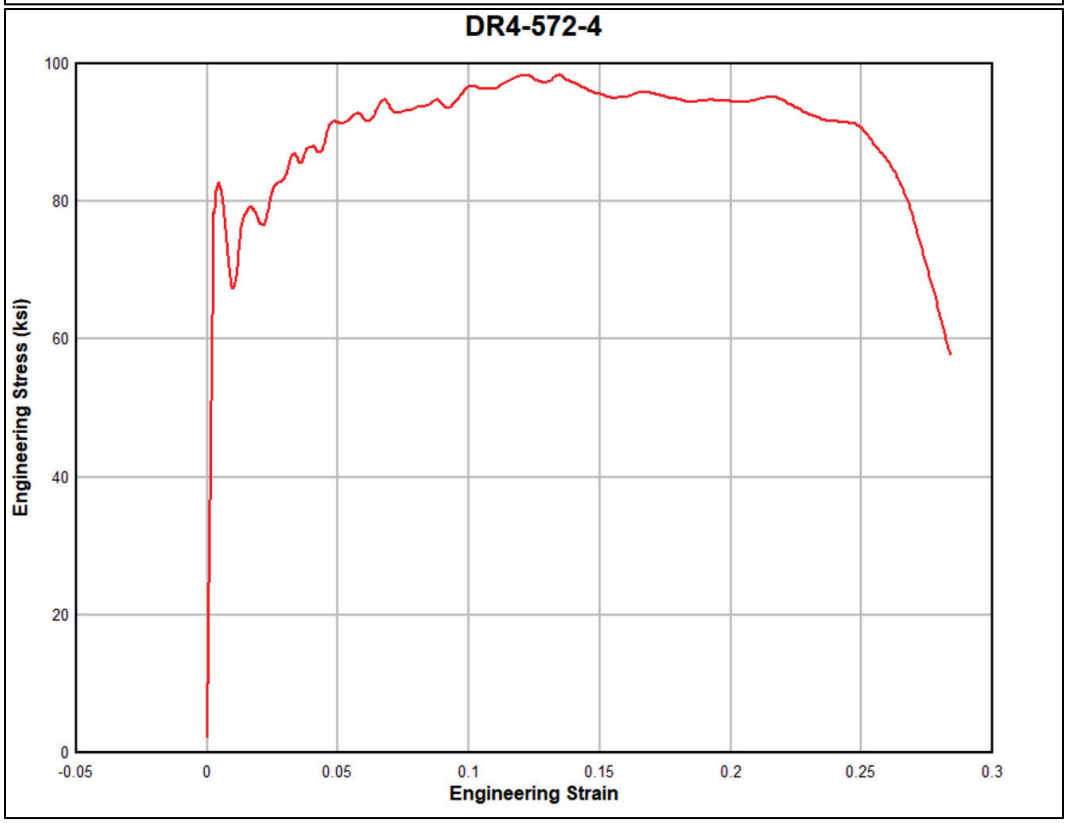
DR4-572-4
Engineering Stress (ksi)
100
80
60
40
20
0
-0.05
0
0.05
0.1
0.15
0.2
0.25
0.3
Engineering Strain

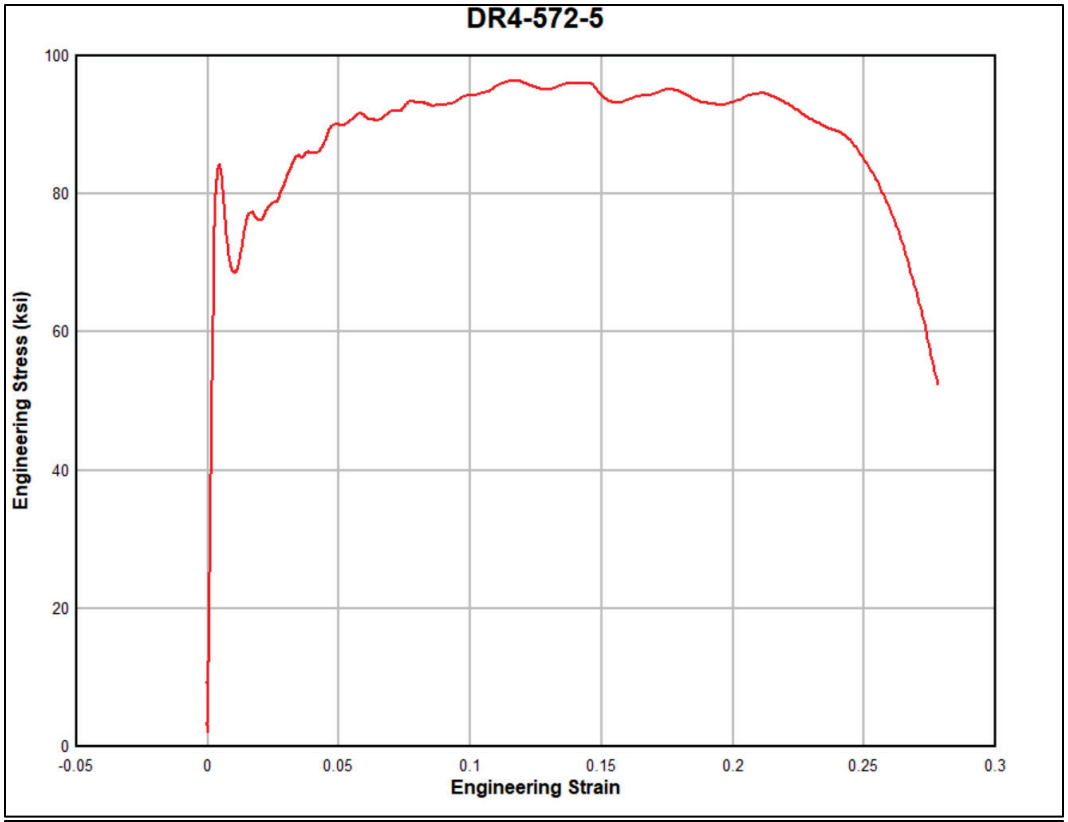
DR4-572-5
Engineering Stress (ksi)
100
80
60
40
20
0
-0.05
0
0.05
0.1
0.15
0.2
0.25
0.3
Engineering Strain

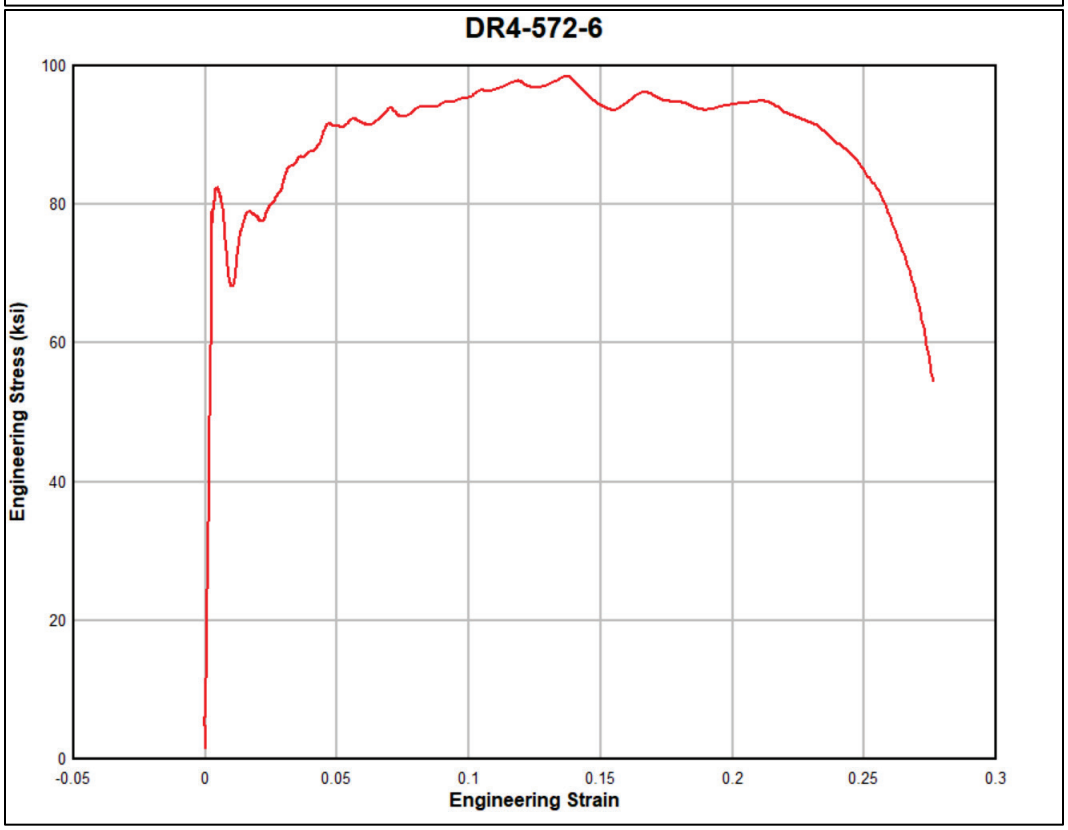
DR4-572-6
Engineering Stress (ksi)
100
80
60
40
20
0
-0.05
0
0.05
0.1
0.15
0.2
0.25
0.3
Engineering Strain

Appendix B: ASTM A992 Stress-Strain Diagrams

The following 41 figures present ASTM A992 stress-strain diagrams.

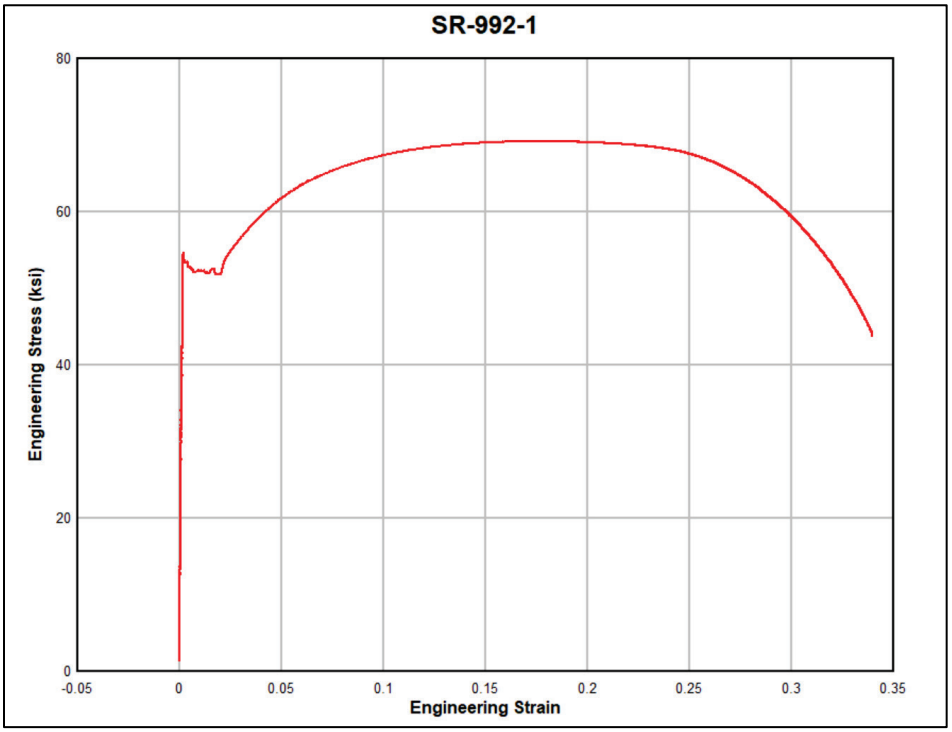

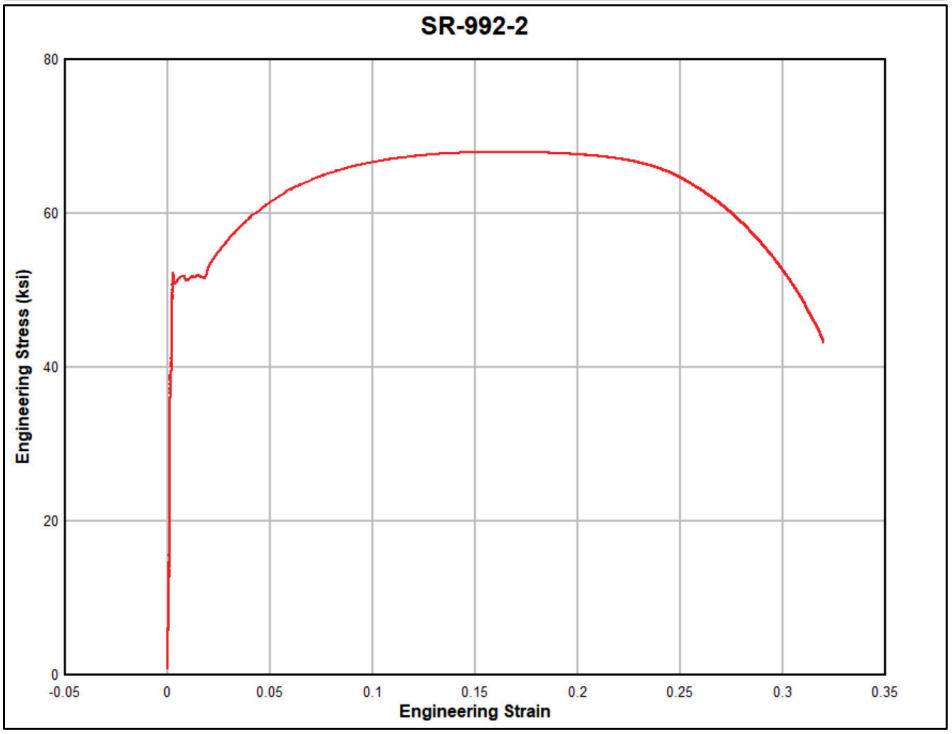

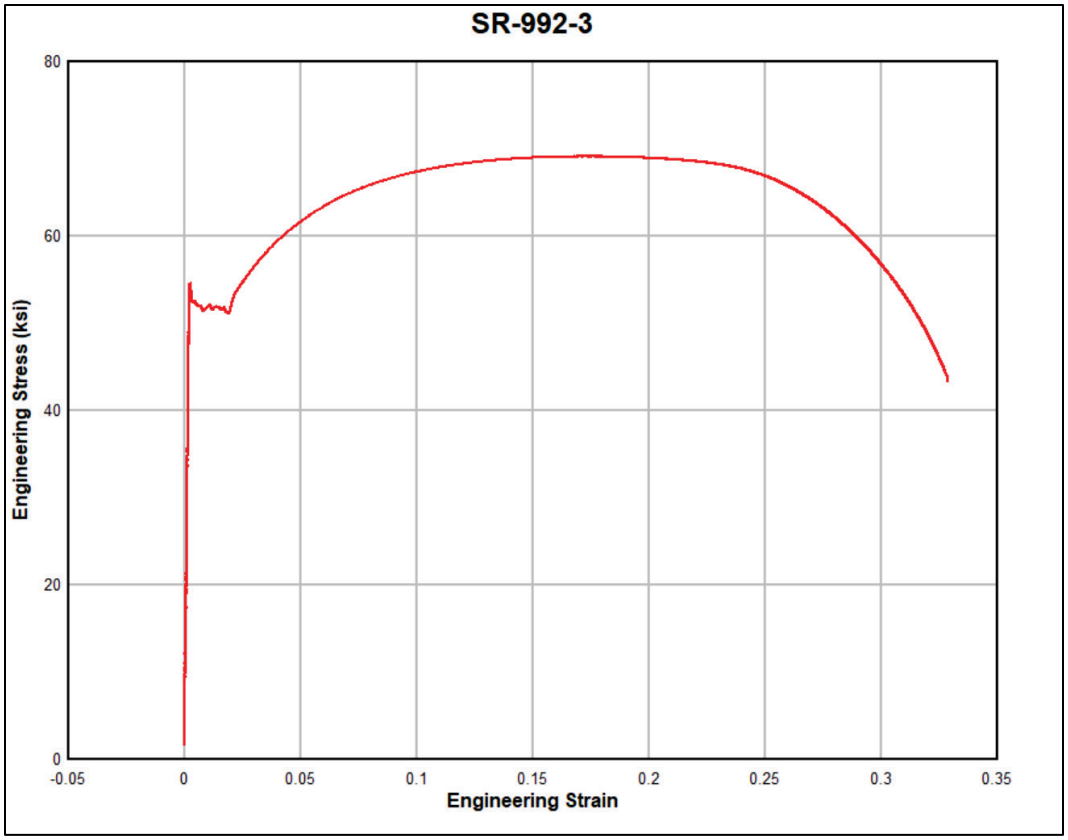
SR-992-3
Engineering Stress (ksi)
80
60
40
20
0
-0.05
0
0.05
0.1
0.15
0.2
0.25
0.3
0.35
Engineering Strain

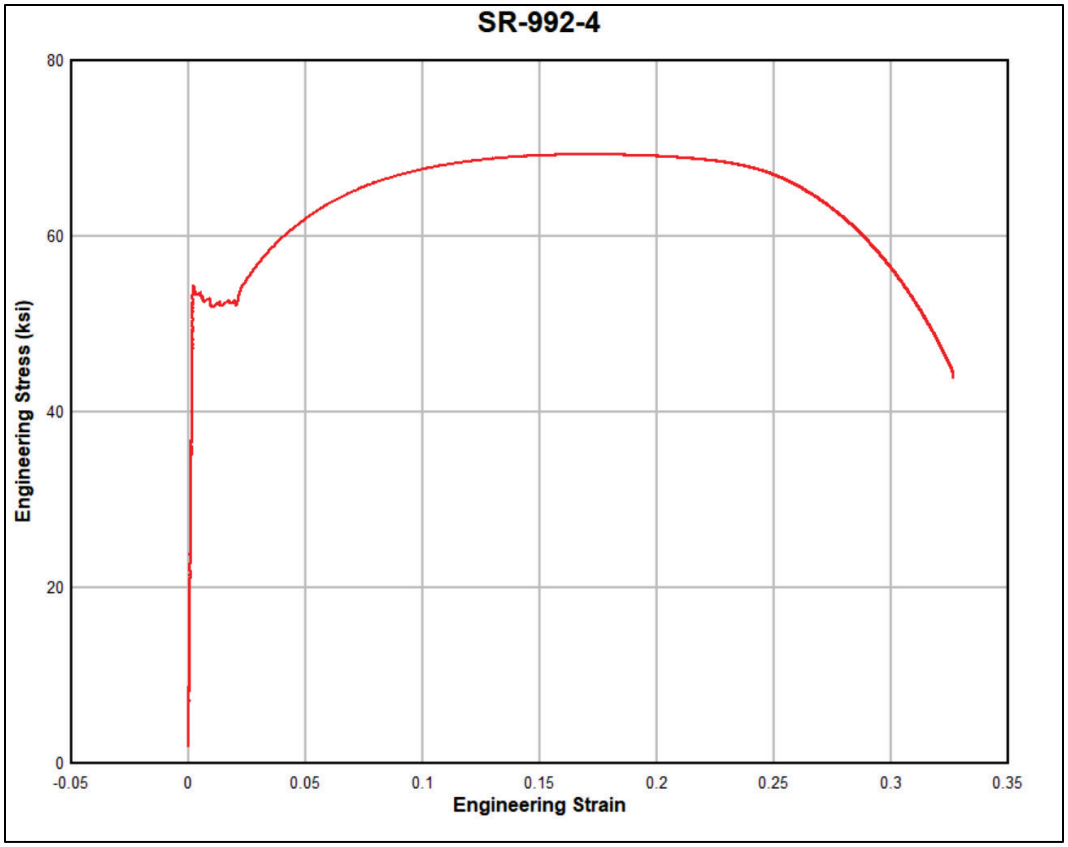
SR-992-4
Engineering Stress (ksi)
80
60
40
20
0
-0.05
0
0.05
0.1
0.15
0.2
0.25
0.3
0.35
Engineering Strain

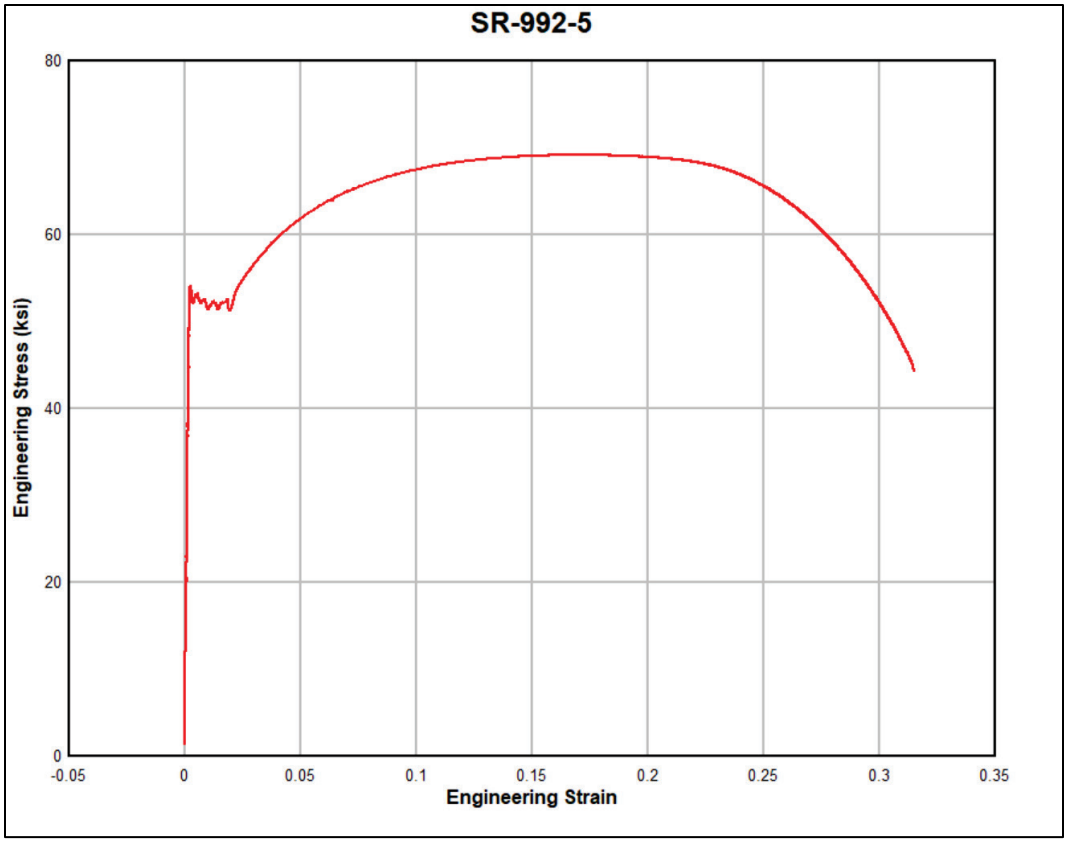
SR-992-5
Engineering Stress (ksi)
80
60
40
20
0
-0.05
0
0.05
0.1
0.15
0.2
0.25
0.3
0.35
Engineering Strain

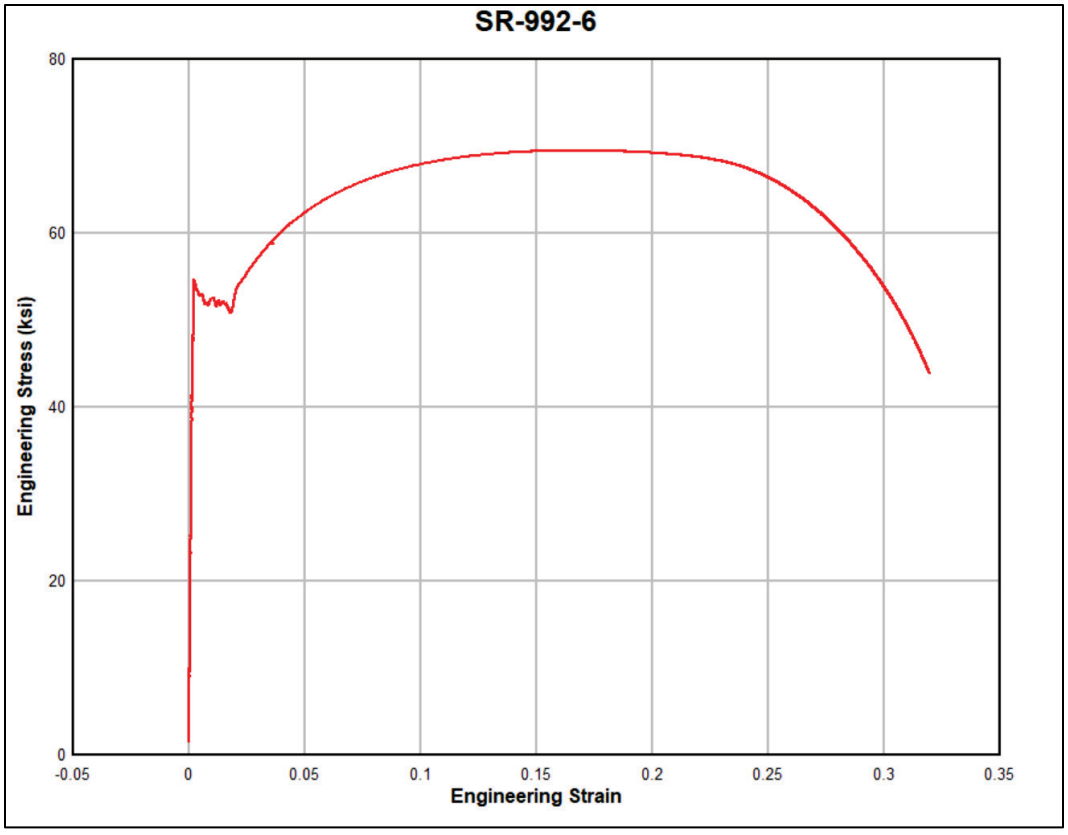
SR-992-6
Engineering Stress (ksi)
80
60
40
20
0
-0.05
0
0.05
0.1
0.15
0.2
0.25
0.3
0.35
Engineering Strain

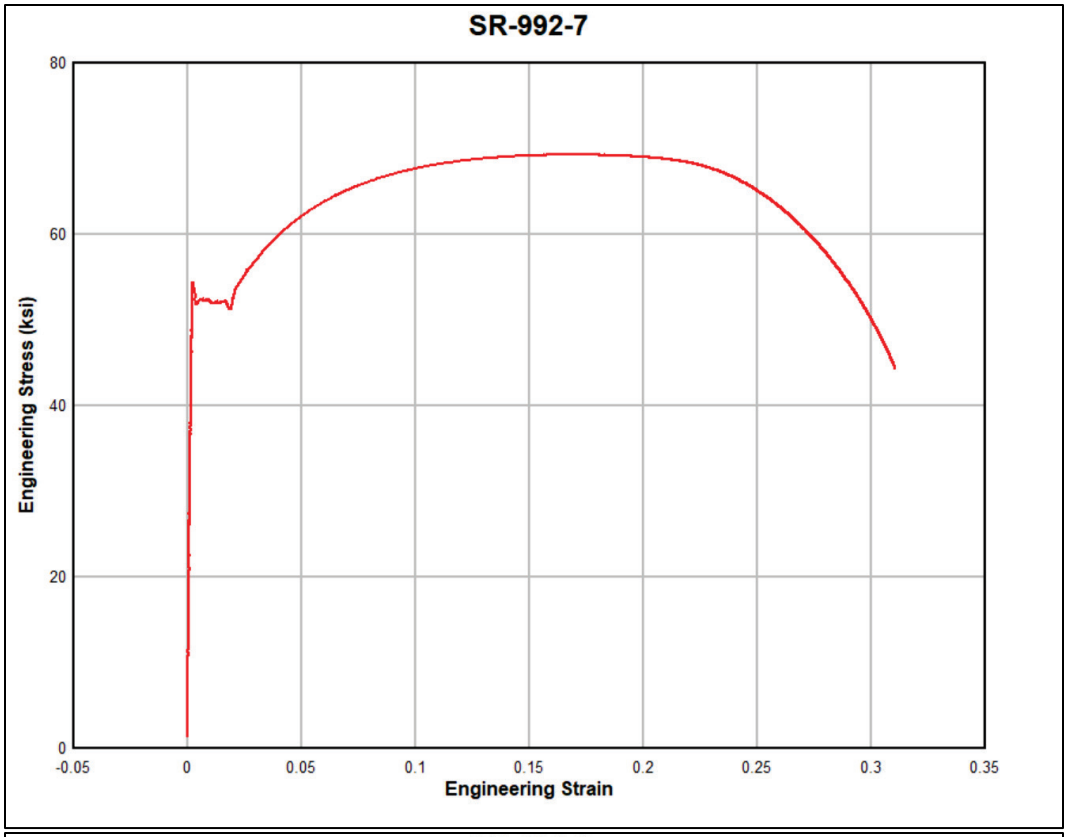
SR-992-7
Engineering Stress (ksi)
80
60
40
20
0
-0.05
0
0.05
0.1
0.15
0.2
0.25
0.3
0.35
Engineering Strain

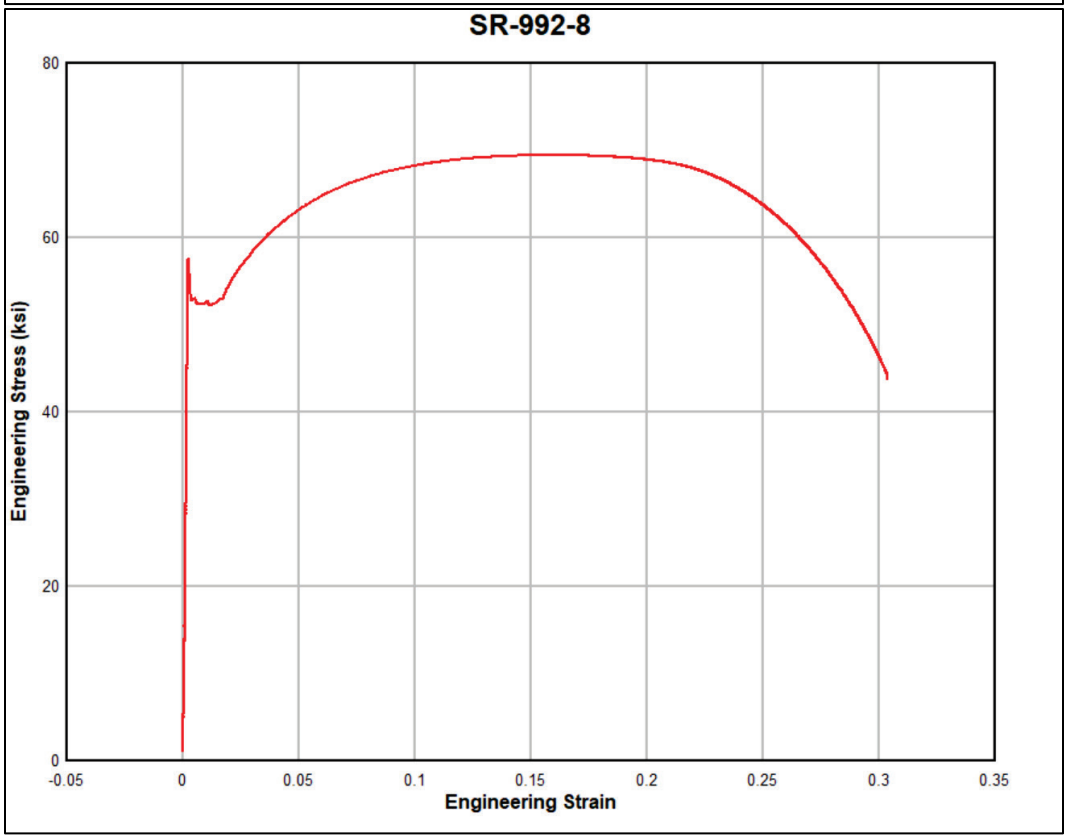
SR-992-8
Engineering Stress (ksi)
80
60
40
20
0
-0.05
0
0.05
0.1
0.15
0.2
0.25
0.3
0.35
Engineering Strain

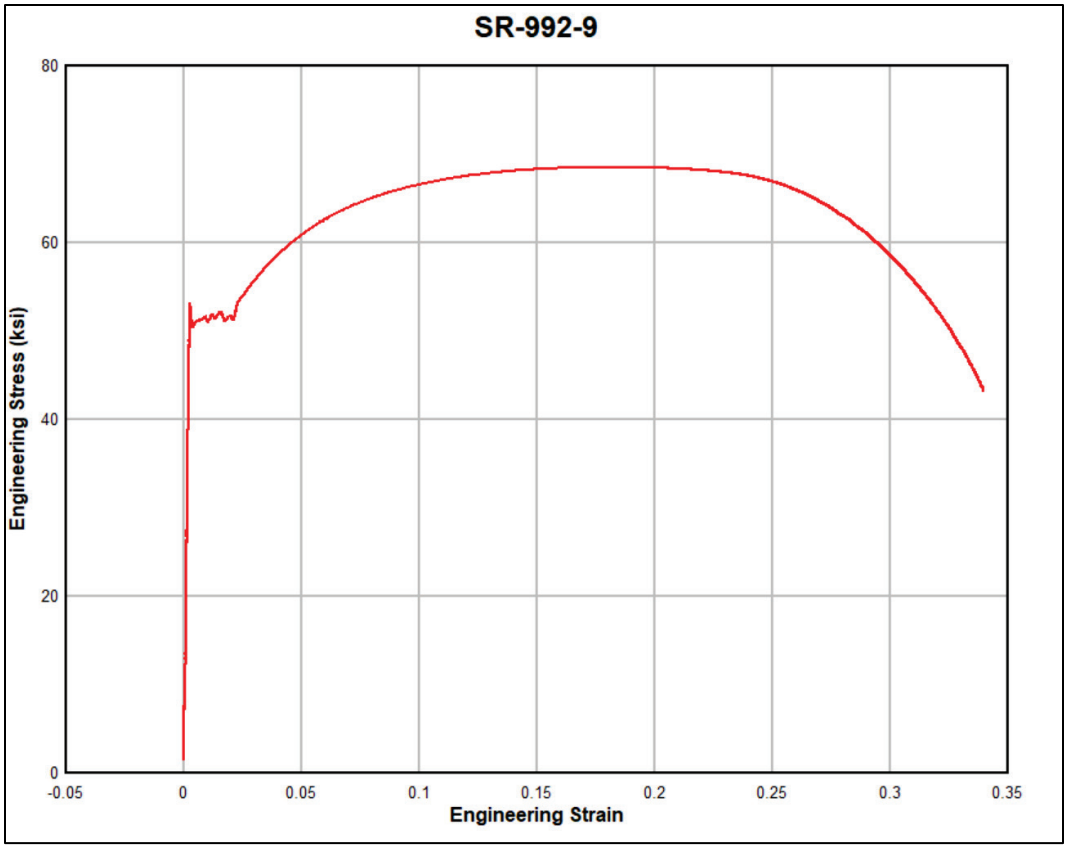
SR-992-9
Engineering Stress (ksi)
80
60
40
20
0
-0.05
0
0.05
0.1
0.15
0.2
0.25
0.3
0.35
Engineering Strain

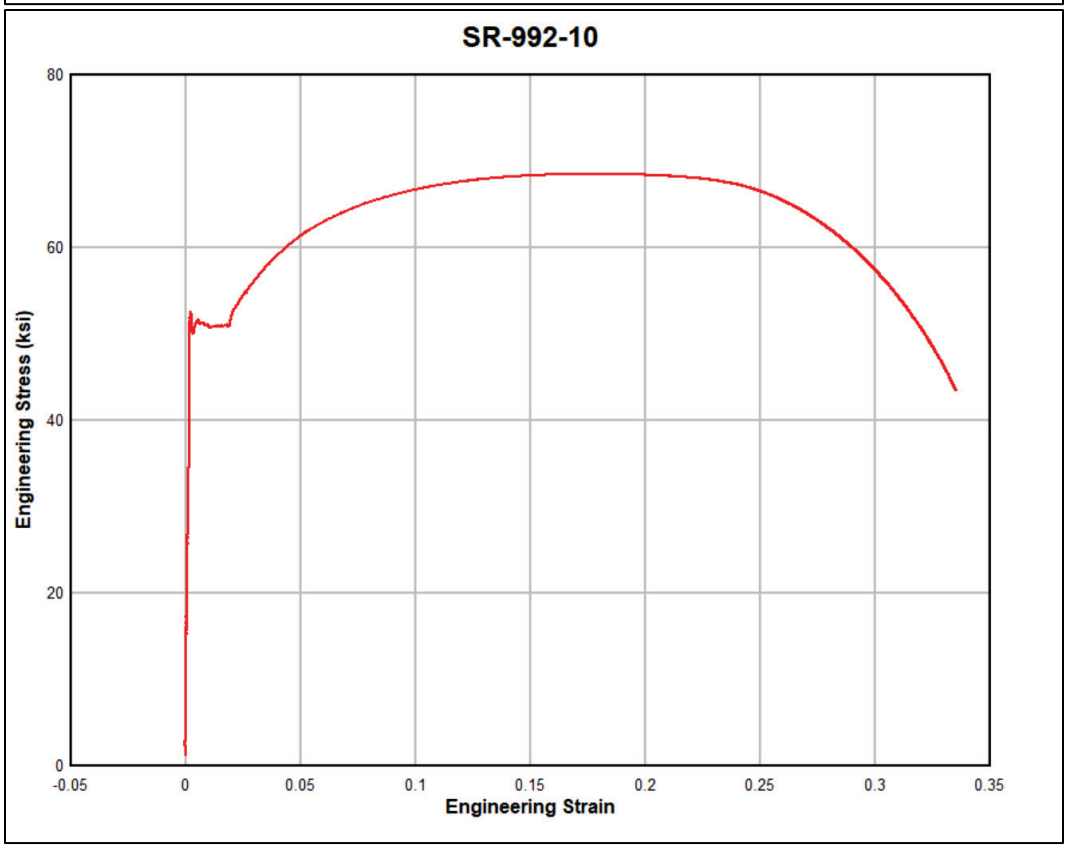
SR-992-10
Engineering Stress (ksi)
80
60
40
20
0
-0.05
0
0.05
0.1
0.15
0.2
0.25
0.3
0.35
Engineering Strain

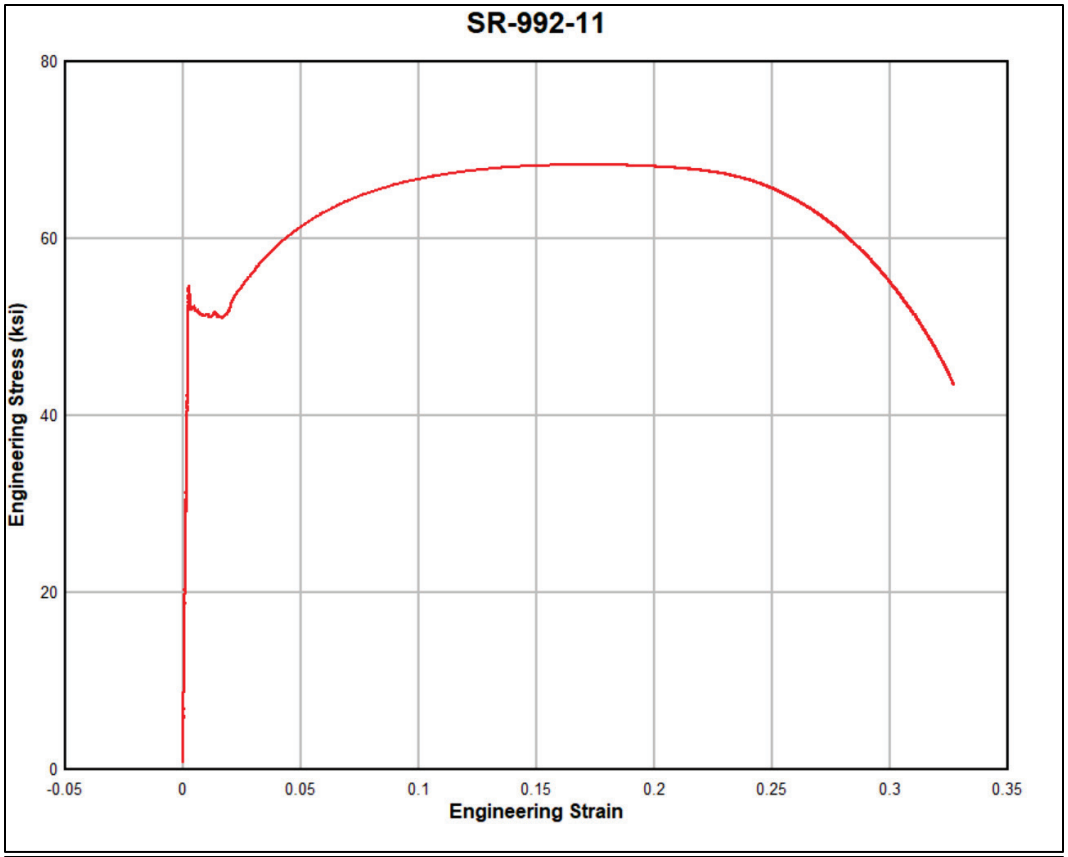
SR-992-11
Engineering Stress (ksi)
80
60
40
20
0
-0.05
0
0.05
0.1
0.15
0.2
0.25
0.3
0.35
Engineering Strain

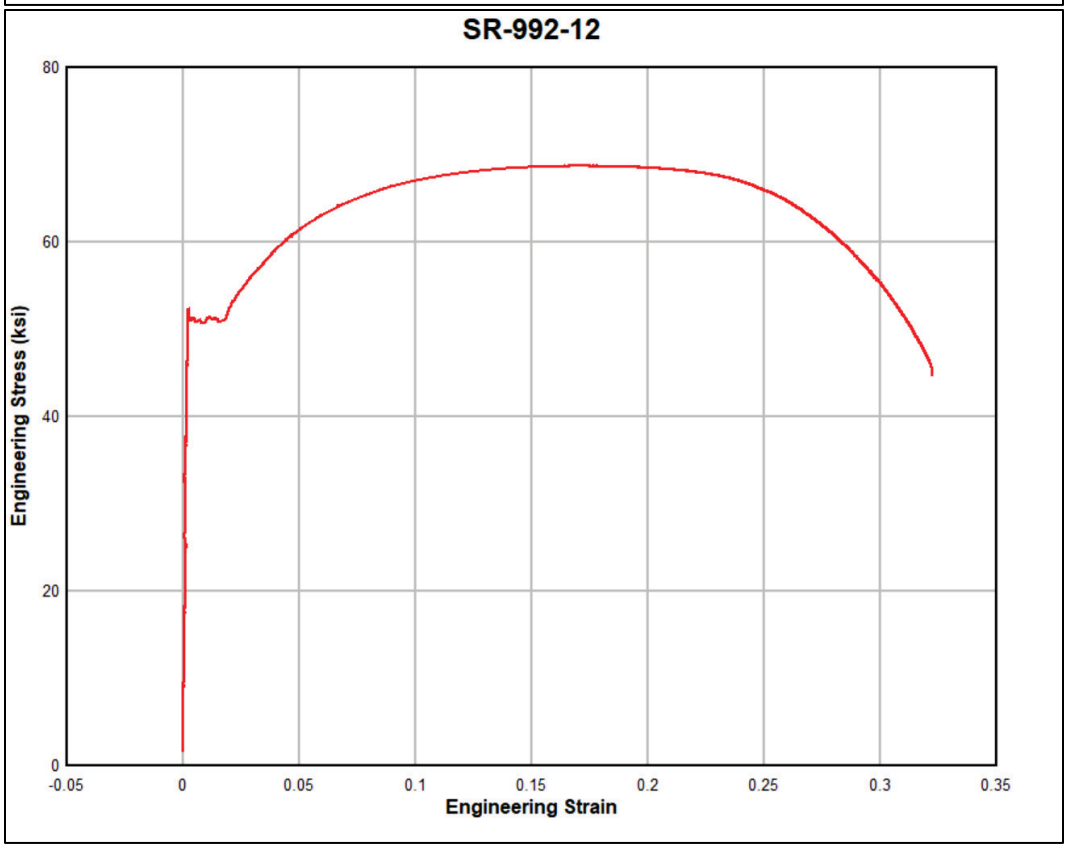
SR-992-12
Engineering Stress (ksi)
80
60
40
20
0
-0.05
0
0.05
0.1
0.15
0.2
0.25
0.3
0.35
Engineering Strain

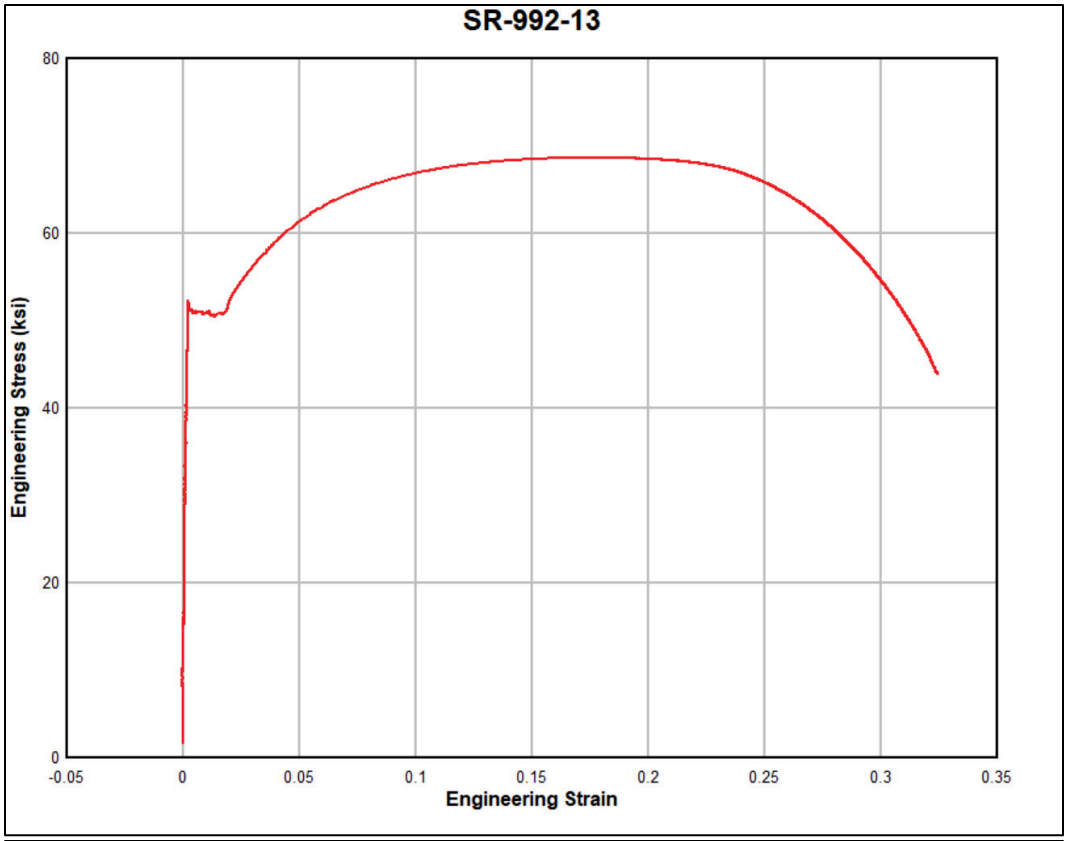
SR-992-13
Engineering Stress (ksi)
80
60
40
20
0
-0.05
0
0.05
0.1
0.15
0.2
0.25
0.3
0.35
Engineering Strain

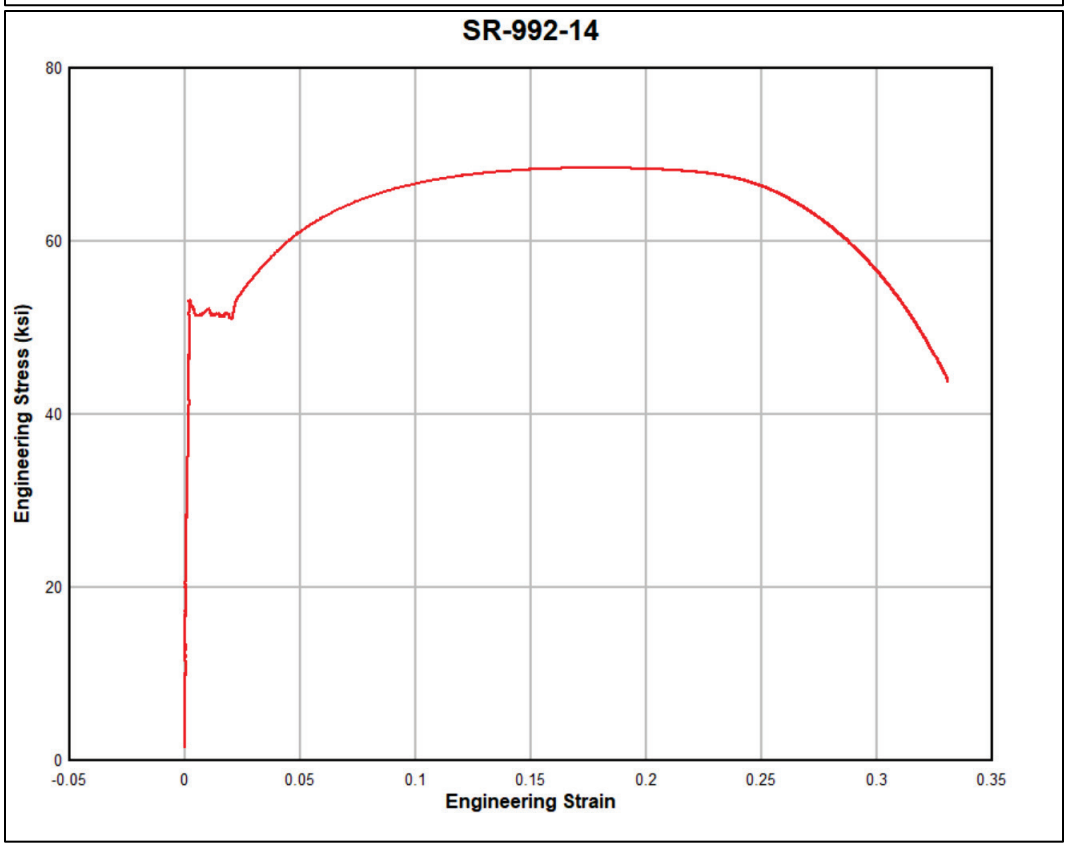
SR-992-14
Engineering Stress (ksi)
80
60
40
20
0
-0.05
0
0.05
0.1
0.15
0.2
0.25
0.3
0.35
Engineering Strain

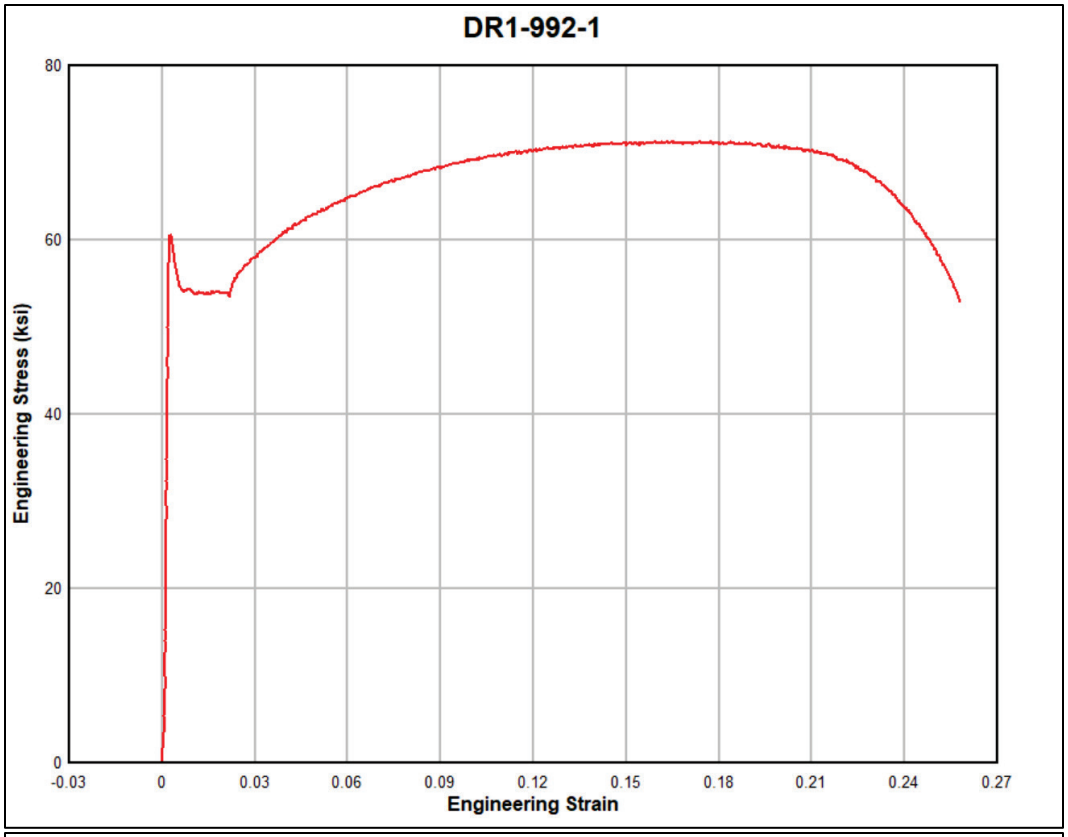
DR1-992-1
Engineering Stress (ksi)
80
60
40
20
0
-0.03
0
0.03
0.06
0.09
0.12
0.15
0.18
0.21
0.24
0.27
Engineering Strain

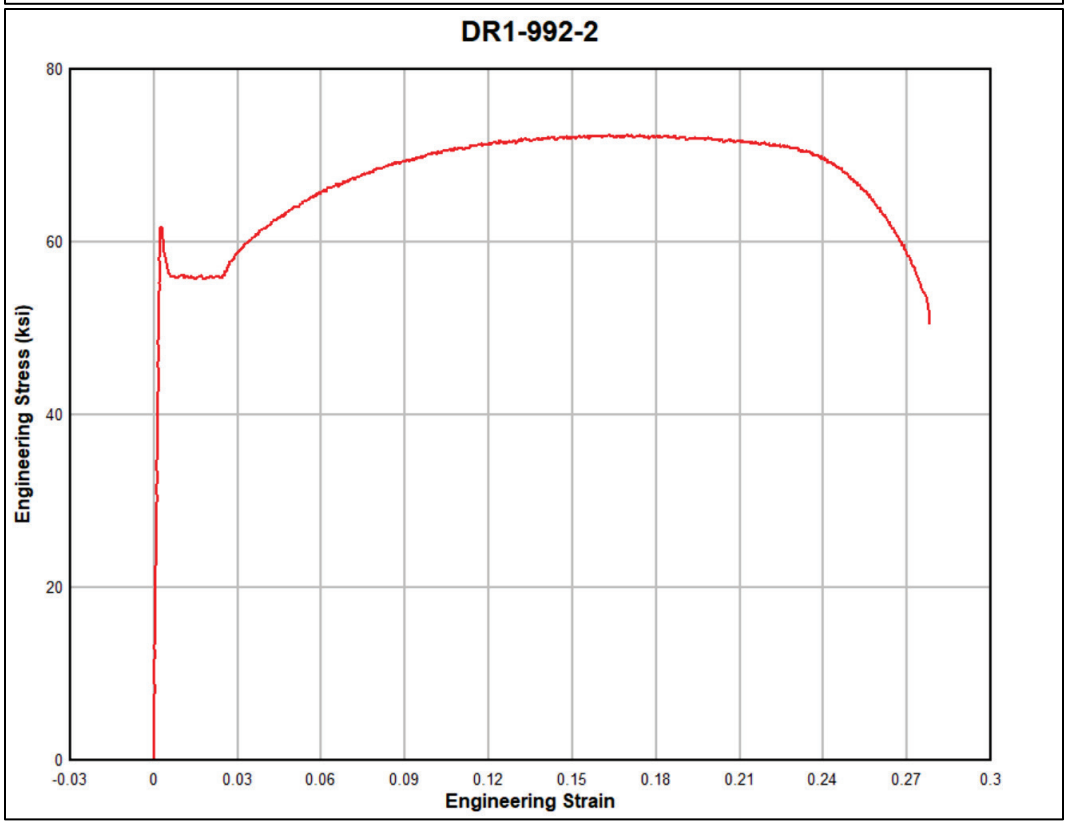
DR1-992-2
Engineering Stress (ksi)
80
60
40
20
0
-0.03
0
0.03
0.06
0.09
0.12
0.15
0.18
0.21
0.24
0.27
0.3
Engineering Strain

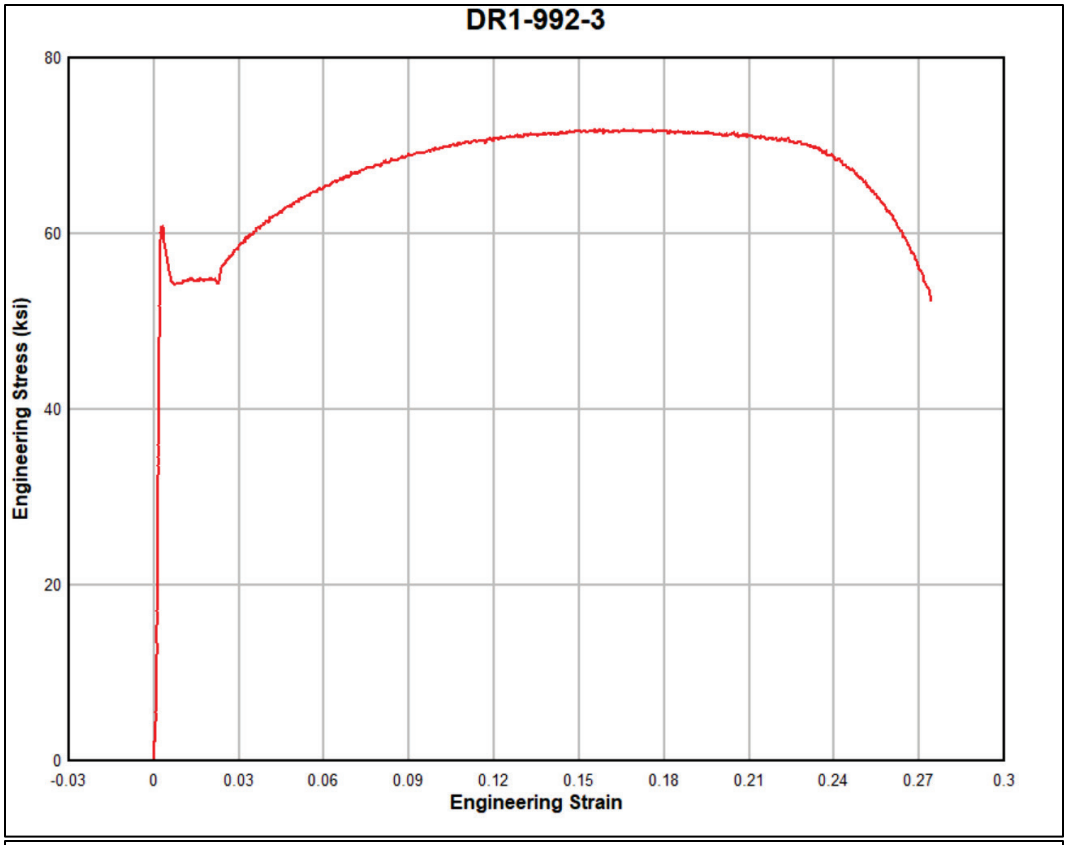
DR1-992-3
Engineering Stress (ksi)
80
60
40
20
0
-0.03
0
0.03
0.06
0.09
0.12
0.15
0.18
0.21
0.24
0.27
0.3
Engineering Strain

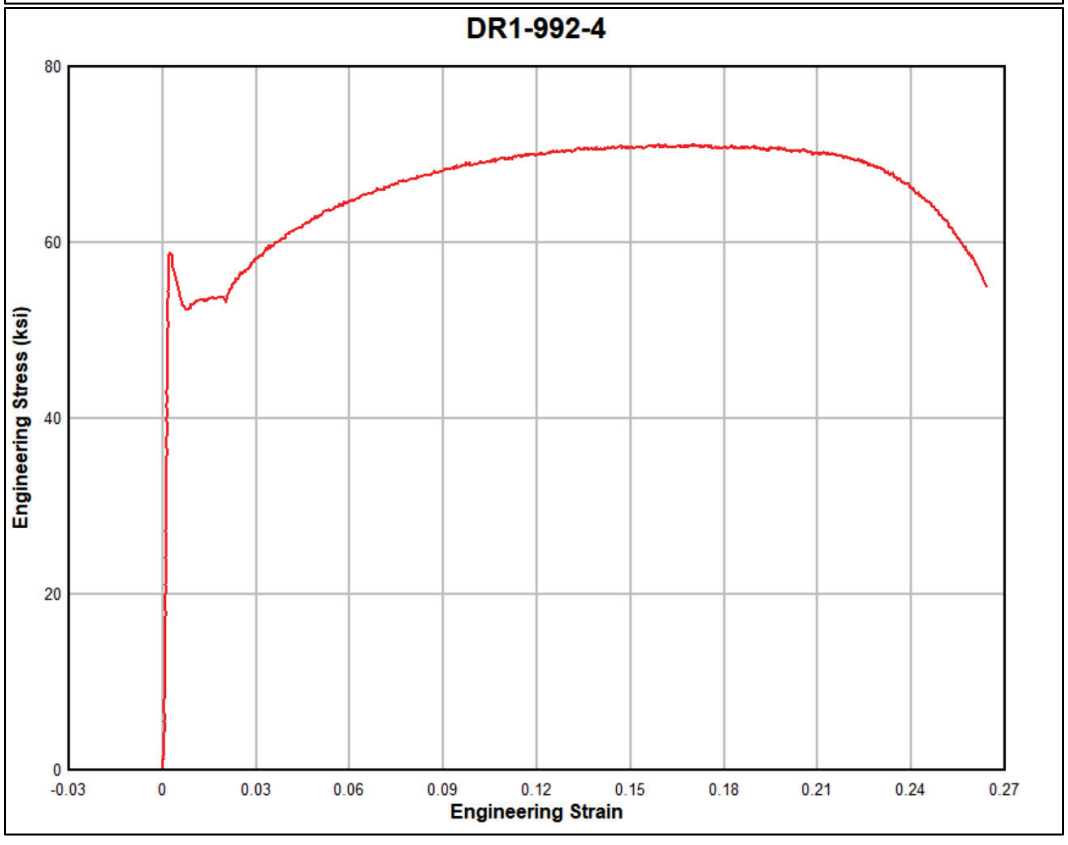
DR1-992-4
Engineering Stress (ksi)
80
60
40
20
0
-0.03
0
0.03
0.06
0.09
0.12
0.15
0.18
0.21
0.24
0.27
Engineering Strain

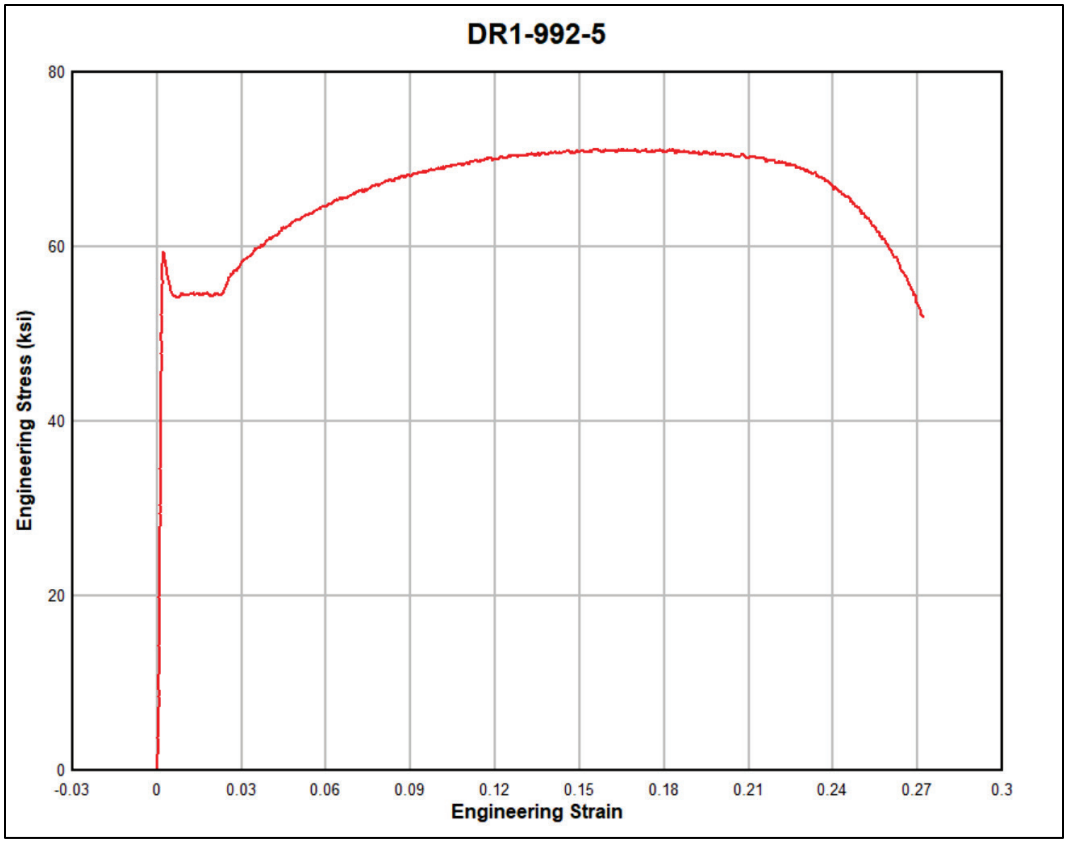
DR1-992-5
Engineering Stress (ksi)
80
60
40
20
0
-0.03
0
0.03
0.06
0.09
0.12
0.15
0.18
0.21
0.24
0.27
0.3
Engineering Strain

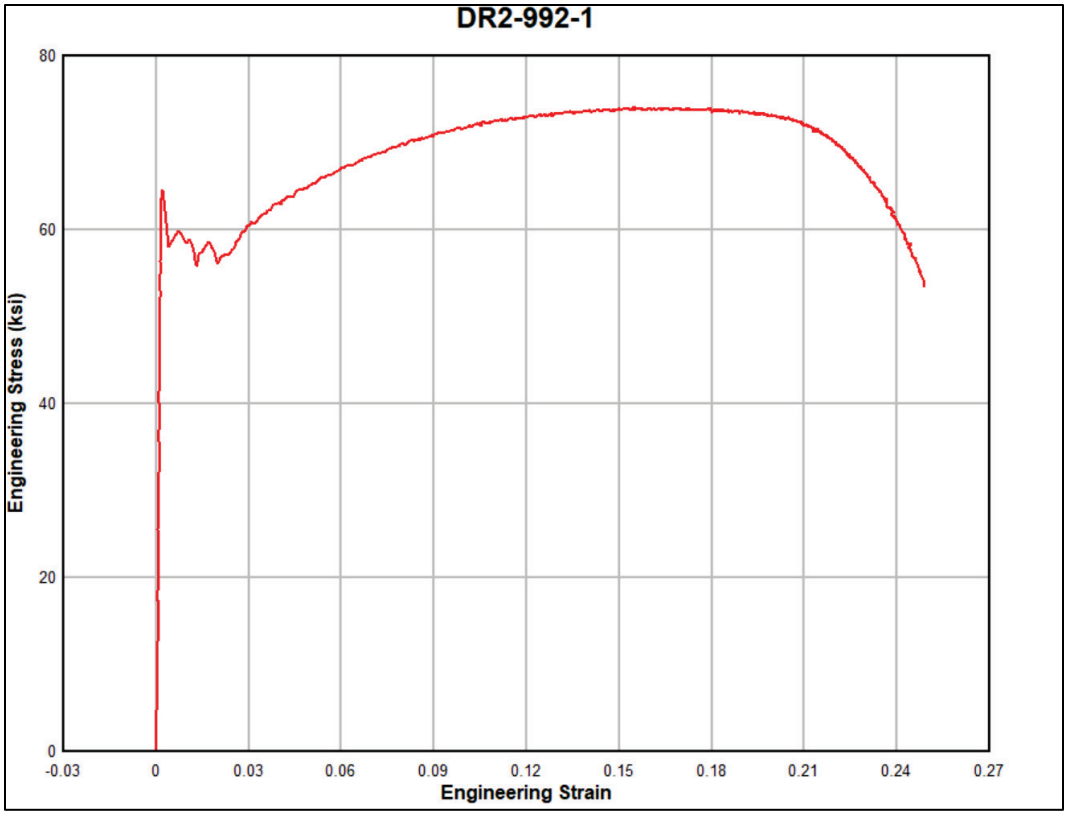
DR2-992-1
Engineering Stress (ksi)
80
60
40
20
0
-0.03
0
0.03
0.06
0.09
0.12
0.15
0.18
0.21
0.24
0.27
Engineering Strain

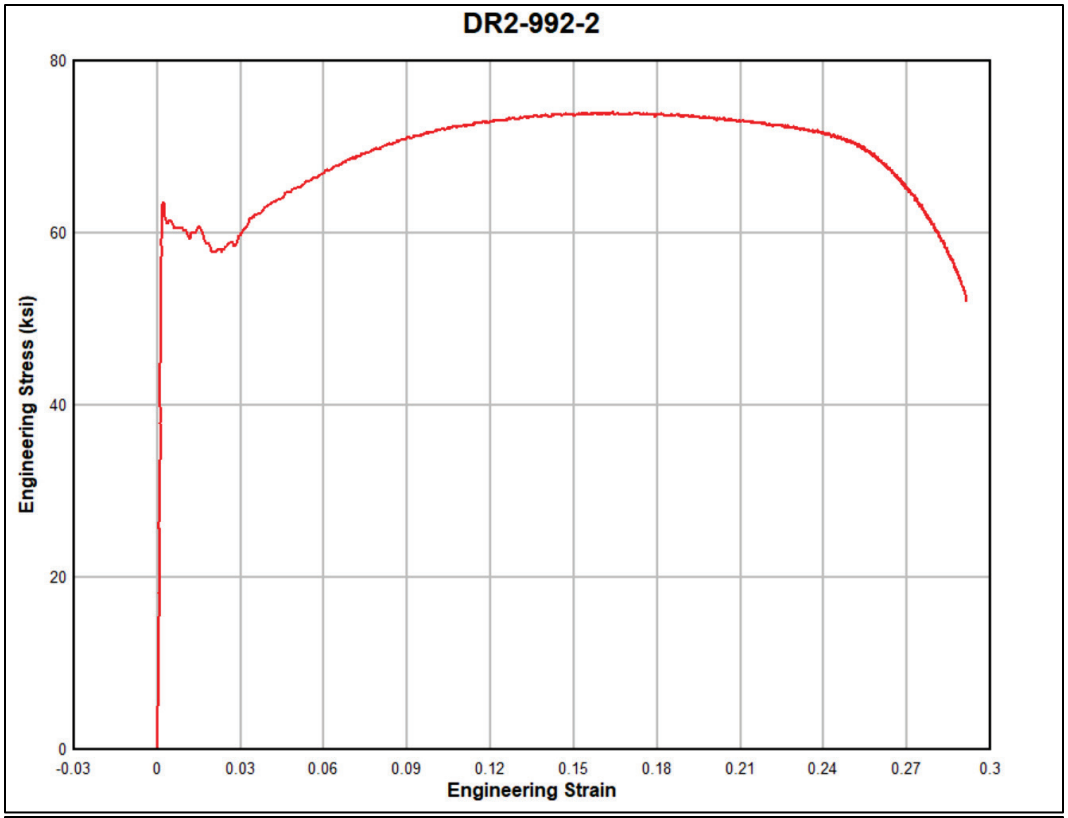
DR2-992-2
Engineering Stress (ksi)
80
60
40
20
0
-0.03
0
0.03
0.06
0.09
0.12
0.15
0.18
0.21
0.24
0.27
0.3
Engineering Strain

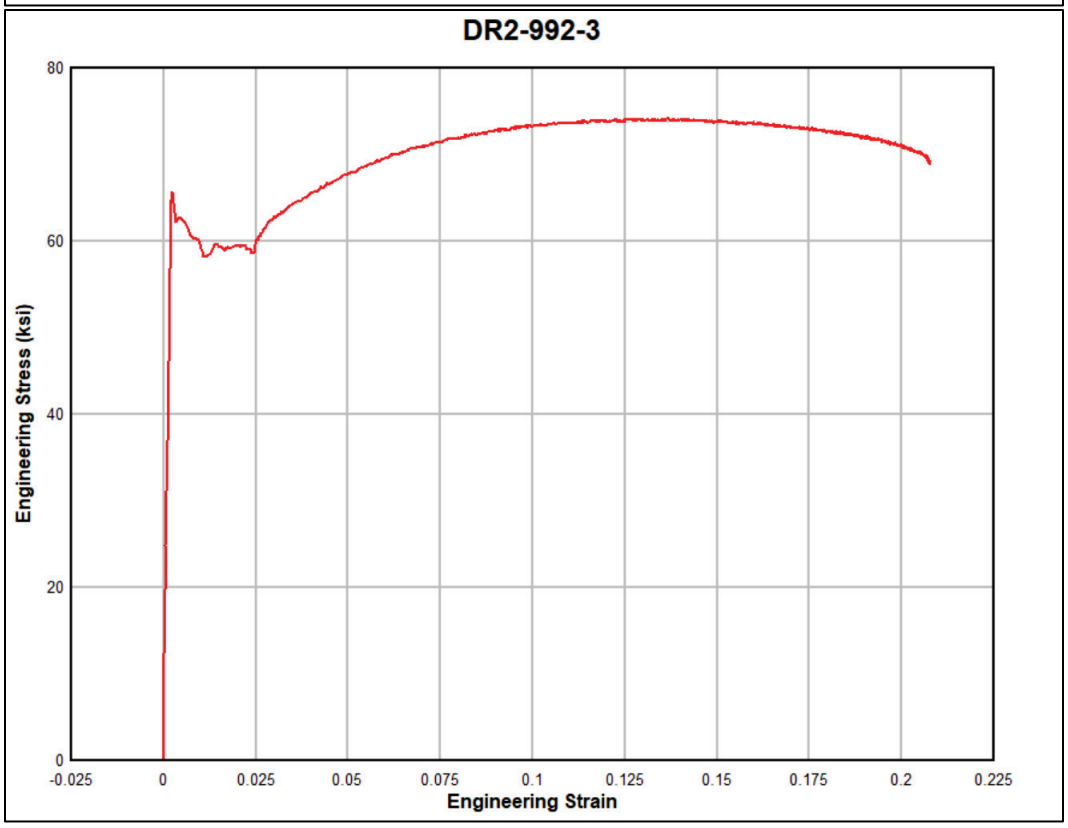
DR2-992-3
Engineering Stress (ksi)
80
60
40
20
0
-0.025
0
0.025
0.05
0.075
0.1
0.125
0.15
0.175
0.2
0.225
Engineering Strain

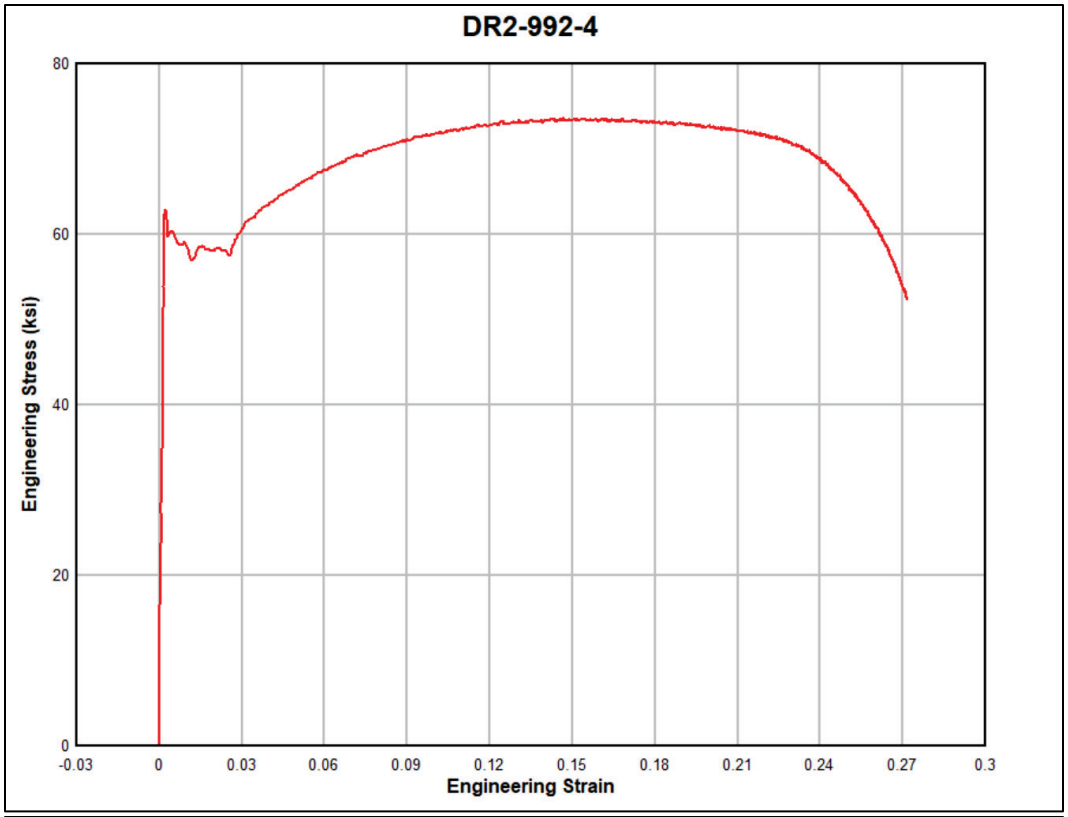
DR2-992-4
Engineering Stress (ksi)
80
60
40
20
0
-0.03
0
0.03
0.06
0.09
0.12
0.15
0.18
0.21
0.24
0.27
0.3
Engineering Strain

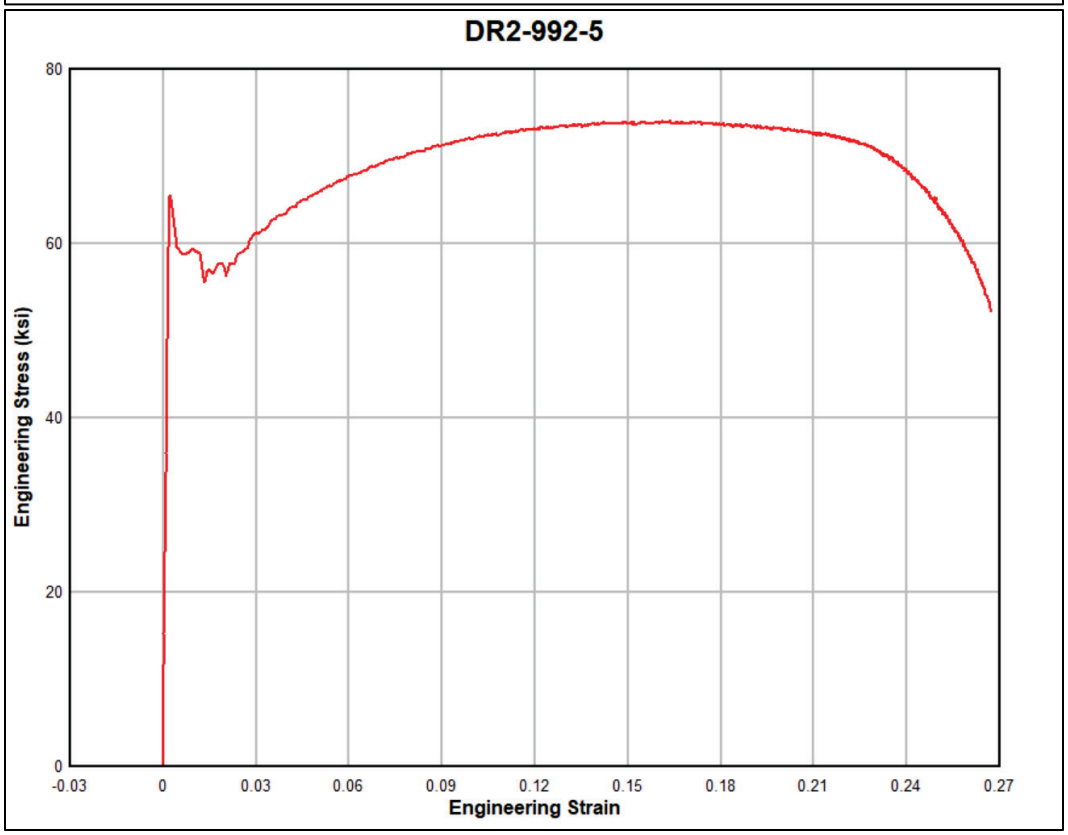
DR2-992-5
Engineering Stress (ksi)
80
60
40
20
0
-0.03
0
0.03
0.06
0.09
0.12
0.15
0.18
0.21
0.24
0.27
Engineering Strain

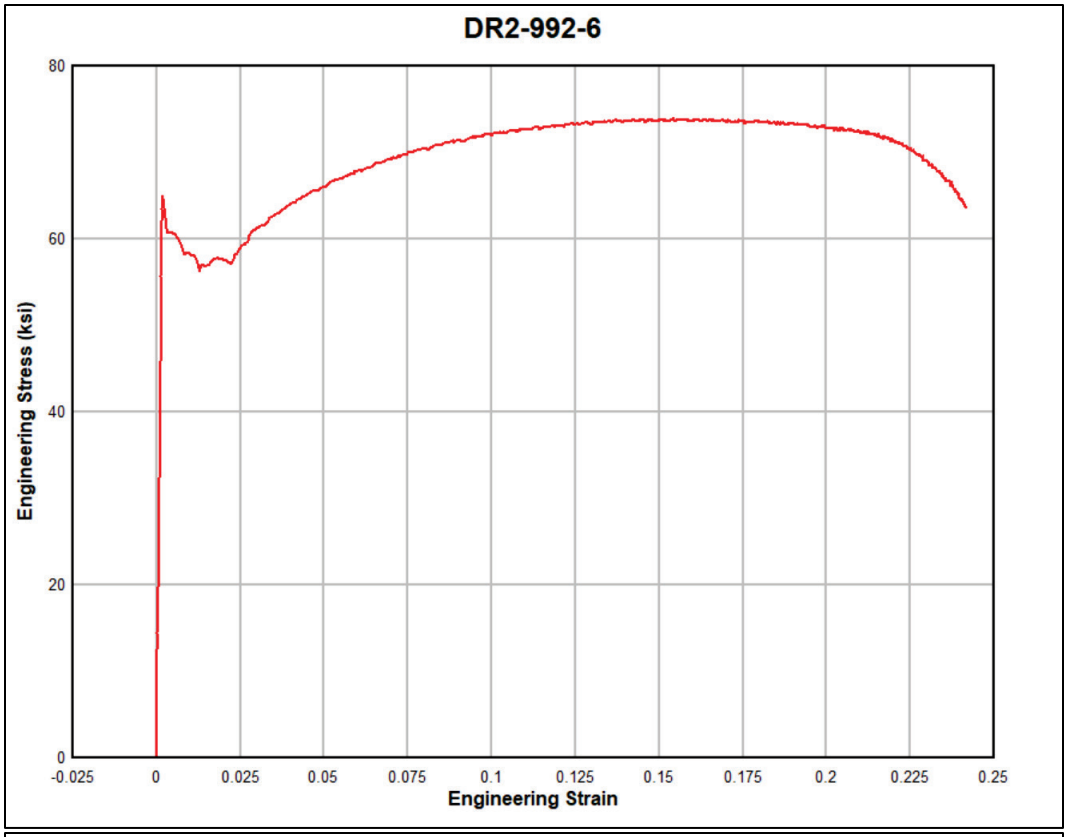
DR2-992-6
Engineering Stress (ksi)
80
60
40
20
0
-0.025
0
0.025
0.05
0.075
0.1
0.125
0.15
0.175
0.2
0.225
0.25
Engineering Strain

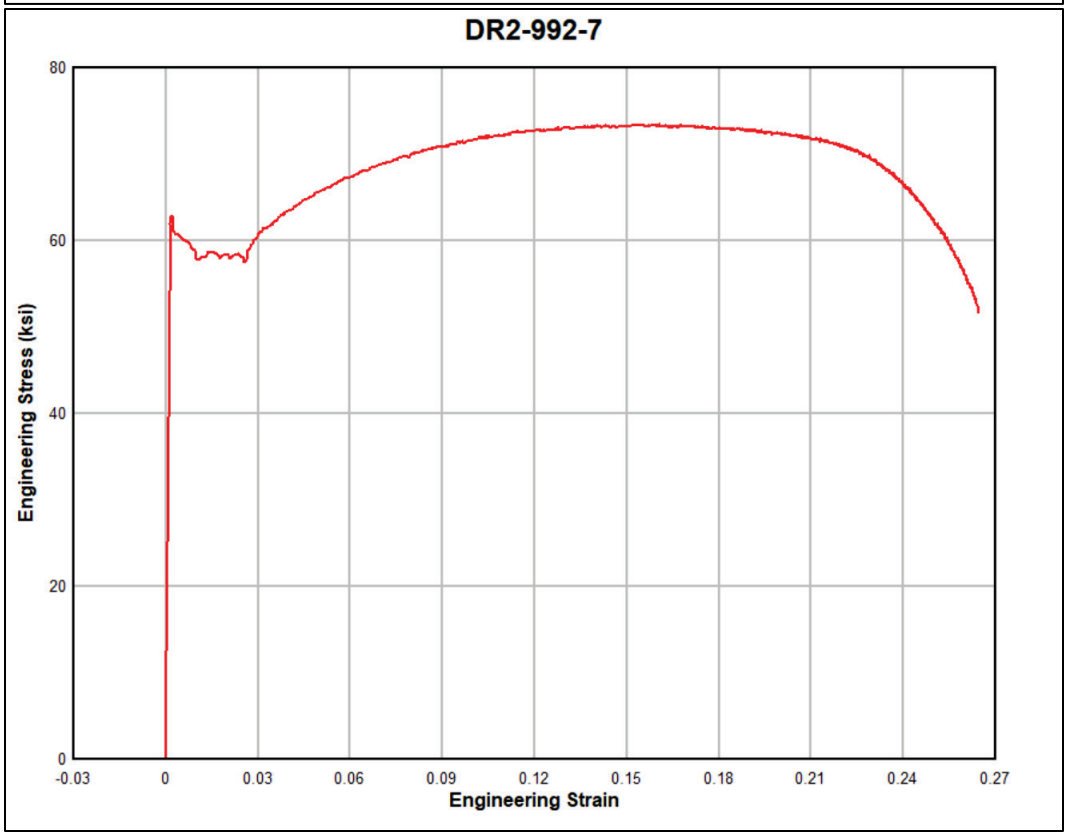
DR2-992-7
Engineering Stress (ksi)
80
60
40
20
0
-0.03
0
0.03
0.06
0.09
0.12
0.15
0.18
0.21
0.24
0.27
Engineering Strain

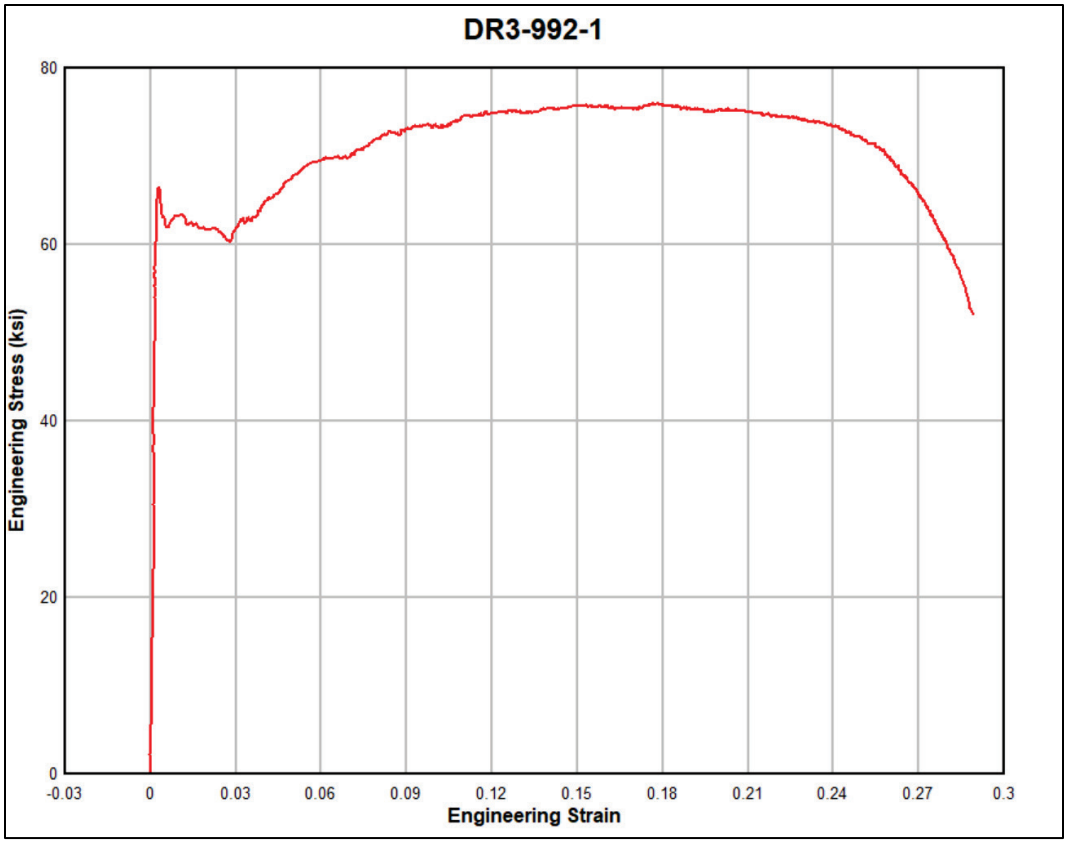
DR3-992-1
Engineering Stress (ksi)
80
60
40
20
0
-0.03
0
0.03
0.06
0.09
0.12
0.15
0.18
0.21
0.24
0.27
0.3
Engineering Strain

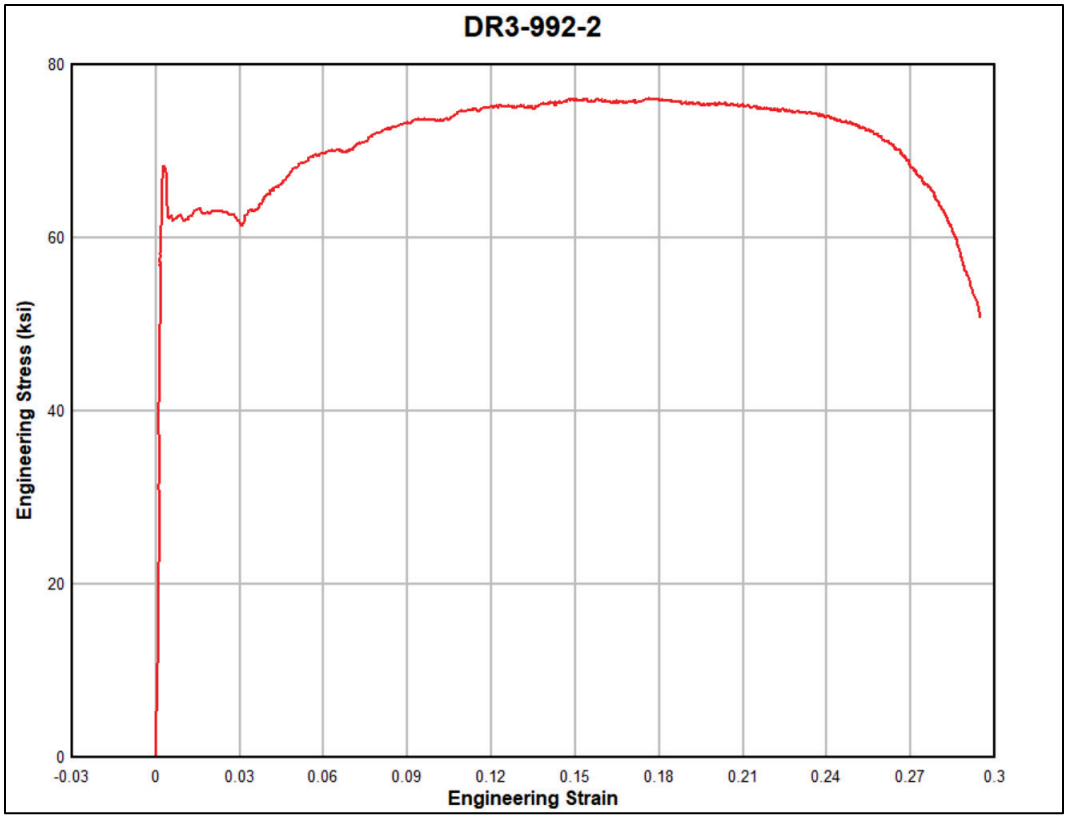
DR3-992-2
Engineering Stress (ksi)
80
60
40
20
0
-0.03
0
0.03
0.06
0.09
0.12
0.15
0.18
0.21
0.24
0.27
0.3
Engineering Strain

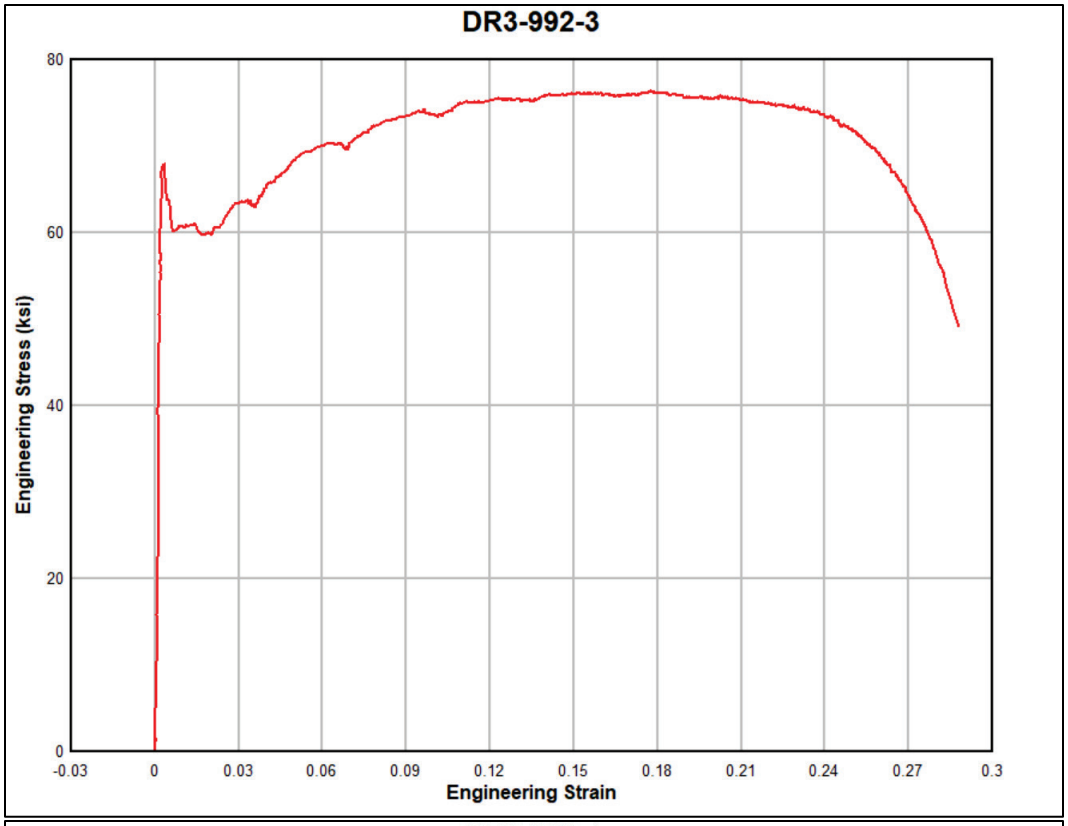
DR3-992-3
Engineering Stress (ksi)
80
60
40
20
0
-0.03
0
0.03
0.06
0.09
0.12
0.15
0.18
0.21
0.24
0.27
0.3
Engineering Strain

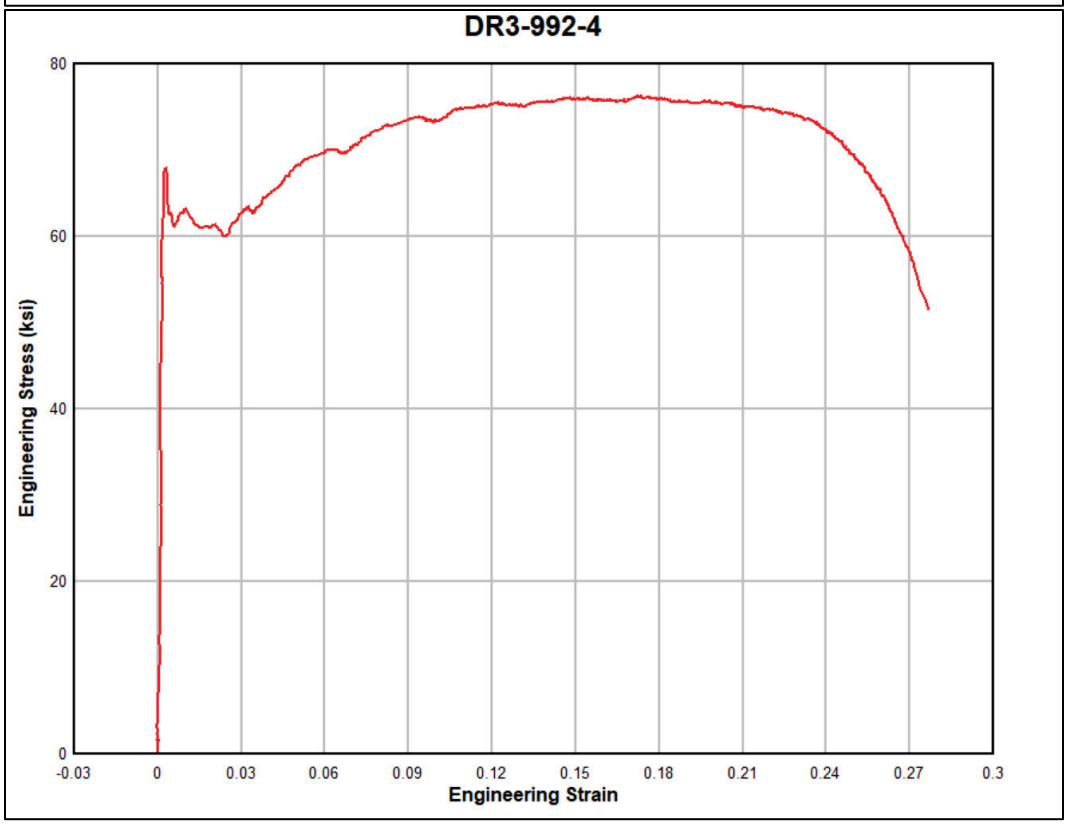
DR3-992-4
Engineering Stress (ksi)
80
60
40
20
0
-0.03
0
0.03
0.06
0.09
0.12
0.15
0.18
0.21
0.24
0.27
0.3
Engineering Strain

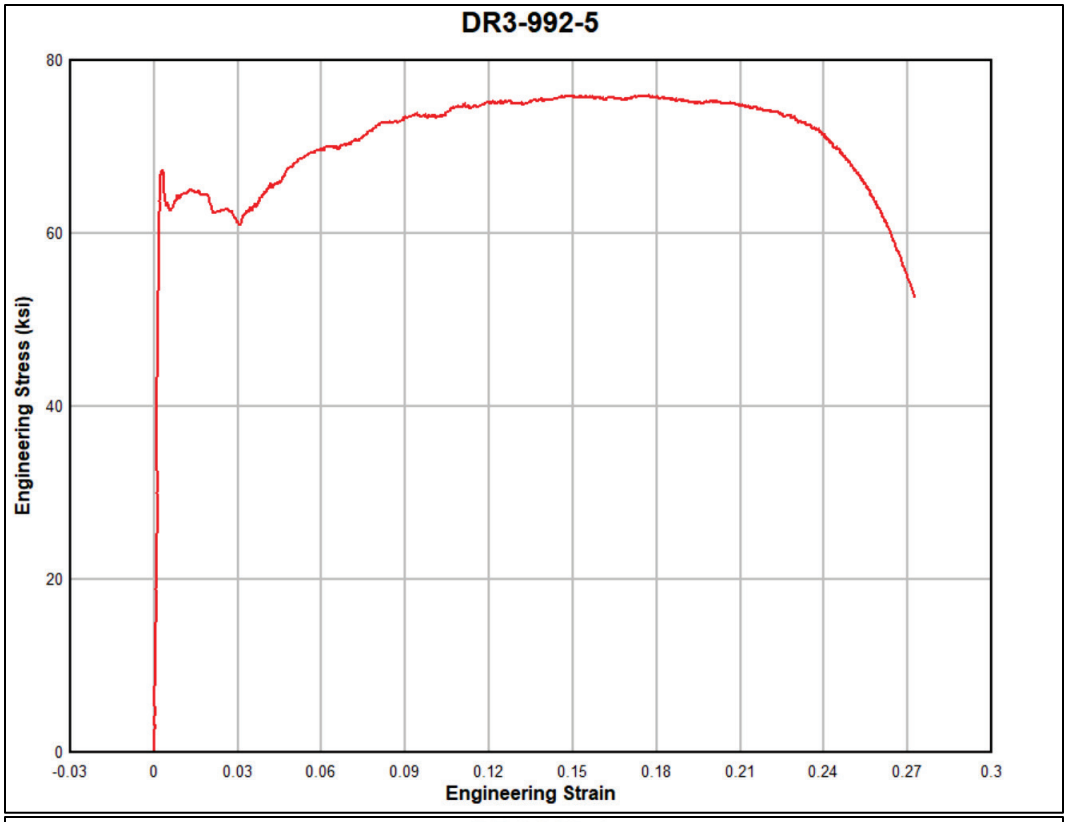
DR3-992-5
Engineering Stress (ksi)
80
60
40
20
0
-0.03
0
0.03
0.06
0.09
0.12
0.15
0.18
0.21
0.24
0.27
0.3
Engineering Strain

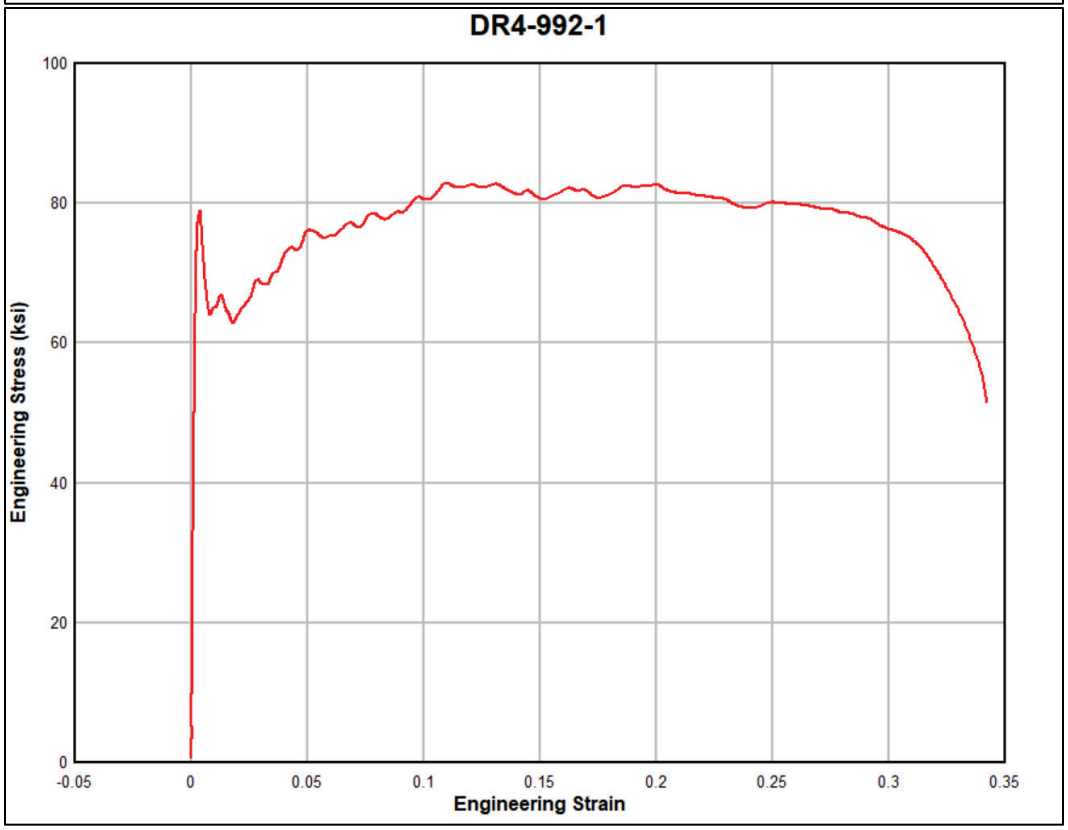
DR4-992-1
Engineering Stress (ksi)
100
80
60
40
20
0
-0.05
0
0.05
0.1
0.15
0.2
0.25
0.3
0.35
Engineering Strain

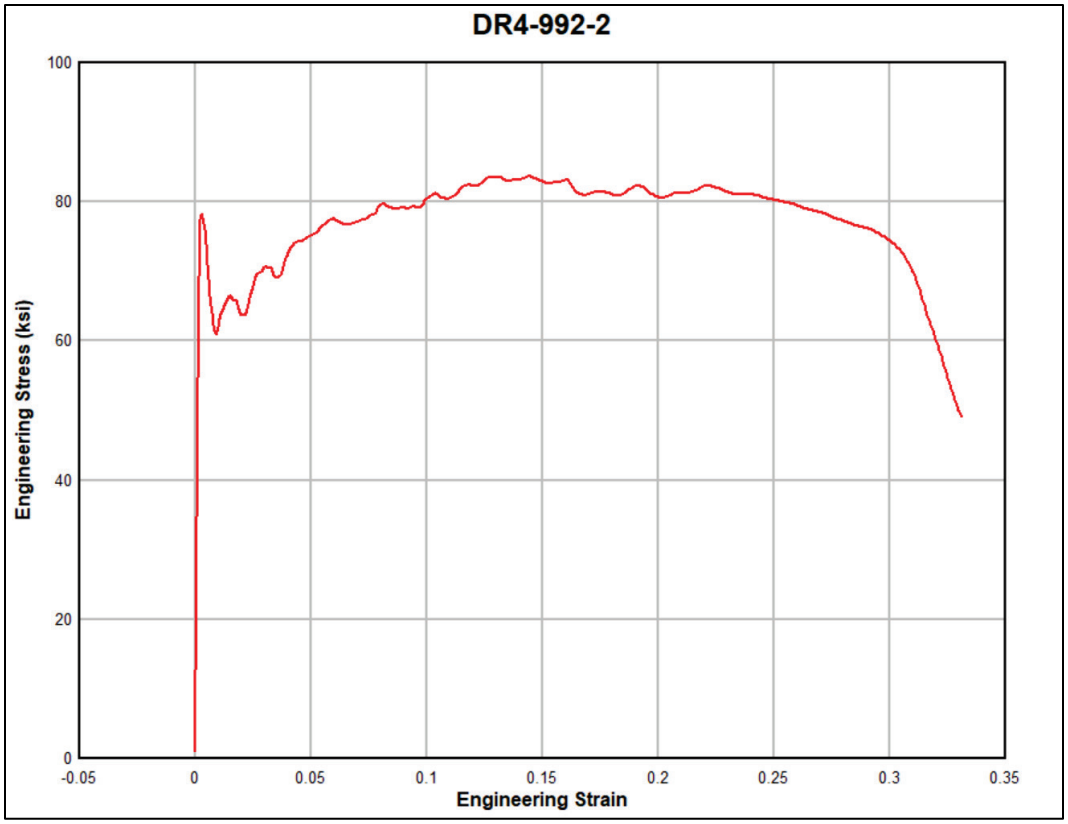
DR4-992-2
Engineering Stress (ksi)
100
80
60
40
20
0
-0.05
0
0.05
0.1
0.15
0.2
0.25
0.3
0.35
Engineering Strain

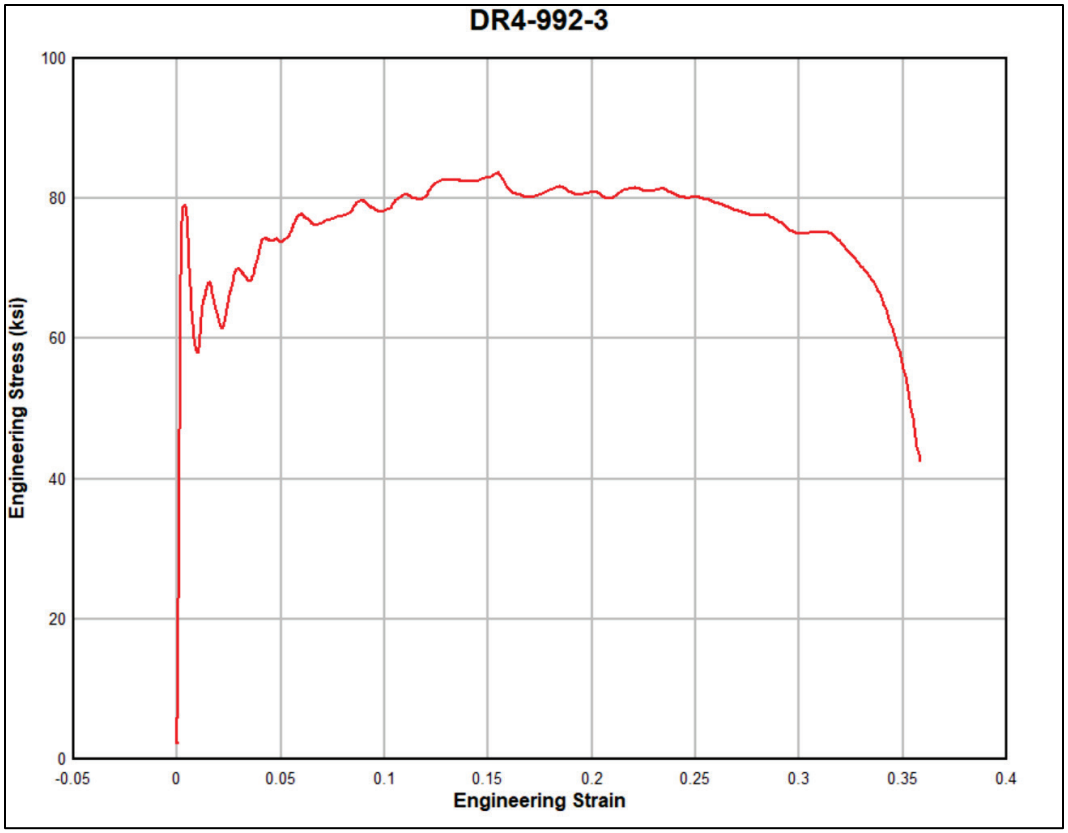
DR4-992-3
Engineering Stress (ksi)
100
80
60
40
20
0
-0.05
0
0.05
0.1
0.15
0.2
0.25
0.3
0.35
0.4
Engineering Strain

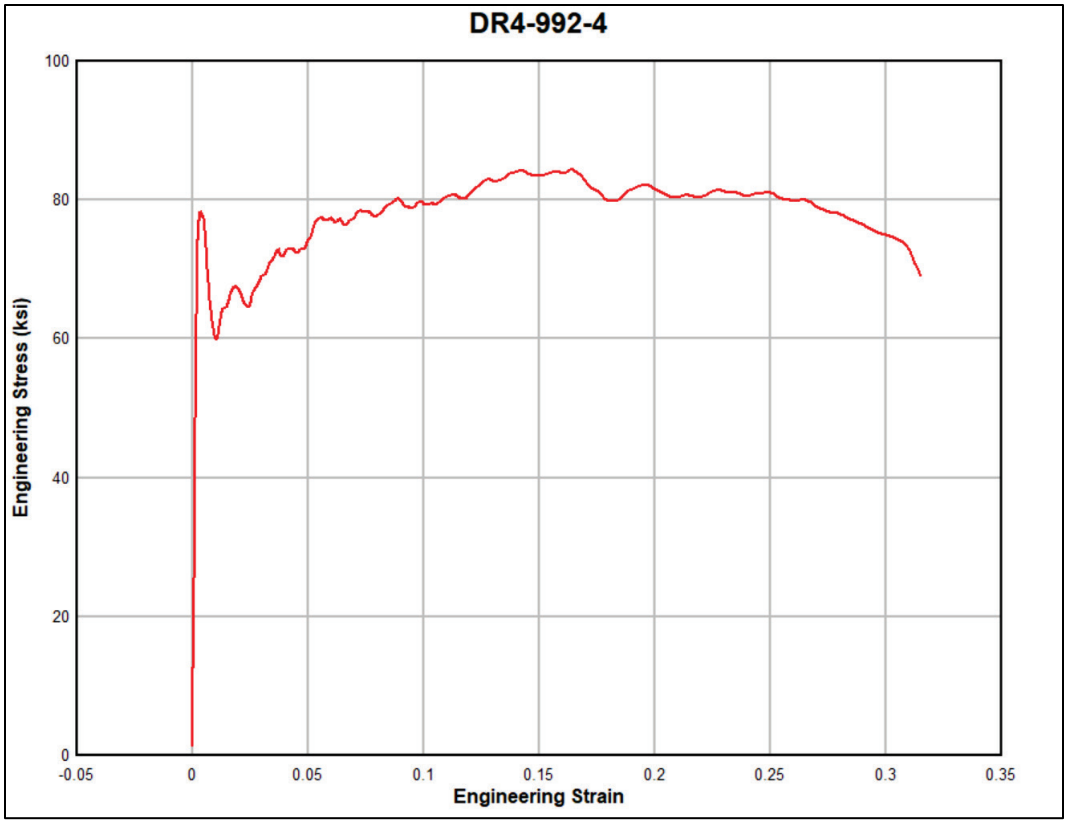
DR4-992-4
Engineering Stress (ksi)
100
80
60
40
20
0
-0.05
0
0.05
0.1
0.15
0.2
0.25
0.3
0.35
Engineering Strain

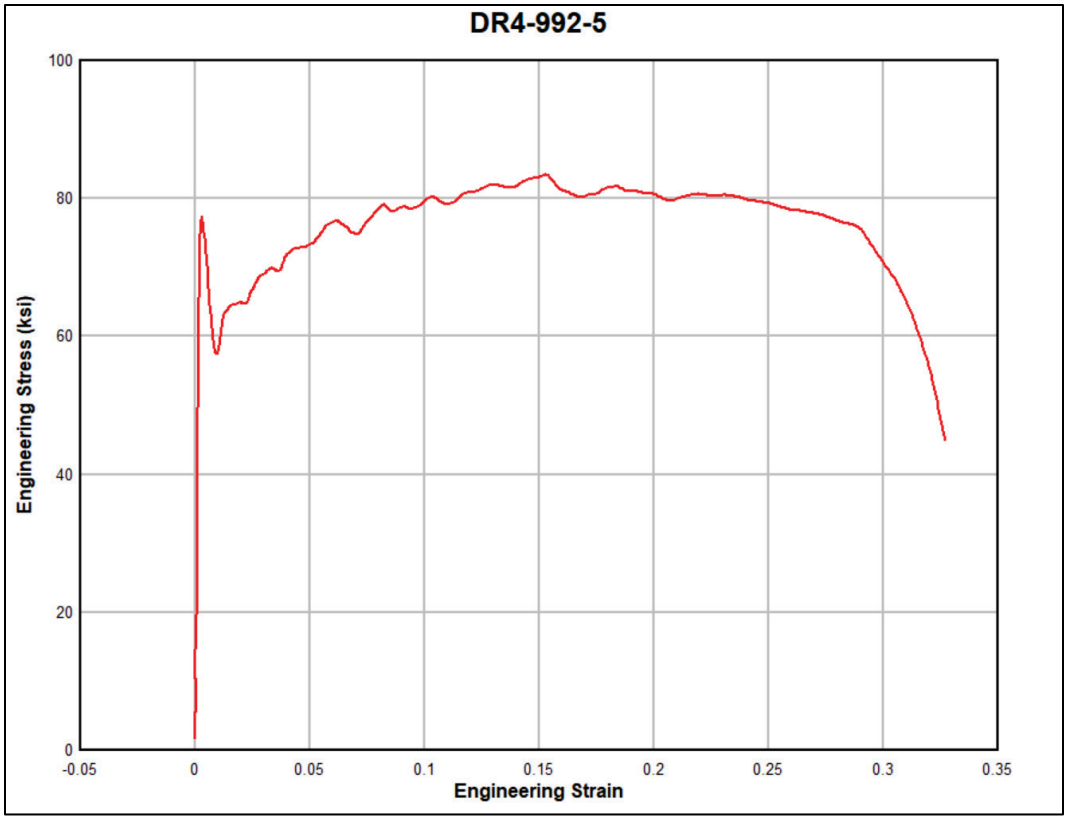
DR4-992-5
Engineering Stress (ksi)
100
80
60
40
20
0
-0.05
0
0.05
0.1
0.15
0.2
0.25
0.3
0.35
Engineering Strain

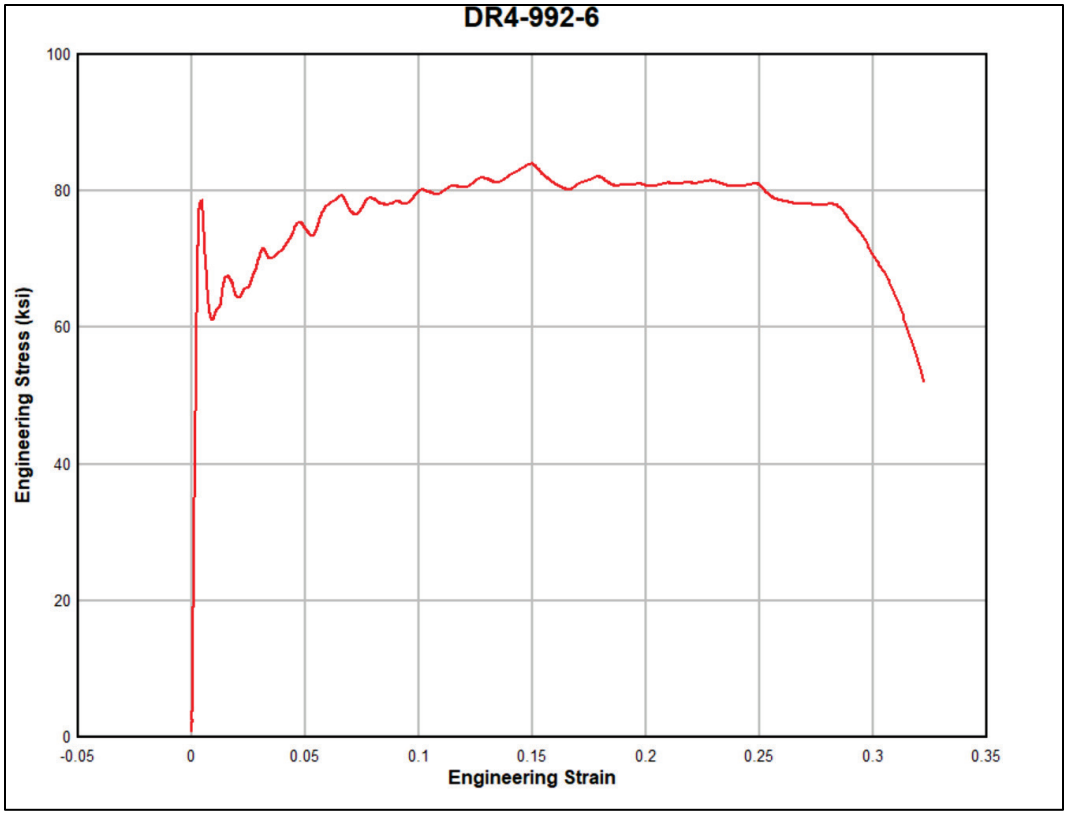
DR4-992-6
Engineering Stress (ksi)
100
80
60
40
20
0
-0.05
0
0.05
0.1
0.15
0.2
0.25
0.3
0.35
Engineering Strain

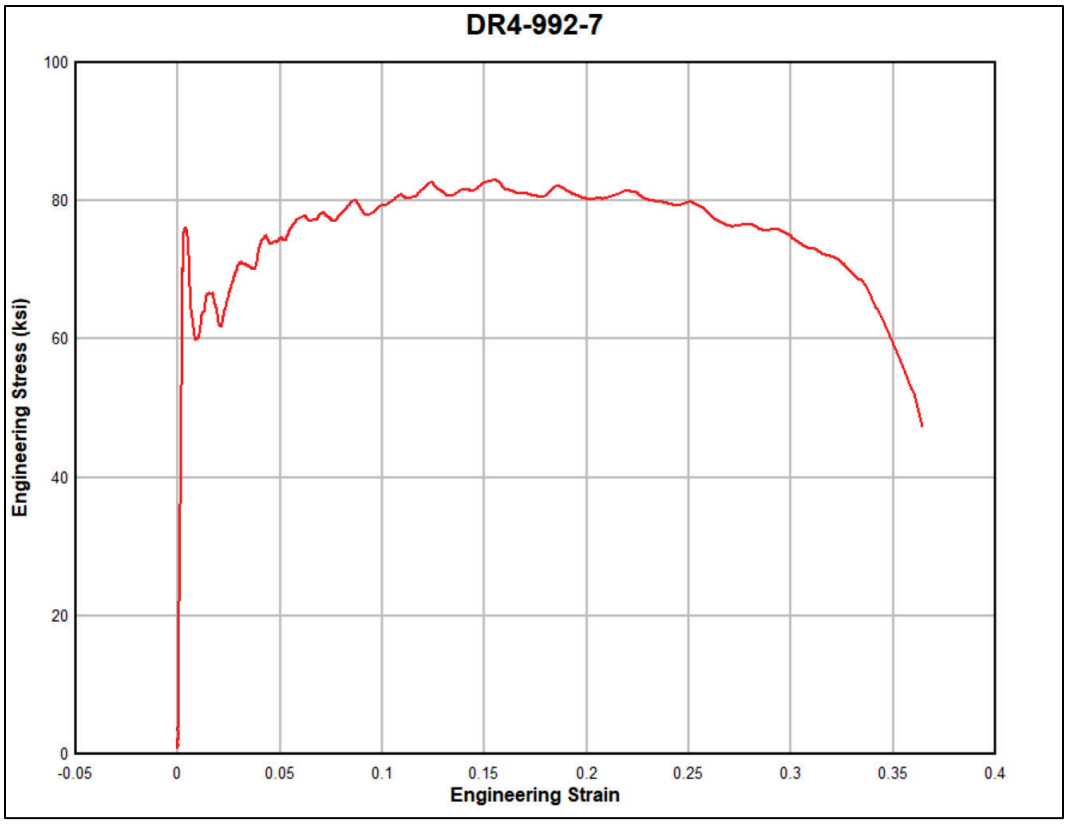
DR4-992-7
Engineering Stress (ksi)
100
80
60
40
20
0
-0.05
0
0.05
0.1
0.15
0.2
0.25
0.3
0.35
0.4
Engineering Strain

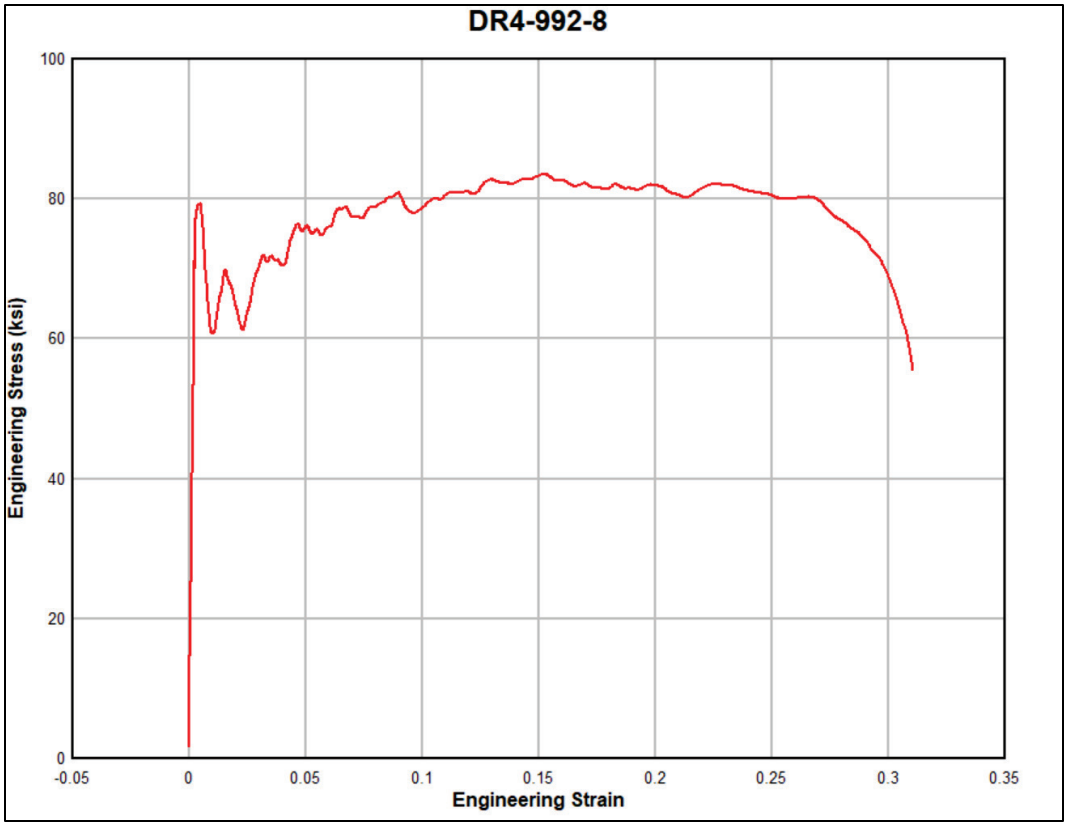
DR4-992-8
Engineering Stress (ksi)
100
80
60
40
20
0
-0.05
0
0.05
0.1
0.15
0.2
0.25
0.3
0.35
Engineering Strain

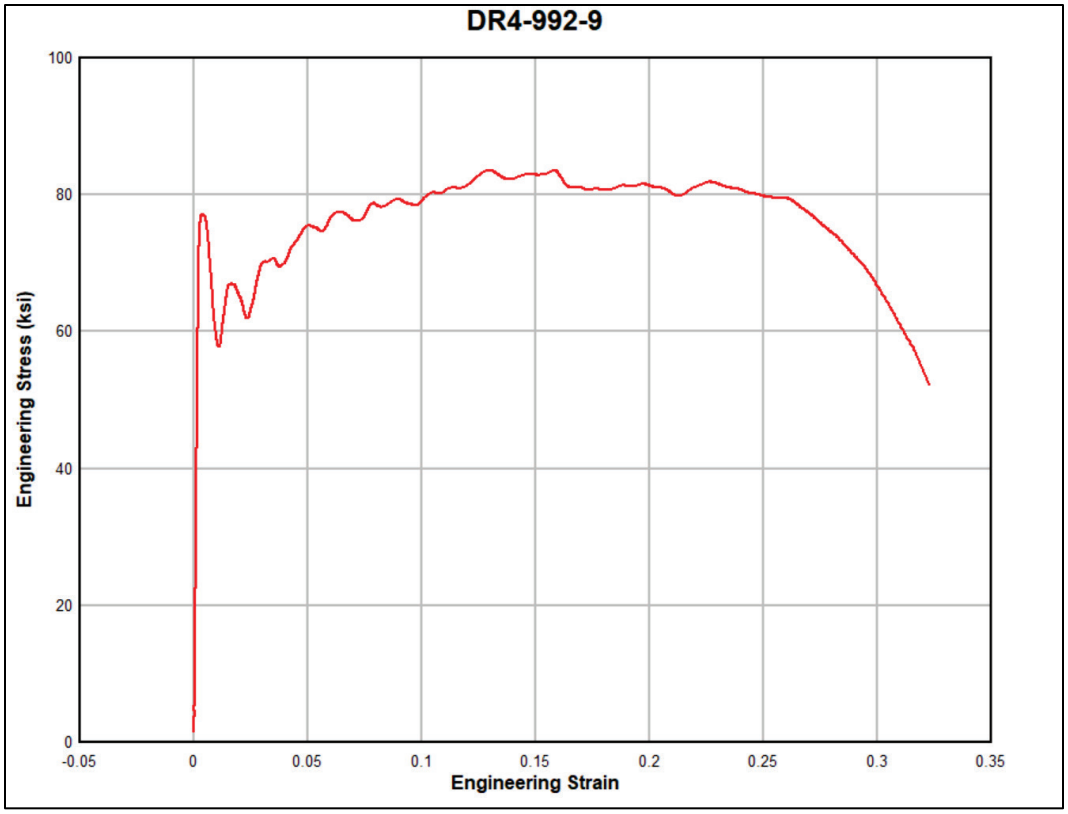
DR4-992-9
Engineering Stress (ksi)
100
80
60
40
20
0
-0.05
0
0.05
0.1
0.15
0.2
0.25
0.3
0.35
Engineering Strain

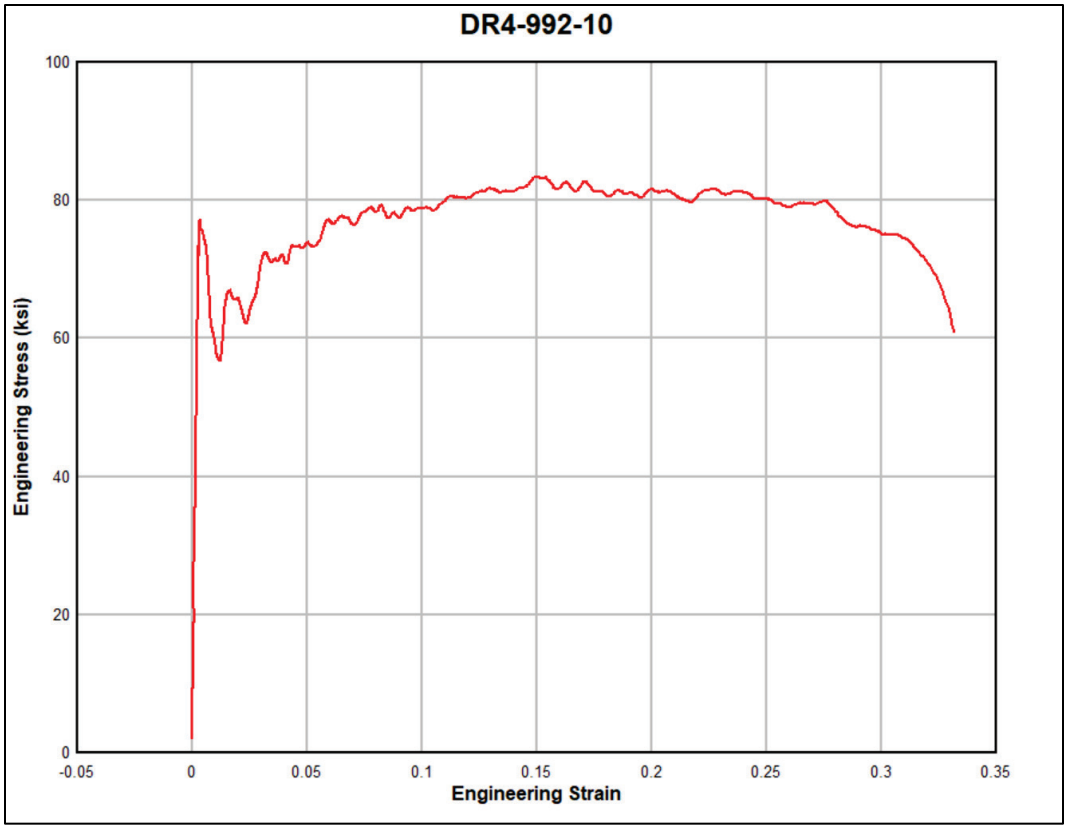
DR4-992-10
Engineering Stress (ksi)
100
80
60
40
20
0
-0.05
0
0.05
0.1
0.15
0.2
0.25
0.3
0.35
Engineering Strain

Abbreviations

Al	Aluminum
ASTM	American Society for Testing Materials International
C	Carbon
Cb	Columbium
Cr	Chromium
CU	Copper
DDESB	Department of Defense Explosive Safety Board
DIF	Dynamic increase factor
DR	Dynamic rate
fps	Frames per second
GSL	Geotechnical and Structures Laboratory
HS	High-speed
MN	Manganese
Mo	Molybdenum
MTR	Mill test report
Nb	Niobium
Ni	Nickel
P	Phosphorous
S	Sulfur
Si	Silicon

SR	Static Rate
TEMA	Track Eye Motion Analysis
Ti	Titanium
V	Vanadium
UFC	Unified Facilities Criteria
USACE	US Army Corps of Engineers
UTS	Ultimate tensile strength

REPORT DOCUMENTATION PAGE

1. REPORT DATE	2. REPORT TYPE	3. DATES COVERED	
		START DATE	END DATE
August 2023	Final report	FY17	FY18

4. TITLE AND SUBTITLE

Dynamic Material Properties of Grade 50 Steel: Effects of High Strain Rates on ASTM A992 and A572 Grade 50 Steels

5a. CONTRACT NUMBER	5b. GRANT NUMBER	5c. PROGRAM ELEMENT
5d. PROJECT NUMBER	**5e. TASK NUMBER**	**5f. WORK UNIT NUMBER**

6. AUTHOR(S)

Matthew P. Murray, Trace A. Thornton, Stephen P. Rowell, and Clifford E. Grey

7. PERFORMING ORGANIZATION NAME(S) AND ADDRESS(ES)

US Army Engineer Research and Development Center
Geotechnical and Structures Laboratory
3909 Halls Ferry Road
Vicksburg, MS 39180-6199

US Army Engineer Research and Development Center
Information Technology Laboratory
3909 Halls Ferry Road
Vicksburg, MS 39180-6199

8. PERFORMING ORGANIZATION REPORT NUMBER

ERDC TR-23-11

9. SPONSORING/MONITORING AGENCY NAME(S) AND ADDRESS(ES)

Department of Defense Explosives Safety Board
4800 Mark Center Drive
Alexandria, VA 22350-3606

10. SPONSOR/MONITOR'S ACRONYM(S)

11. SPONSOR/MONITOR'S REPORT NUMBER(S)

12. DISTRIBUTION/AVAILABILITY STATEMENT

Distribution Statement A. Approved for public release: distribution is unlimited.

13. SUPPLEMENTARY NOTES

Funding provided under MIPR 11052312

14. ABSTRACT

Uniaxial tensile tests were conducted on American Society for Testing Materials International (ASTM) A992 and A572 Grade 50 steels at increasing strain rates to determine the material strength properties of structural members subjected to dynamic loadings. The increase in dynamic yield strength and ultimate tensile strength was determined to update design criteria within UFC 3-340-02, which are currently limited to ASTM A36 and A514 steels. The proposed updates will provide the necessary information required to design blast-resistant structures utilizing modern-day structural steels. The dynamic material properties determined by high-rate tensile tests were compared to static values obtained from ASTM E8 standard tensile tests. The comparisons were used to calculate dynamic increase factors (DIFs) for each steel at strain rates from 2E-3 to 2E0 inch/inch/second. The experiments revealed that the A992 steel exhibited an increase in yield strength up to 45% and ultimate tensile strength up to 20% as strain rate increased over the range tested. The A572-50 steel exhibited a similar increase in yield strength up to 35% and ultimate tensile strength up to 20%. The DIF design curves developed during this research will allow engineers to more efficiently design structural steel components of hardened structures for the protection of our nation's critical infrastructure.

15. SUBJECT TERMS

Steel, Structural--Dynamic testing; Steel, Structural--Mechanical properties; Strains and stresses

16. SECURITY CLASSIFICATION OF:			17. LIMITATION OF ABSTRACT	18. NUMBER OF PAGES
a. REPORT	b. ABSTRACT	C. THIS PAGE		
Unclassified	Unclassified	Unclassified	SAR	95

19a. NAME OF RESPONSIBLE PERSON	19b. TELEPHONE NUMBER (include area code)
Matthew P. Murray	(601) 529-9316